UC Berkeley
UC Berkeley Electronic Theses and Dissertations

Title
Regulation and Assembly of the Proteasome Base

Permalink
https://escholarship.org/uc/item/4vh4t9nq

Author
Goodall, Ellen Alethea

Publication Date
2017

Peer reviewed|Thesis/dissertation

eScholarship.org Powered by the California Digital Library
University of California

Regulation and Assembly of the Proteasome Base

By

Ellen A Goodall

A dissertation submitted in partial satisfaction of the

requirements for the degree of

Doctor of Philosophy

in

Molecular & Cell Biology

in the

Graduate Division

of the

University of California, Berkeley

Committee in charge:

Professor Andreas Martin, Chair
Professor Susan Marqusee
Professor David G Drubin
Professor Arash Komeili

Summer 2017

Abstract

Regulation and Assembly of the Proteasome Base

by

Ellen A Goodall

Doctor of Philosophy in Molecular & Cell Biology

University of California, Berkeley

Professor Andreas Martin, Chair

The ubiquitin-proteasome system is largely responsible for the turnover of proteins in the eukaryotic cell. The proteasome is a compartmental protease of the AAA+ family, and it mechanically unfolds ubiquitinated substrates into a proteolytic chamber in an ATP-dependent manner for degradation. This mechanical unfolding is performed by the proteasome base, but the AAA-motor can only function as a part of the larger proteasome complex. In addition to unfolding, the proteasome must first be recognize substrates by their attached ubiquitin chains and thread them into the motor. Ubiquitin modifications must be removed by the deubiquitinase Rpn11. This dissertation focuses on the effect of substoichiometric proteasome components in the assembly and function of the base. First, this dissertation focuses on how substoichiometric proteasome components Ubp6 and Rad23 affect proteasomal degradation through their interactions with the base.

Ubp6, a deubiquitinase, affects the conformational state of the proteasome through direct interaction with the N-ring in the base in addition to interactions with base subunit Rpn1. By enforcing a substrate-engaged conformation in the proteasome, ubiquitin-bound Ubp6 inhibits Rpn11, stimulates ATPase activity, and shuts down substrate turnover. Ubp6 acts more slowly on ubiquitin-protein substrates than Rpn11 but displays higher activity towards non-translocation dependent ubiquitin substrates. Rad23 also binds to Rpn1 and serves as a ubiquitin receptor at the proteasome. Substrates delivered through Rad23 are deubiquitinated and degraded more slowly than those delivered through the intrinsic ubiquitin receptor, Rpn10. However, substrates delivered through either receptor are deubiquitinated by Ubp6 at similar rates.

Finally, this dissertation examines the importance of four base-specific assembly factors in heterologous expression of the base. These assembly factors, Nas6, Rpn14, Hsm3, and Nas2, help to stabilize base subunits, which allows for assembly, but they are unable to prevent the assembly of base subunits into incorrect complexes. In addition, other components of the proteasome, Ubp6 and core, discriminate between properly and improperly assembled base.

Table of Contents

Table of Figures

Chapter 1: Introduction to the ubiquitin-proteasome system

The need for protein turnover in the cell

The fundamental processes of a cell are carried out by its proteins. In order to respond to changes in its environment a cell must be able to rapidly and selectively change its suite of proteins. In addition, proteins that have been damaged need to be recognized and removed by degradation. In eukaryotes, targeted protein turnover is performed by the ubiquitin-proteasome system, where the proteasome is responsible for the destruction of ubiquitin-tagged proteins (Finley, 2009). Protein degradation needs to occur in a timely manner: regulatory proteins such as those governing the cell cycle must be turned over, but degradation must also be generalizable so that cells may target any given protein.

To accomplish this a variety of E3 ligases are specialized for recognition of specific targets to be marked with ubiquitin for targeting to the proteasome. Proteins are targeted for degradation throughout their life cycle beginning with the recognition of translation errors on the ribosome (Bengtson and Joazeiro 2010; Brandman et al., 2012). Off the ribosome, E3 ligases recognize misfolded proteins in both the nucleus and the cytoplasm, as well as in subcellular compartments such as at the endoplasmic reticulum (Kriegenburg, Ellgaard, and Hartmann-Petersen, 2012). Many of these processes also require the action of Cdc48/VCP/p97, a AAA-type motor to extract ubiquitinated proteins from macromolecular complexes or membranes before they are accessible to the proteasome. In addition to quality control, the proteasome is essential for signaling events through the turnover of short-lived regulatory proteins. Perhaps best studied is the role of the proteasome, with the SCF and anaphase promoting complex E3 ligases, in governing the transition between phases of the cell cycle (Vodermaier, 2004).

In all of these processes proteins are targeted to the proteasome by the covalent addition of ubiquitin to lysine side chains. Attachment of ubiquitin chains to a protein can target a substrate to the proteasome, however an unstructured tail is also required for engagement by the proteasome motor for degradation (Prakash et al., 2004; Thrower et al., 2000; Yu et al., 2015). Ubiquitin is involved in a variety of cellular process including in signaling that does not ultimately result in the degradation of the ubiquitinated substrate, and ubiquitin is key to the targeting of proteins for proteasomal degradation.

Making ubiquitin chains

For a substrate to be recognized by the 26S proteasome, it is covalently modified by the small protein ubiquitin. A cascade of enzymes termed E1, E2, and E3 can attach the C-terminus of ubiquitin to a lysine side chain of a substrate, forming an isopeptide bond (Figure 1.1). First, E1 activates the C-terminus of ubiquitin in an ATP-consuming step, transferring the ubiquitin to a cysteine side chain in its active site linked through a high-energy thioester. E1 recruits an E2 and transfers the ubiquitin to a cysteine on the E2. E3 enzymes then transfer the ubiquitin to a lysine in a substrate. Homology to E6AP containing (HECT) E3 ligases transfer the ubiquitin to a catalytic cysteine on themselves before transferring the ubiquitin to the substrate lysine (Kim and Huibregtse, 2009). Another major class of E3 ligases, Really interesting new gene (RING), do not transfer the ubiquitin to an E3 cysteine, but stimulate a bound E2 to transfer the E2-attached ubiquitin to a substrate (Pruneda et al., 2012). After discharge of the ubiquitin from the E2 or E3 to the substrate, another charged E2 can bind and transfer another ubiquitin. Through this repeated process substrates can be modified with ubiquitin at multiple lysines and chains of ubiquitin can be built off of lysines on ubiquitin itself (Komander and Rape, 2012) (Figure 1.2a).

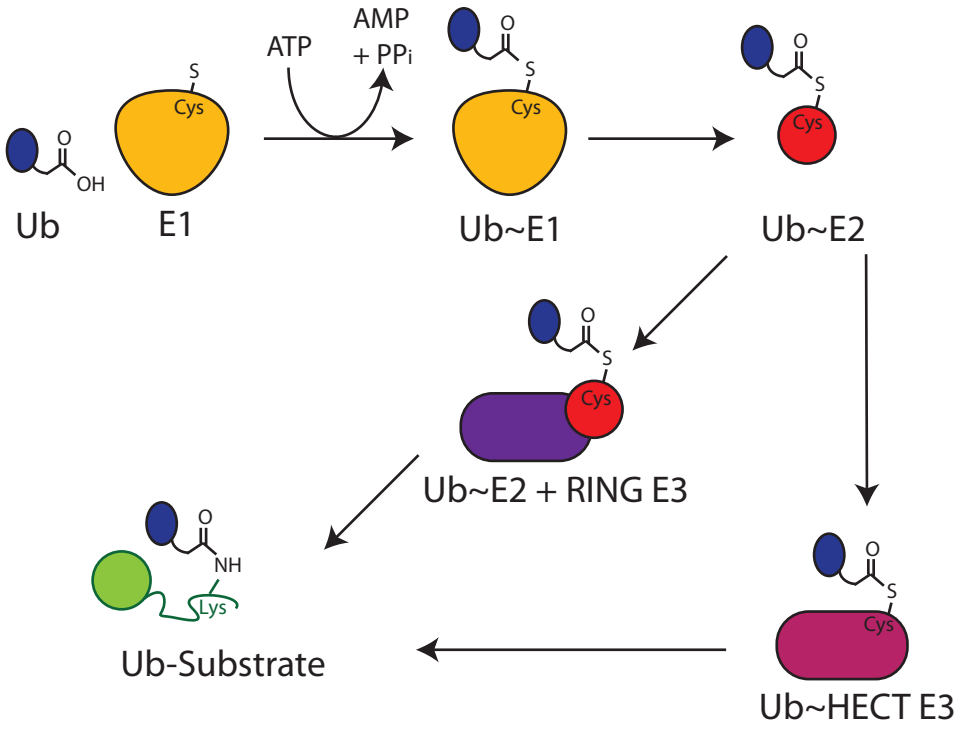

Figure 1.1: The Ubiquitination cascade: Ubiquitin (navy blue) is attached to substrate lysines (green) through its C-terminus. First, in an ATP-consuming step, ubiquitin is transferred to the active site cysteine of E1 (gold). This high-energy thioester linkage is transferred to the active site cysteine of an E2 (red). An E3 ligase pairs a charged E2 with a substrate and catalyzes ubiquitin transfer. HECT E3 ligases (magenta) transfer the ubiquitin to their own active site cysteine first, while RING E3 ligases (purple) do not. The ubiquitin is transferred to a lysine on the substrate resulting in an isopeptide bond.

Ubiquitin contains lysines at six positions (K6, K11, K29, K33, K48, K63), and any of these along with the N-terminus can accept ubiquitin. Ubiquitin chains of different linkage types can be specifically recognized due to the differences in orientation of ubiquitins to each other (Ye et al., 2012) (Figure 1.2b). This allows a wide variety of different linkage type ubiquitin chains to be built on substrates: not only can information be encoded in which lysines are ubiquitinated on a substrate, but differences in number and placement of ubiquitins can also. In analyses of different linkage types in both mammalian cells and yeast, percentages of each linkage type have varied, but all linkage types are present (Ziv et al., 2011; Kim et al., 2011; Xu et al., 2009). On the substrate side, ubiquitin can be found not just on substrate lysines, but also transferred to the thiol of cysteines or hydroxyls of threonine and serines in a few cases (McDowell and Philpott, 2013), allowing the modification of lysine-free proteins. Use of different E2s and E3s allows for selectivity in linkage type of ubiquitin chains, while the E3 is responsible for substrate specificity.

These differences in ubiquitin chains can be readout by ubiquitin interacting proteins with linkage specificity (Husnjak and Dikic, 2012). In addition, deubiquitinases (DUBs) can remove ubiquitin from substrates, sparing proteins from proteasomal degradation, and can also have specificity to linkage type (Ye et al., 2012). Even when a substrate has been targeted for degradation either at the

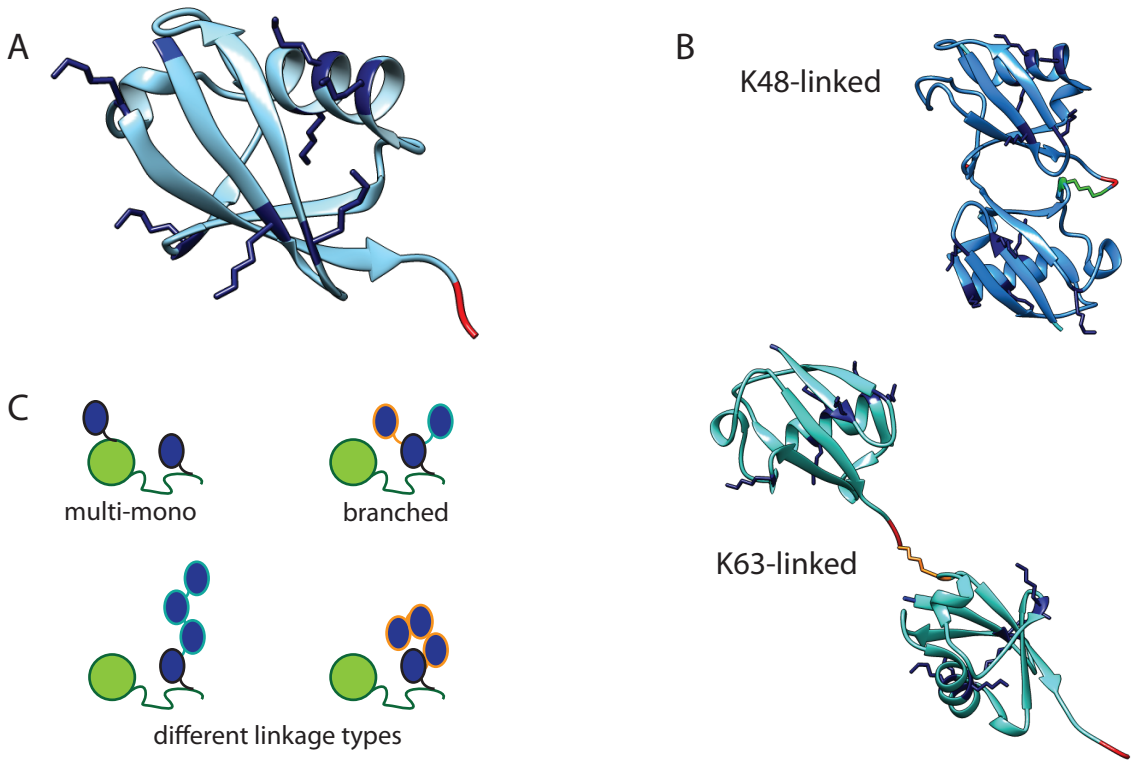

Figure 1.2: Ubiquitin linkages. (A) Ubiquitin contains six lysines and an N-terminus (navy blue) that can all be linked to the C-terminus (red) of another ubiquitin to form ubiquitin chains of different linkage types (PDB: 1UBQ, Vijay-Kumar, Bugg and Cook, 1987). (B) Different linkage types have different properties due to differences in the geometry of ubiquitins to each other in a chain. Chains formed through K48 (blue, lysine in green) can adopt a compact conformation (PDB: 2O6V, Eddins et al., 2006), while chains formed through K63 (structure in aquamarine, lysine in gold) are extended. (C) Substrates (green) can be modified through multiple lysines, chains of different linkages types, (highlighted as teal or orange) and branched chains.

proteasome or through the lysosome, the attached ubiquitin that targets substrates is removed by DUBs to be recycled rather than co-degraded. While some linkage types, such as K63-linked ubiquitin chains, are infrequently associated with proteasomal degradation *in vivo*, *in vitro* these chains efficiently target substrates for degradation by the proteasome (Saeki, Isono, and Toh-E, 2005; Nathan et al., 2013).

Proteasome structure and assembly

While there are many E3 ligases and DUBs that constitute the ubiquitin code, in targeted protein degradation all of these substrates end up at the proteasome for proteolytic cleavage. The proteasome is a complex molecular machine composed of at least 33 different subunits in one or two copies (Figure 1.3 Figure 1.4a, Table 1.1). The proteasome holoenzyme can be biochemically dissociated into the base, lid and core subcomplexes that also act as the assembly building blocks of the proteasome holoenzyme. The barrel-shaped 20S core peptidase is capped on one or both ends by the 19S regulatory particle. This 20S core peptidase contains the proteolytic active sites in an internal chamber, sequestering them from the cytosol. It is composed of two copies of 14 different α and β-subunits that form four stacked rings (α_7-β_7-β_7-α_7) (Groll et al., 1997). Three of the β-

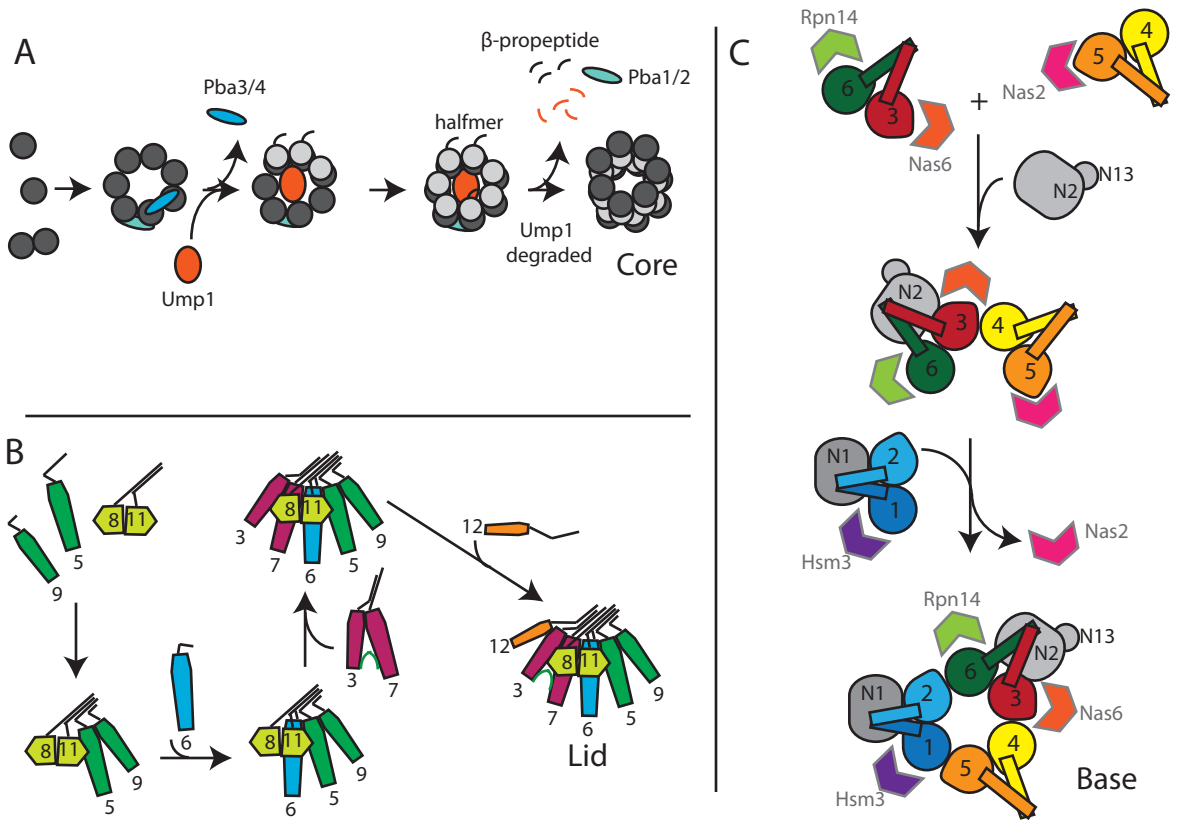

Figure 1.3: Assembly of proteasome subcomplexes from subunits. (A) Assembly of the 20S core occurs through ordered steps with the aid of dedicated assembly factors. First, α subunits (dark grey) assemble to form a heptameric ring with the aid of Pba1/2 and Pba3/4. The α-ring, with the aid of β-propeptides, assembles a ring of β subunits (light grey) to form a 'halfmer' containing one α and one β-ring. Joining of two halfmers completes core assembly with the release of Pba1/2 and activation of the peptidases. This results in the degradation of assembly factor Ump1 and the β-propeptides. (B) Lid assembly is driven by interaction between C-terminal helices of each subunit. Specific interactions between the MPN domains of Rpn8 and Rpn11 (light green) pair these two subunits, while Sem1 (dark green line) pairs Rpn3 and Rpn7. Rpn12 (gold) is the last subunit to join the lid and requires the incorporation of the other Rpns. (C) Base assembly occurs through the joining of coiled-coiled pairs of ATPase subunit modules. Rpt3 (dark green) and Rpt6 (red) form a module with Rpn14 (light green) and Nas6 (dark orange). This module pairs with a module containing Rpt4 (yellow), Rpt5 (light orange), and Nas2 (pink) and is joined by Rpn2 and Rpn13 (grey). Addition of Hsm3 (purple), Rpt1 (blue) Rpt2 (cyan) and Rpn1 as a module displaces Nas2 from Rpt5.

(Following page) Table 1.1: Stable subunits of the proteasome organized by proteasome subcomplex. Domains and motifs responsible for enzymatic activities, interaction with other subunits, and assembly are listed for each subunit.

Subcomplex	Name	Function/ activities	Domains/motifs
19S Regulatory particle - Base			
	Rpn1	Ubiquitin binding, UBL binding (Rad23, Ubp6)	α-solenoid of PC repeats
	Rpn2		α-solenoid of PC repeats
	Rpn13	Ubiquitin binding, UBL binding (Dsk2)	PH
	Rpt1	ATPase unfoldase	coiled-coil, OB, AAA
	Rpt2	ATPase unfoldase, core gate opening	coiled-coil, OB, AAA, HbYX
	Rpt3	ATPase unfoldase, core gate opening	coiled-coil, OB, AAA, HbYX
	Rpt4	ATPase unfoldase	coiled-coil, OB, AAA
	Rpt5	ATPase unfoldase, core gate opening	coiled-coil, OB, AAA, HbYX
	Rpt6	ATPase unfoldase	coiled-coil, OB, AAA
19S Regulatory particle - Lid			
	Rpn3		TPR, PCI, helix in bundle
	Rpn5		TPR, PCI, helix in bundle
	Rpn6		TPR, PCI, helix in bundle
	Rpn7		TPR, PCI, helix in bundle
	Rpn9		TPR, PCI, helix in bundle
	Rpn12		TPR, PCI, helix in bundle
	Rpn8	Dimer with Rpn11	MPN, helix in bundle
	Rpn11	JAMM Deubiquitinase	MPN, helix in bundle
	Sem1		
	Rpn10	Ubiquitin binding, through UIM	VWA, UIM
20S Core Particle	**α1-7**	Gating entry to core	
	β1-7	β1, β2, β5 are active Thr-proteases	

subunits are the active proteases with active sites facing the interior of the core peptidase. These subunits, β1, β2, and β5, are threonine peptidases with differing specificity and activity (Groll et al., 1997; Dick et al., 1998). The β1 subunit shows caspase-like activity and cleaves after acidic residues, the β2 subunit shows trypsin-like activity and cleaves after arginine residues, and the most active β5 shows chymotrypsin-like activity and cleaves after hydrophobic residues.

Assembly of the core involves several core-dedicated assembly factors, but also specificity encoded in the proteasome subunits themselves (Figure 1.3a). For example, the N-terminal propeptides of the β-subunits promote core assembly (Arendt and Hochstrasser 1999). Core-dedicated assembly factors aid assembly by stabilizing and pairing core subunits. Pba3/4 aids in the assembly of the α-ring through interactions with α5, while a stable intermediate of the completed α-ring with three of the seven β-subunits is formed with the aid of Pba1/2, Ump1, and the propeptides of β-subunits (Kunjappu and Hochstrasser, 2014). A 'halfmer,'containing one full ring each of α and β-subunits, joins with another halfmer and this joining is linked to the activation of the β-subunits and Ump1 degradation (Kunjappu and Hochstrasser, 2014). This assembly mechanism ensures that only core particles that are capable of acting as peptidases are assembled. In the assembled core, α-subunits contain the closed gates on either end of the 20S core that can be opened by the binding the 19S regulatory particle (Smith et al., 2007).

The 19S regulatory particle is responsible for the deubiquitination, unfolding, and translocation of protein substrates into the core and can be further divided into the base and lid subcomplexes. The

base contains the AAA-type unfoldase responsible for unfolding and threading proteasome substrates into the core. The lid contains the essential DUB of the proteasome, and along with eight other subunits, hugs the side of the complex making contacts with both the base and core complexes (Lander et al., 2012, Lasker et al., 2012).

In contrast to the core, the lid does not require dedicated assembly chaperones for assembly, despite also being assembled from subunits that are each structurally to each other (Figure 1.3b). The six PCI (proteasome-CSN-eIF3) containing subunits are arranged in a horseshoe-shaped structure through lateral interactions of winged-helix domains. The N-terminal TPRs (tetratricopeptide repeat) that project outwards from the winged helix domains and make contacts with the base and core (Lander et al., 2012). The DUB Rpn11 forms a heterodimer with the related, but catalytically inactive Rpn8 (Lasker et al., 2012). C-terminal helices present in eight subunit of the lid are the drivers of the specific assembly of the lid (Estrin et al., 2013). Modules of fewer subunits join together to form the lid and addition of the final subunit, Rpn12, acts as a capstone for proper assembly of the lid (Estrin et al., 2013; Tomko and Hochstrasser, 2011a, Tomko et al., 2015). Sem1, a small disordered protein that does not participate in the C-terminal helix bundle, helps pair two of the PCI containing subunits together and remains bound in the final lid complex, acting as a 'molecular glue' (Tomko and Hochstrasser, 2014).

Similar to the lid, the base assembles from sets of related subunits (Figure 1.3c). The AAA-type unfoldase of the proteasome is unique in the AAA+ family as it is composed of six different subunits (Rpts1-6) that assembly into a heterohexamer in the specific order Rpt1-Rpt2-Rpt6-Rpt3-Rp4-Rpt5 (Tomko and Hochstrasser, 2011b). The ATPase subunits are homologous to the homohexameric PAN, an archeal unfoldase that also binds to a heptameric protease. In both the proteasome base and PAN, the N-terminal portion of each ATPase subunit contains a coiled coil and an OB-fold. Together these form a hexameric N-ring consisting of an OB fold contributed by each subunit that sits atop the AAA ring (Lander et al., 2012; Zhang et al., 2009). Three pairs of coiled-coils, formed from neighboring subunits, project from the N-ring and make additional contacts with other base and lid subunits in the proteasome. In PAN, the N-domains self assemble into hexamers, while the AAA domains do not assemble in the absence of N-domains. The AAA hexamer forms a second ring with each Rpt contributing one AAA domain. On the C-terminus of PAN, a tripeptide motif of the sequence hydrophobic-Tyr-any amino acid (HbYX) in alternating ATPase subunits docks into the core peptidase to open the α-gates (Smith et al., 2007). In the proteasome, only the three alternating subunits (Rpt2, Rpt3, and Rpt5) retain this motif, and dock into hydrophobic pockets between α-subunits of 20S core (Table 1.1). The two large non-ATPase subunits of the base, Rpn1 and Rpn2, do not make extensive with each other, but make contacts with the coiled coils of the ATPases. Rpn1 and Rpn2's PC (proteasome-cyclosome) α-helical solenoid domains interact with ubiquitin, ubiquitin receptors, and DUBs, and along with Rpn13 are responsible for scaffolding and ubiquitin recognition (Shi et al., 2016; Husnjak et al., 2008; Schreiner et al., 2008).

In its assembly, the base is more similar to the core than the lid: four RP-dedicated assembly 'chaperones' (RACs) aid in assembly of the base subcomplex (Roelofs et al., 2009; Funakoshi et al., 2009; Saeki et al., 2009, Le Tallec et al., 2009) (Figure 1.3c). These RACs, Rpn14, Hsm3, Nas6, and Nas2, each interact with specific ATPase subunits of the base and were originally thought to be subunits of the proteasome holoenzyme. Whereas Rpn14, Hsm3 and Nas6 all remain bound in the final assembled based before assembly of the core and lid with the base displaces them, Nas2 is

released during the base assembly process because Nas2 binds to the same face of Rpt5 as Rpt1 in the assembled base (Singh et al., 2014). Rpn14, Nas6, and Hsm3 each bind to the small-AAA domains of specific Rpts and are released when the base is assembled into proteasome as they sterically clash with core and lid binding to base (Park et al., 2013; Li et al., 2017). When base assembly is disrupted, modules containing subsets of base subunits are observed in yeast and are therefore thought to be the building blocks of base assembly (Park et al., 2009). Each module also contains at least one chaperone: Hsm3-Rpn1-Rpt1-Rpt2 form one module, Nas2-Rpt4-Rpt5 form another, and Rpn14-Rpt6-Rpt3-Nas6 form a third. These modules assemble to form the base, displacing Nas2 and adding Rpn2 and Rpn13 during the process. Similar to the lid, elements of the base subunits themselves contribute to specificity in pairing. Each base module contains a coiled-coil pair of ATPase subunits. Removal of the N-terminal α-helices from any Rpt subunit is not tolerated in yeast, suggesting the coiled coils are important in forming these modules and in base assembly (Inobe and Genmei, 2015). While the binding specificity of these chaperones and high-resolution structures of these factors are known, how exactly they are able to sense and aid the assembly of the base remains an open question (Kim et al., 2010; Barrault et al., 2012; Singh et al., 2014; Takagi et al., 2012; Nakamura et al., 2007).

While each subcomplex of the proteasome is capable of fully assembling before joining to form the proteasome, the role of each subcomplex acting either a as template for assembly by other mechanisms or as gatekeepers of proper assembly has not been ruled out (Beckwith et al., 2013; Lander et al., 2012). The RACs location on the face of the base that interacts with the core suggests that they may regulate the base-core interaction to prevent premature interaction. Nas2 blocks the C-terminus of Rpt5 from interacting with the core, and the C-terminal peptide of Rpt5 is promiscuous in core α-pocket binding (Singh et al., 2014). In the absence of assembled base, this Rpt5 peptide alone is capable of binding to several α-core pockets and has highest affinity for an incorrect pocket (Park et al., 2013).

Though it is tempting to suggest that these subcomplexes may have biological functions outside of the proteasome, a common theme in assembly of these complexes is inhibition of activity in the subcomplex before incorporation into the proteasome holoenzyme (Smith et al., 2007). The lid's DUB activity is autoinhibited by interactions between Rpn11 and Rpn5 that are relieved upon lid incorporation into holoenzyme (Dambacher et al., 2016). Similarly, although the base contains intrinsic ubiquitin receptors and contains ATPase activity in the absence of other complexes, regulatory particle is unable to unfold proteasome substrates (Lu et al., 2016). Assembly of each of these complexes touches on common problems faced in the assembly of many large protein complexes: differentiation between related subunits to form a complex of specific organization and gatekeeping mechanisms to prevent assembly of incorrect subcomplexes from poisoning the whole complex.

Degrading a substrate

Once the proteasome is assembled many similar communications between subunits occur to ensure the efficient degradation of substrates. Through structural characterization of the proteasome, it was revealed that a series of conformational changes are associated with the steps of degradation (Matyskiela et al., 2013; Śledź et al., 2013; Wehmer et al., 2017). First, the ubiquitin chain attached to a substrate is recognized by the proteasome through one or more of several ubiquitin receptors. Rpn13, Rpn10 and Rpn1 all contain intrinsic ubiquitin binding sites on the proteasome (Shi et al., 2016; Husnjak et al., 2008; Elsasser et al., 2004). In addition, 'shuttle receptors' can deliver

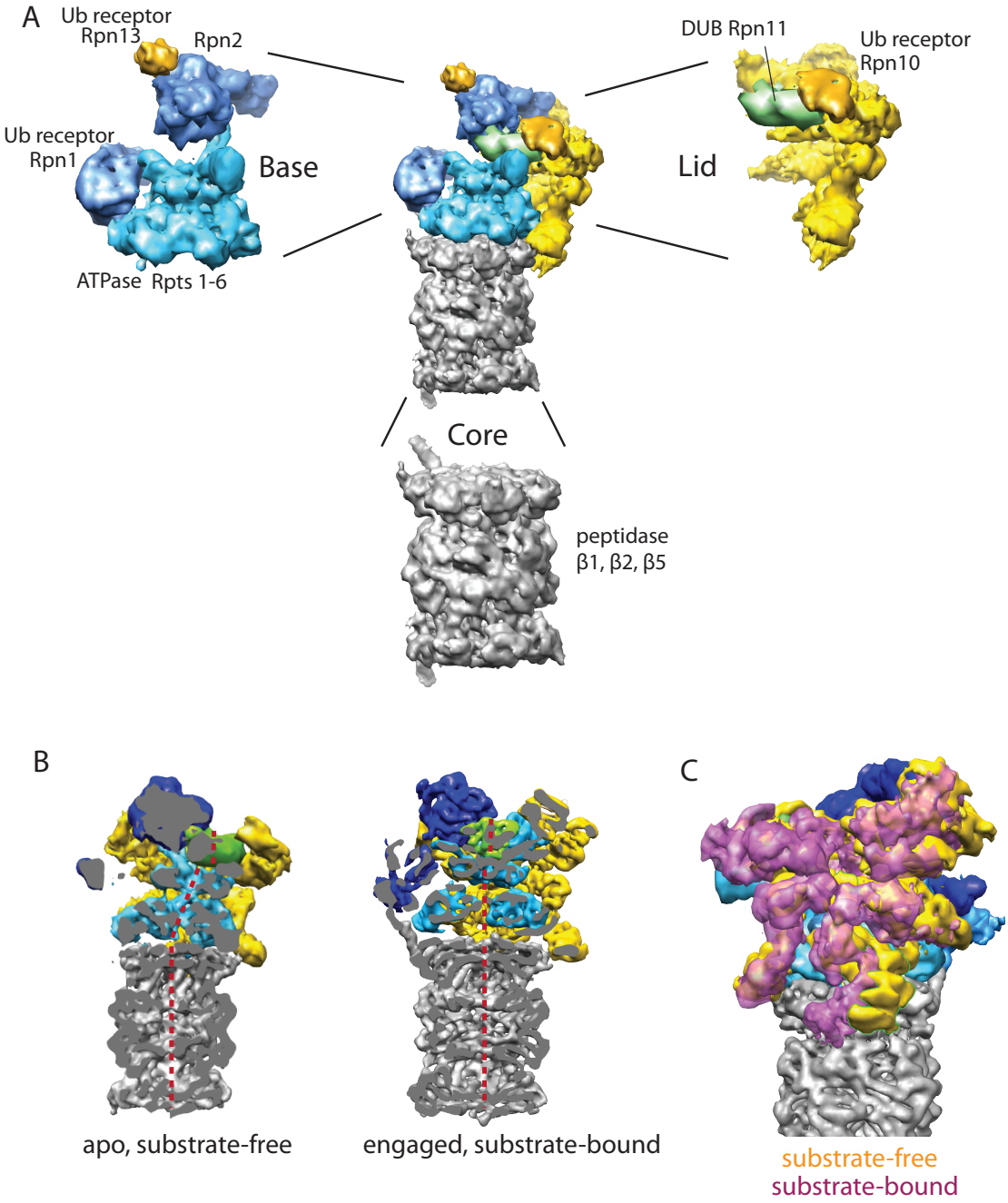

Figure 1.4: Architecture and conformational changes of the 26S proteasome. (A) The proteasome is composed of the base, lid, and core complexes. The base contains the AAA unfoldase (cyan) and ubiquitin receptors Rpn13 (gold) and Rpn1 (blue). The lid hugs the side of the proteasome with its TPRs (yellow) and contains the DUB Rpn11 (green) as well as ubiquitin receptor Rpn10 (gold) The regulatory particle sits atop the core and controls access to the interior of the core particle (grey) containing proteases. (B) Conformational changes induced by substrate or ATPγS result in an alignment of the base ATPase channel (cyan) and Rpn11 DUB (green) active site as seen in a cut through of the proteasome pore highlighted with dashed red lines. (C) From outside the proteasome, rotation in the lid PCI horseshoe occurs in this conformational change.

substrates through transient interactions with the proteasome and will be discussed in more detail in the following section (Elsasser et al., 2004). An unstructured segment of the substrate is fed into the N-ring and ATPase ring of the proteasome. Once substrate is engaged by the proteasome, a large conformational change occurs, rearranging the base ATPases into a planar ring that is aligned with the gated pore of the core peptidase (Matyskiela et al., 2013; Śledź et al., 2013)(Figure 1.4b). A rotation of the lid also brings the essential DUB Rpn11 above the pore of the N-ring, aligning it with the core pore as well. From knowledge of related motors and additional conformations captured of the proteasome bound to non-hydrolyzable nucleotide analogs, ATP hydrolysis causes movements in proteasome ATPase domains and these movements allow pore loop tyrosines to translocate the substrate (Wehmer et al., 2017; Ding et al., 2017; Martin, Baker, and Sauer, 2008). As the ATPase translocates a polypeptide, Rpn11 cleaves attached ubiquitin chains *en bloc* from the substrate. Work by the ATPase motor pulls substrates into the ATPase, unfolding them and feeding the unfolded polypeptide into the core peptidase (Matyskiela and Martin, 2013). Once in the peptidase, the three active β-subunits clip the substrate into peptides in the core. After fully translocating and degrading a substrate, the proteasome likely switches back to the substrate-free conformation to repeat the process with another substrate.

Additional factors at the proteasome: shuttle factors

In addition to the proteasome subunits described above, a suite of non-stoichiometric or loosely bound proteasome interacting proteins (PIPs) are involved in proteasome function. For the most part these PIPs have not yet been structurally localized to the proteasome. Given the broad characterization of these factors, it is likely that they will impact the proteasome in many different ways. However, a few of these PIPs have direct impact on substrate degradation at the proteasome. In *Saccharomyces cerevisiae*, three shuttle receptors, Rad23, Dsk2, and Ddi1, have been described and are united in their overall domain architecture. Each contains an N-terminal ubiquitin-like domain (UBL) followed by one or more ubiquitin binding domains (UBAs, ubiquitin-associated). These shuttle receptors can interact with either E3 ligases or the proteasome through their UBL domain, and bind polyubiquitin through their UBAs (Elsasser et al., 2004; Chen and Madura, 2002; Kim, Mi, and Rao, 2004). This gives rise to the shuttling model where a shuttle receptor binds to an E3 ligase, binding a ubiquitinated substrate as the E3 ligase adds ubiquitin and then delivers the substrate to the proteasome where the substrate is degraded. The shuttling is thought to be controlled by the interplay of overlapping, competing binding surfaces. Shuttle receptors can form intramolecular interactions between the UBL and the UBA, or the UBA can interact with ubiquitin chains while the UBL interacts with either the proteasome or an E3 ligase (Goh et al., 2008). Consistent with other proteasome ubiquitin receptors, deletion is not lethal, but is associated with accumulation of polyubiquitin (Saeki et al., 2002). Rad23 expressed in *Escherichia coli* can restore degradation of a polyubiquitinated substrate *in vitro* when proteasomes lack Rpn10 (Verma et al., 2004). The shuttle receptors bind to different sites, but bind to overlapping sites. Rad23 and Ddi1 are reported to bind to Rpn1, while Dsk2 binds Rpn13 (Gomez et al., 2011; Chen et al., 2016). Although shuttle receptors are recruited to the proteasome, they avoid degradation as they lack a sufficient unstructured tail to be engaged by the motor (Fishbain et al., 2011).

While shuttle receptors have similar domain architecture and have all been described in delivery of ubiquitinated substrates to the proteasome, mutation of individual shuttle receptors has specific effects. Indeed, their names allude to their initial discoveries not as shuttle receptors for the proteasome, but in a variety of different processes. Ddi1 is a DNA damage-induced factor required for the ubiquitination and proteasomal degradation of Ho endonuclease and its F-box adaptor Ufo1

(Voloshin et al., 2012). For these substrates Rad23 and Dsk2 cannot substitute and Ho accumulates in the cytoplasm in the absence of Ddi1. Dsk2 was originally discovered as a mediator of spindle pole body duplication, and while overexpression is lethal, deletion is not (Biggins, Ivanovska, and Rose, 1996). In humans, Dsk2-like genes have been duplicated giving rise to the ubiquilin family of UBL-UBA proteins. Mutation of ubiquilin 2 is a dominant, causative mutation seen in some cases of familial amyotrophic lateral sclerosis (Deng et al., 2011). Introduction of these mutations into cells impairs degradation by the proteasome. However, the links between Dsk2's role in spindle pole body duplication and proteasomal degradation are unclear. Similarly, Rad23 was originally characterized in its role in nucleotide excision repair, where Rad23 forms a heterodimer with the DNA-damage recognizing protein XPC (Rad4 in *S. cerevisiae*). The nucleotide excision repair pathway does use ubiquitination in later steps, but the role of Rad23 as a shuttle to the proteasome is in this process is unclear. As Rad23 is found in excess over Rad4, Rad23 certainly has other roles outside of nucleotide excision repair. Indeed the same domain responsible for Rad4 dimerization binds Png1, an N-glycanase in the delivery of ERAD (ER-associated degradation) substrates to the proteasome (Datuma, Heinen, and Hoogstraten, 2009).

In ERAD, Rad23 and Dsk2 are essential components, and this role is likely due to their shuttling capabilities. Both interact with Ufd2, a Cdc48-associated E3 ligase, and are thought to shuttle Cdc48/Ufd2 substrates to the proteasome (Kim, Mi, and Rao, 2004). The specific roles of shuttle factors is clouded by a lack of understanding of what makes each shuttle different from each other in proteasome delivery, either in their substrate specificity or in their binding sites on the proteasome. As a result of their shuttling between E3 ligases and the proteasome, overexpression and deletion phenotypes have been somewhat misleading due to the importance of dosage in their action. For example, while Rad23 can deliver substrates to the proteasome, in excess it prevents delivery by sequestering ubiquitin chains from the proteasome (Raasi and Pickart, 2003). In addition, different shuttle factors can interact with each other, and it is unclear whether coordination of multiple shuttle factors is involved in the interaction with ubiquitinated substrates, ligases and the proteasome (Kang et al., 2013). To gain a clearer understanding of how the shuttle receptors deliver substrates, an *in vitro*, mechanistic characterization of these factors is required.

Ubp6

In addition to the shuttle receptors, Ubp6, a proteasome associated DUB, is also recruited to the proteasome through its N-terminal UBL domain. Ubp6 binding, although still on Rpn1 is to a distinct location, and Ubp6 and Rad23 do not compete for binding (Elsasser et al., 2004). Binding studies with Ubp6 to Rpn1 alone suggest Ubp6 has an additional binding site other than the UBL (Rosenzweig et al., 2012). Ubp6 modulates the activity of the proteasome through both catalytic and noncatalytic mechanisms. Ubp6 stimulates ATPase activity of the base and can also stimulate core gate opening by the base (Hanna et al., 2006; Peth et al., 2009). Conversely, Ubp6 inhibits the activity of Rpn11 (Hanna et al., 2006). Ubp6 has been implicated in maintaining ubiquitin levels in the cell, leading to the model that Ubp6 acts as a timer on the proteasome, decreasing a substrates chances of being degraded by removing ubiquitin chains targeting it to the proteasome (Hanna, Leggett, and Finley, 2003). Recent work suggests that Ubp6 may efficiently remove all but the last ubiquitin chain from substrates during proteasome degradation (Lee et al., 2016). However, inhibitory effects on protein degradation are also seen with catalytically inactive Ubp6 (Hanna et al., 2006). Inhibition of Rpn11 and decreased degradation of ubiquitinated substrate does not require the catalytic cysteine of Ubp6.

In vivo, perturbation of Ubp6 can alter cellular function. Loss of Ubp6 confers an increased tolerance of aneuploidy (Torres et al., 2010). In cancer, higher expression of the human homolog of Ubp6, Usp14, is associated with worse outcomes, while knockdown of Usp14 slows cell growth (Wu et al., 2013; D'Arcy et al., 2011). Together these suggest that Ubp6's paradoxical roles in activating some aspects of proteasome activity while inhibiting others may offer an interesting allosteric regulation point in the proteasome to maintain homoeostasis. However, a mechanistic understanding of Ubp6's location and biochemical interaction with the proteasome is required to understand its role.

Open Questions

Recent structural and biochemical work on the proteasome has led to major advances in our understanding of the architecture of the proteasome and its conformational during substrate degradation, however we do not understand the allosteric network of driving these conformational changes. In addition, we do not understand how the proteasome subunits and assembly factors assemble into the final proteasome structure. This dissertation aims to address these questions by focusing on Rpn1 and its interactors. Here we have localized Ubp6 and find that it makes direct contacts with the N-ring of the base. This interaction offers an explanation for how Ubp6 affects the activity of the proteasome and a tool for further exploring the conformational changes necessary for proteasome degradation. In addition, I have also used a variety of approaches to localize the binding sites on Rpn1 for the shuttle receptor Rad23 and developed fluorescence-based approaches for understanding the delivery of substrates. Finally, I have uncovered a role for Rpn1 in ensuring proper assembly of the base and investigated this in the context of the role of assembly factors mediating base assembly and in the role of proteasome interacting proteins in recognizing properly assembled base.

Chapter 2: Ubp6 deubiquitinase senses and controls conformational dynamics and substrate degradation of the proteasome

Portions of work presented in this chapter have previously been published in:

> Bashore C, Dambacher CM, Goodall EA, Matyskiela ME, Lander GC, Martin A. Ubp6 deubiquitinase controls conformational dynamics and substrate degradation of the 26S proteasome. Nat Struct Mol Biol. 2015 Sep; 22(9):712-9.

CB, AM, and I designed and performed biochemical experiments with Ubp6. MEM designed and constructed the artificial proteasome-recruitment system. CMD and GCL performed the negative stain EM. The subsections of this chapter titled '*Defining Ubp6 Substrates*' and '*Using Ubp6 as a tool to test conformational state of proteasome mutants*' are not a part of the previously published work.

Introduction

In the eukaryotic cell, proteins are tagged for degradation with the small protein modifier ubiquitin, and recognition of ubiquitin chains, along with an unstructured segment, constitute the recognition signal by the proteasome (Thrower et al., 2000; Prakash et al., 2004). Following recognition, ubiquitin chains must be removed to be recycled to the cell, but removal of ubiquitin chains must be timed so that substrates are not deubiquitinated before they are committed to degradation. The proteasome contains two deubiquitinases (DUBs): the essential, zinc-dependent Rpn11, and Ubp6, a non-essential, cysteine protease-type DUB (Yao and Cohen, 2002; Verma et al. 2002; Leggett et al., 2002). Structural studies from our lab and others have identified large conformational changes in the proteasome in response to substrate that bring Rpn11 to a position just above the central pore, where it is positioned to act on a threaded substrate (Matyskiela et al., 2013; Unverdorben et al. 2013). Rpn11 lacks the binding sites for ubiquitin seen in other DUBs and only makes interactions with the C-terminus of ubiquitin in its active site. As a result, Rpn11 has poor affinity for its substrates and requires the threading of the proteasome motor to deliver substrates directly to its active site (Worden, Padovani, and Martin, 2013). How the other proteasome DUB, Ubp6, acts with Rpn11 and is integrated into the degradation process was unclear.

Ubp6 is activated by binding to the proteasome (Leggett et al., 2002). In addition, it has been reported to have both activating and inhibitory effects on the activity of the proteasome. Ubiquitin chains activate core gate opening, but only when Ubp6 is present (Peth, Besche, and Goldberg, 2009). Conversely, mutation of the catalytic cysteine of Ubp6 or treatment with a suicide substrate (Ub-vinyl sulfone or aldehyde) can inhibit degradation of ubiquitinated substrates, including inhibiting the activity of Rpn11 (Hanna et al., 2006). Loss of Ubp6 in yeast confers aneuploidy tolerance, and loss of proteasome binding of the human homolog, Usp14, results in an increase in proteasome degradation rates (Torres et al., 2010; Walters et al., 2014). In the hippocampus this interferes with pre-synaptic formation and can be rescued by overexpression of the catalytically inactive mutant of Usp14 (Walters et al., 2014).

Using the reconstituted proteasome system we were able to more clearly define the biochemical interactions of Ubp6 and the proteasome. Together with structural studies, we show here that Ubp6 can sense and affect the conformational state of the proteasome. Using Ubp6 activity as a sensor of conformational state of the proteasome, I have examined other mutations in the proteasome and found that Walker-B mutation in Rpt4 biases the proteasome towards a substrate-engaged state.

Results

Ubp6 responds to the proteasome.

Ubp6 has been previously reported to be activated by the proteasome (Leggett et al. 2002). To determine the requirements for this activation we used cleavage of ubiquitin-4-amino-methyl-coumarin (Ub-AMC) a model DUB substrate to study the activity of Ubp6 in the context of the proteasome. Ubp6 binds to Rpn1, a subunit of the base, but this interaction is insufficient to stimulate the activity of Ubp6 (Figure 2.1a). Incubation of Ubp6 with the base subcomplex achieves stimulation similar to proteasome in ATP, but only in the proteasome holoenzyme context is Ubp6's activity further stimulated by the incubation with ATPγS (Figure 2.1a).

Stimulation of Ubp6 activity by ATPγS is observed not just in reconstituted holoenzymes, but also in holoenzymes purified from *S. cerevisiae* (Figure 2.1b). The proteasome contains another DUB, Rpn11, but it shows much lower activity towards Ub-AMC and this activity is not stimulated by ATPγS (Figure 2.1a,b). Inhibition of ubp6Δ proteasome with *o*-phenanthroline, an inhibitor of Rpn11, abolishes Ub-AMC activity (Figure 2.1c).

The proteasome responds to Ubp6

Poly-ubiquitin-bound Ubp6 has also been observed to activate the proteasome, in both core gate opening and ATPase activity (Peth, Besche, and Goldberg, 2009; Hanna et al., 2006). However, investigating the allosteric effects of Ubp6 in the context of an actively degrading substrate proved difficult because of the dual role of ubiquitin for both targeting a substrate to the proteasome independent of Ubp6 and interacting with Ubp6 for allosteric regulation of the proteasome. To address this, we turned to a system from *E. coli* to develop ubiquitin-independent substrate delivery to the proteasome. In bacteria, $SspB_2$ recruits substrates containing the 11 amino acid ssrA tag to the ClpXP protease, a AAA+ protein degradation machine (Levchenko et al., 2000). We fused a permutant of the $SspB_2$ dimer to the N-terminus of Rpt2 (Figure 2.2a). By including the ssrA tag in our model proteasome substrate, degradation by this $SspB_2$-fused proteasome could occur in either a ubiquitin-independent manner or mediated by a poly-ubiquitin chain on a substrate (Figure 2.2b, 2.3a). The $SspB_2$-fused proteasomes behave similarly to wild type proteasome in their response to Ubp6 (Figure 2.2c). ATPase activity of $SspB_2$-fused and wild type proteasomes is similarly stimulated 1.8-fold by ubiquitin-bound Ubp6 (Figure 2.2b). Ubiquitin-bound Ubp6 is achieved either by treating Ubp6 with the suicide substrate, ubiquitin-vinyl sulfone (Ub-VS) or by incubating catalytically inactive Ubp6 with K48-linked ubiquitin dimers (Figure 2.3b). Using the ubiquitin-independent substrate recruitment system, we separately determined proteasome ATPase stimulation of the proteasome by ubiquitin-bound Ubp6 and by substrate. Substrate stimulates proteasome ATPase activity 3.3-fold, but ubiquitin-bound Ubp6 does not lead to further stimulation (Figure 2.2c, 2.3c). This suggests that Ubp6-mediated stimulation of ATPase activity is due to partial stabilization of the proteasome state during substrate degradation. Ubiquitin-bound Ubp6 shifts the conformational equilibrium of the proteasome to a lesser extent than substrate degradation, leading to a weaker stimulation of ATPase activity.

Given that proteasomes engaged on substrate or ATPγS seem to induce a similar conformational change in the AAA-type ATPases of the proteasome and that Ubp6 activity responds to ATPγS, we suspected that Ubp6 may stabilize a similar state of the proteasome when ubiquitin-bound (Figure 2.S1). Overall, these biochemical data suggest that Ubp6's activity is responsive to the conformational state of the proteasome. Furthermore, ubiquitin-bound Ubp6 biases the proteasome towards a substrate-engaged state.

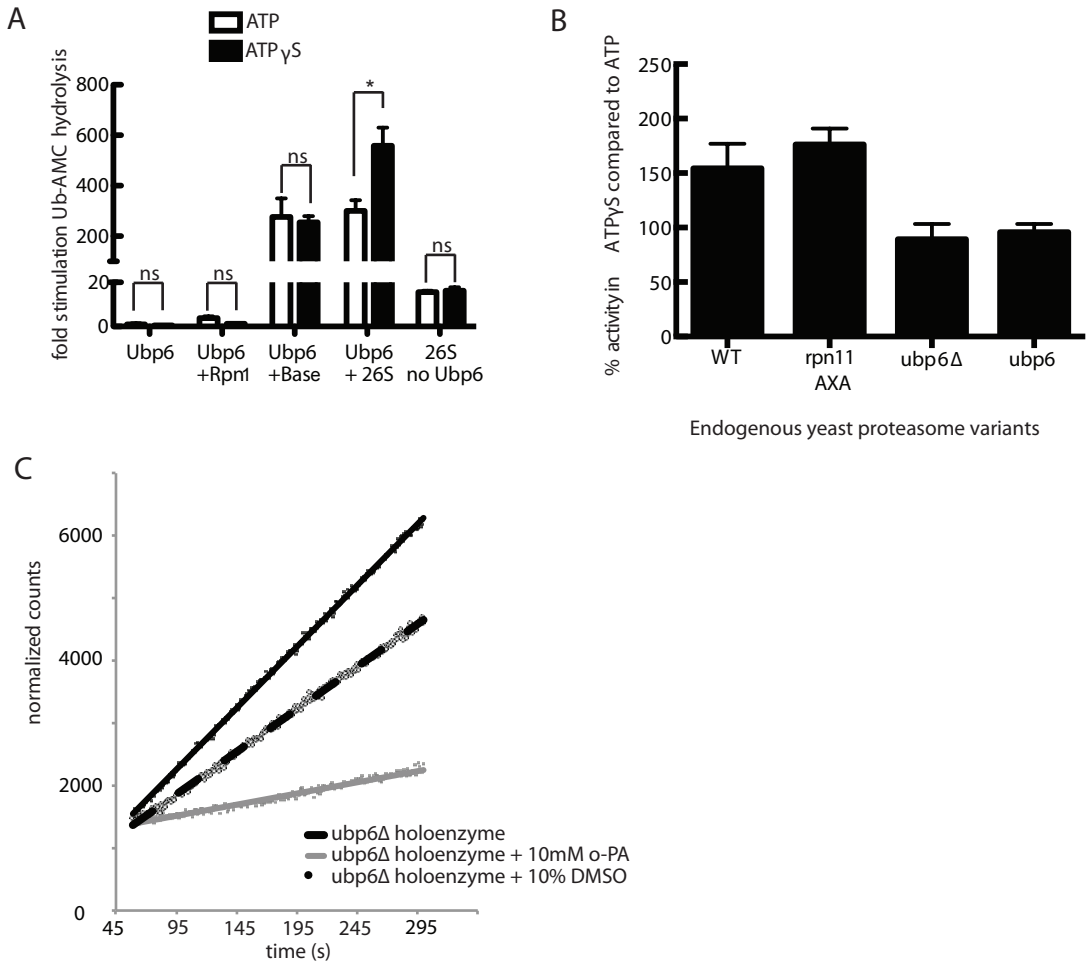

Figure 2.1: Ubp6 deubiquitination activity responds to the conformational state of the proteasome. Ub-AMC cleavage activity of Ubp6 was measured in response to interactions with the proteasomes holoenzyme or isolated subcomplexes. (a) Deubiquitination assays using proteasomes reconstituted with heterologously expressed base subcomplex purified from *E. coli* as well as core and lid subcomplexes purified from yeast, in the presence of ATP or the non-hydrolysable ATPγS that induces the engaged state of the proteasome. (b) Deubiquitination assays using proteasomes purified from yeast strains with wild type, deleted, or inactive (C118A) Ubp6 and an inactive Rpn11 (AXA). Shown are the relative activities in the presence of ATPγS compared to ATP. Data in (a) and (b) are means and s.e.m. of three independent experiments. (c) Ubp6-free holoenzymes were preincubated with buffer, 10% DMSO, or ortho-phenanthroline (o-PA) for 10 minutes before Ub-AMC measurements. Averages of three technical replicates are plotted with corresponding linear regression.

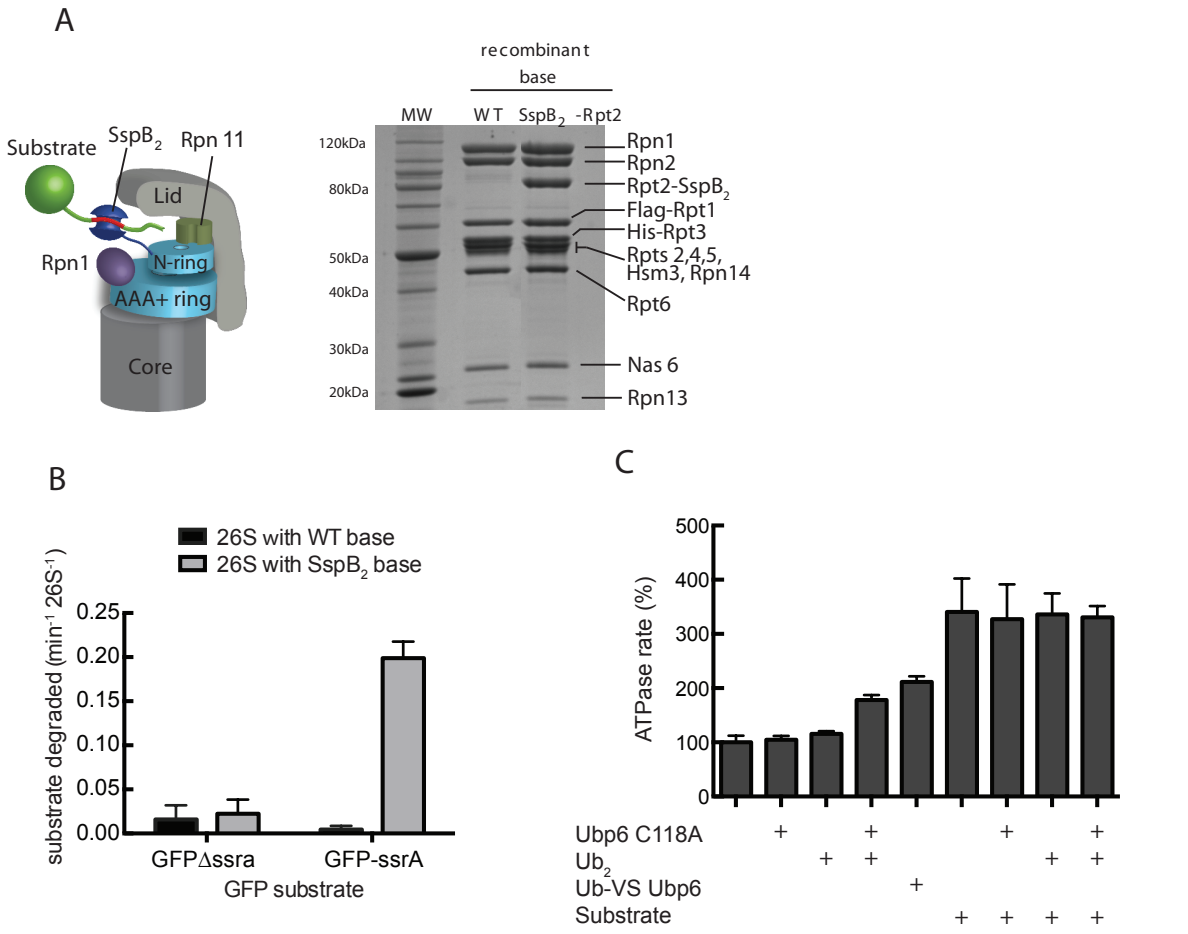

Figure 2.2: Ubiquitin-independent substrate delivery system. To separate ubiquitin processing from substrate engagement and translocation, we designed an ubiquitin-independent recruitment system by fusing a linked permutant of the bacterial dimeric substrate adapter $SspB_2$to Rpt2 of the base. (a) Schematic of a $SspB_2$-fused proteasome recruiting an ssrA tagged substrate and SDS-PAGE of *E. coli*-expressed base subcomplex with either wild-type or $SspB_2$-fused Rpt2. (b) Degradation of a GFP model substrate containing the ssrA recognition motif was measured using proteasomes reconstituted with either wild-type or $SspB_2$-fused base complexes. (c) Ubiquitin-bound Ubp6 (Ubp6 C118A with di-ubiquitin or ubiquitin-vinyl sulfone-fused Ubp6, Ubp6-UbVS) and substrate translocation stimulate the ATPase rate of $SspB_2$-fused proteasomes.

Ubp6 makes direct contacts with the base ATPase

Previous attempts to clearly localize Ubp6 on the proteasome have been unsuccessful. Ubp6 interacts with the proteasome subunit Rpn1 through the 9 kDa UBL domain (Leggett et al., 2002). The small UBL is separated from the larger catalytic USP domain by a 23 amino acid linker, which likely allows the USP domain mobility while remaining tethered to Rpn1 (Wyndham et al., 1999; Rosenzweig et al., 2012). Rpn1 within the proteasome is also highly flexible and is consistently one of the lowest resolution subunits of the proteasome (Unverdorben et al., 2013). Together, these factors have hampered Ubp6 visualization in a proteasome context.

The realization that ubiquitin-bound Ubp6 may have a similar effect on the proteasome as substrate led us to perform negative stain EM on proteasome in the presence of Ubp6 treated with Ub-VS.

Together with the knowledge that Ubp6's activity requires the base and not just Rpn1, suggested to us that we might be able to stabilize proteasome interaction with the USP domain of Ubp6 by forcing Ubp6 to be permanently ubiquitin-bound. Proteasome incubated with Ub-VS-treated Ubp6 exhibited hybrid states as compared with non-ubiquitin bound Ubp6 (Figure 2.S2, S3). While this was suggestive of affecting the conformational state, we could not confidently localize Ubp6 without adding ATPγS in addition to Ub-VS (Figure 2.4, 2.S4). This sample showed a complete absence of the apo state, with all particles adopting a substrate-bound conformation of the proteasome and allowed for 3D reconstruction.

Surprisingly, extra, defined density was seen in contact with the base ATPases, making direct contacts with Rpt1. Using the crystal structure of the human homolog of Ubp6, USP14, bound to ubiquitin we were able to generate a homology model and dock this into the extra density of our 3D reconstruction (Figure 2.4). This density is the appropriate shape and size for the USP domain of Ubp6. Interestingly, 3D reconstruction of proteasomes from tomograms of rat neurons had previously seen density in the same location only in substrate-engaged proteasomes, but this density had not previously been assigned to a specific protein (Asano et al., 2015).

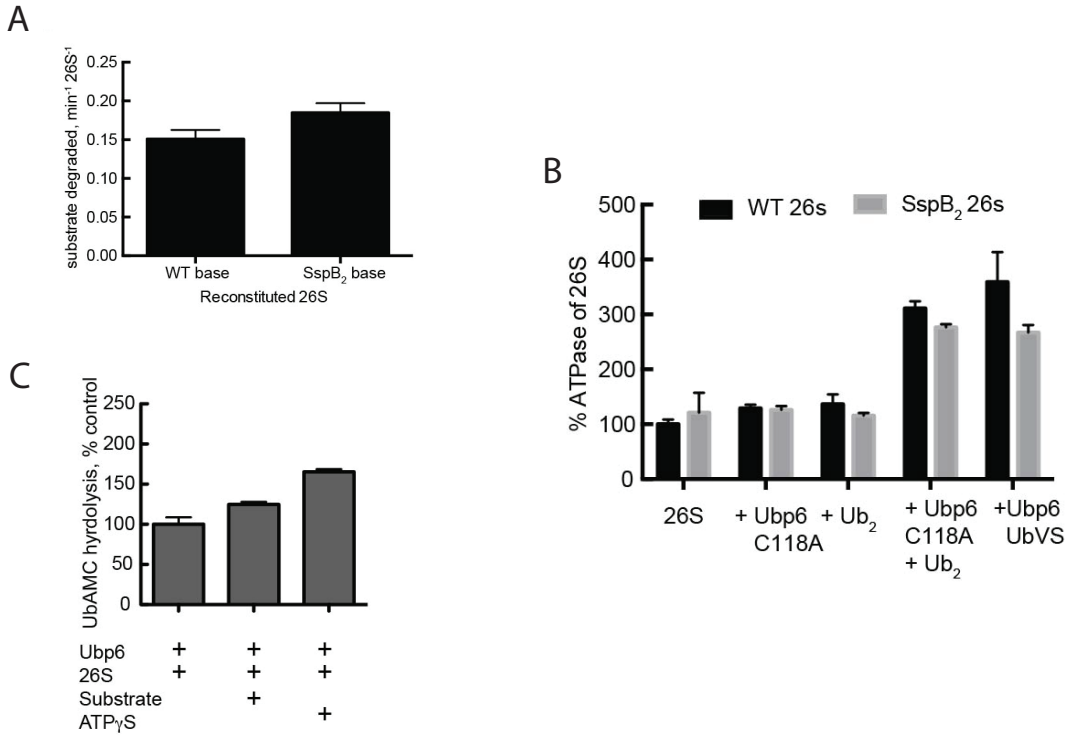

Figure 2.3: Ubiquitin-bound Ubp6 induces a substrate bound state (a) Proteasomes reconstituted with $SspB_2$-Rpt2 base are competent to degrade ubiquitinated substrate. 200 nM WT or $SspB_2$-Rpt2 base was assembled into proteasomes with 600nM Lid, Rpn10, and CP. Degradation of 2μM ubiquitinated EGFP substrate was measured by loss of fluorescence at 511nm. (b) Ubp6 similarly stimulates ATPase rate of proteasomes reconstituted with WT base or $SspB_2$-Rpt2 base. Proteasomes were reconstituted with 200nM WT or $SspB_2$-Rpt2 base and 600nM Lid, Rpn10, and CP. 900nM Ubp6 or 20μM di-ubiquitin was added to show similar stimulations of ATPase rate with the wild-type or $SspB_2$-Rpt2 base. Di-ubiquitin with Ubp6 stimulated proteasomes similarly to UbVS-Ubp6. Error bars represent SEM of at least three independent experiments. (c) Substrate translocation by the proteasome stimulates Ubp6 deubiquitination. Wild-type Ubp6 activity was measured with proteasomes reconstituted with $SspB_2$-Rpt2 base. Addition of saturating amounts of an unfolded substrate increases Ubp6 deubiquitination, although not as much as the addition of ATPγS.

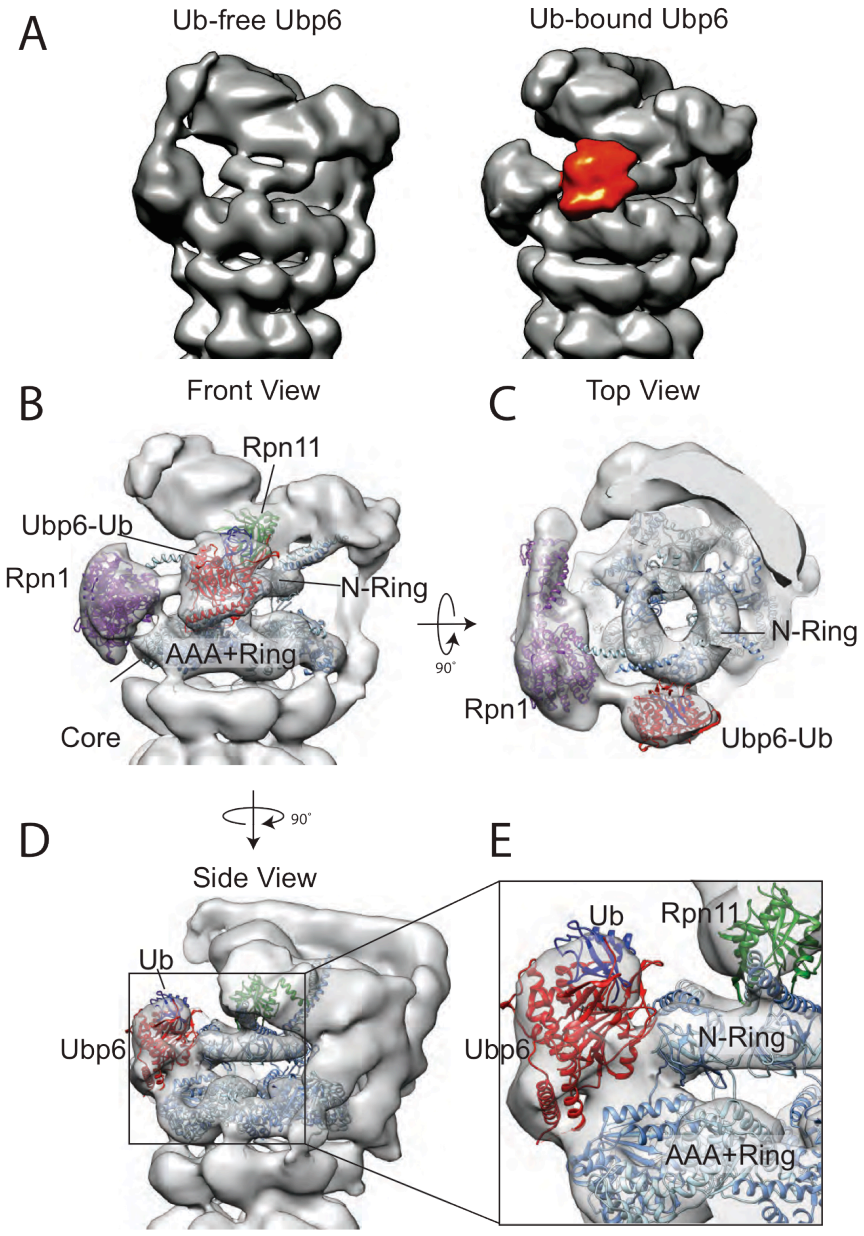

Figure 2.4: Ubiquitin-bound Ubp6 interacts with the Rpt hexamer of the base.
(a) 3D reconstructions of the proteasome holoenzyme in complex with ATPγS and ubiquitin-free (left) or permanently ubiquitin-bound Ubp6 shown in red (right). (b–e) PDB models of various RP subunits were docked into the 3D electron density map obtained from negatively stained samples. Rpn1 is shown in purple (PDB 4CR4 Chain Z), Rpn11 in green (PDB 4O8X), and the ATPase ring in blue (PDB 4CR4, Chains H-M). The Ubp6-Ub homology model was docked into the corresponding density of the 22.3-Å resolution map (Ubp6 is shown in red, ubiquitin in blue). PDB models for all Rpt proteins of the base are alternately colored in two different shades of blue. (b) Front view of the RP. Connecting density is observed between Rpn1 and the catalytic domain of Ubp6, which contacts the Rpt ring directly in front of Rpn11. (c) Top view of the RP. Ubp6 makes specific contacts with the N-terminal domain of Rpt1. (d) Side view of the RP. Ubp6 bridges the N-ring and the AAA+ ring in their coaxially stacked, engaged conformation. The N-domain residues of Rpt1 appear to interact with surface loops of Ubp6, while the AAA+ domain of Rpt1 contacts two C-terminal helices of Ubp6. This architecture places Ubp6 in close proximity to Rpn11 (~20 Å), with its bound ubiquitin only ~30 Å from the Rpn11 active site. (e) Zoomed-in view of (d), highlighting the Ubp6-base

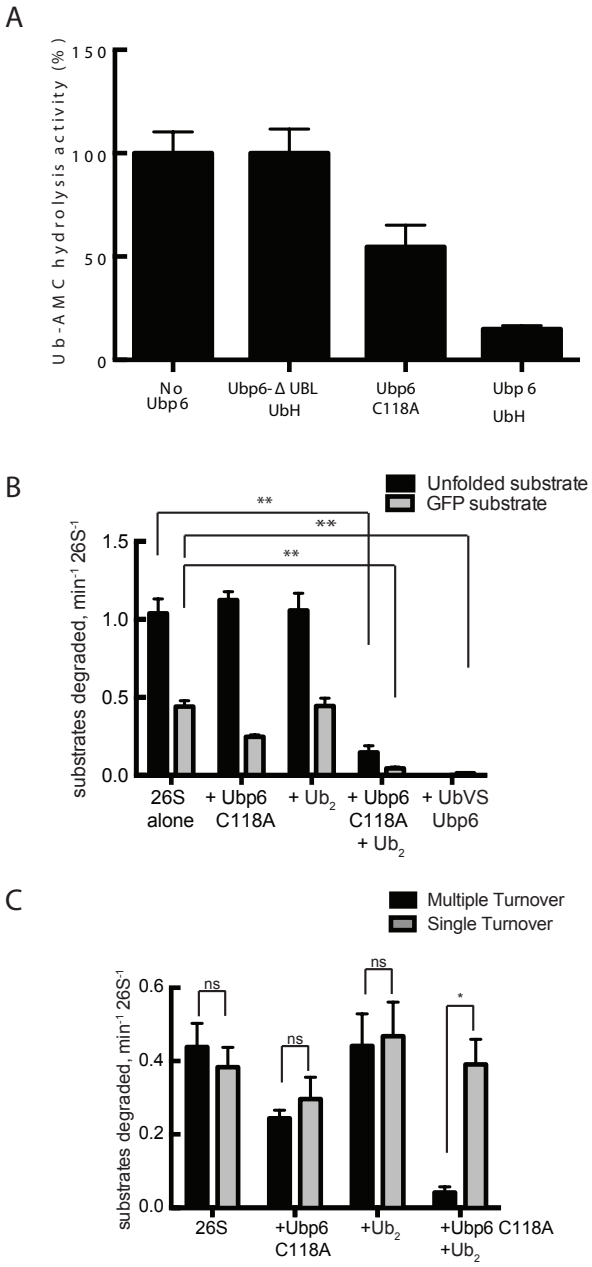

Figure 2.5: Ubp6 affects ubiquitin-independent degradation (a) Ubiquitin binding to Ubp6 strongly inhibits Rpn11 deubiquitination activity. Ubp6 (wild type or C118A) was treated with ubiquitin aldehyde (Ub-H) and added to Ubp6-free holoenzymes purified from yeast. Rpn11 deubiquitination activity was measured by Ub-AMC cleavage. Data are means and s.e.m. of 3 independent experiments. Ubiquitin-independent substrate delivery to the proteasome reveals that ubiquitin-bound Ubp6 allosterically inhibits multiple- but not single-turnover degradation. (b) Multiple-turnover degradation of a permanently unfolded model substrate and a GFP fusion substrate by reconstituted $SspB_2$-Rpt2 proteasomes in the absence or presence of Ubp6 C118A and di-ubiquitin (Ub_2). Data shown are means and s.e.m of three technical replicates. (c) Rate constants for degradation of the GFP fusion substrate under multiple- and single-turnover conditions.

The localization of Ubp6 not only confirms that Ubp6 affects the conformational state of the proteasome similar to substrate, but also explains the crosstalk between the ATPase activity of the proteasome and the Ub-AMC cleavage of Ubp6. Binding of the USP domain to the N-ring moves the BL loops covering the active site of Ubp6 and allowing ubiquitin access to the active site. Simultaneously, binding of the USP domain to the N-ring stabilizes the base ATPase in a substrate-engaged conformation, and this conformational stabilization interferes with Rpn11 activity (Figure 2.5a).

Ubp6 inhibits degradation of proteasome substrates

Using the $SspB_2$-mediated delivery of proteasome substrates we could now test how Ubp6's effect on proteasome conformation affects the degradation of substrates in the absence of ubiquitin. Catalytically inactive Ubp6, (Ubp6-C118A), does not change the degradation rate of either a permanently unfolded or a folded, GFP-containing substrate (Figure 2.5b). In contrast, Ubp6-

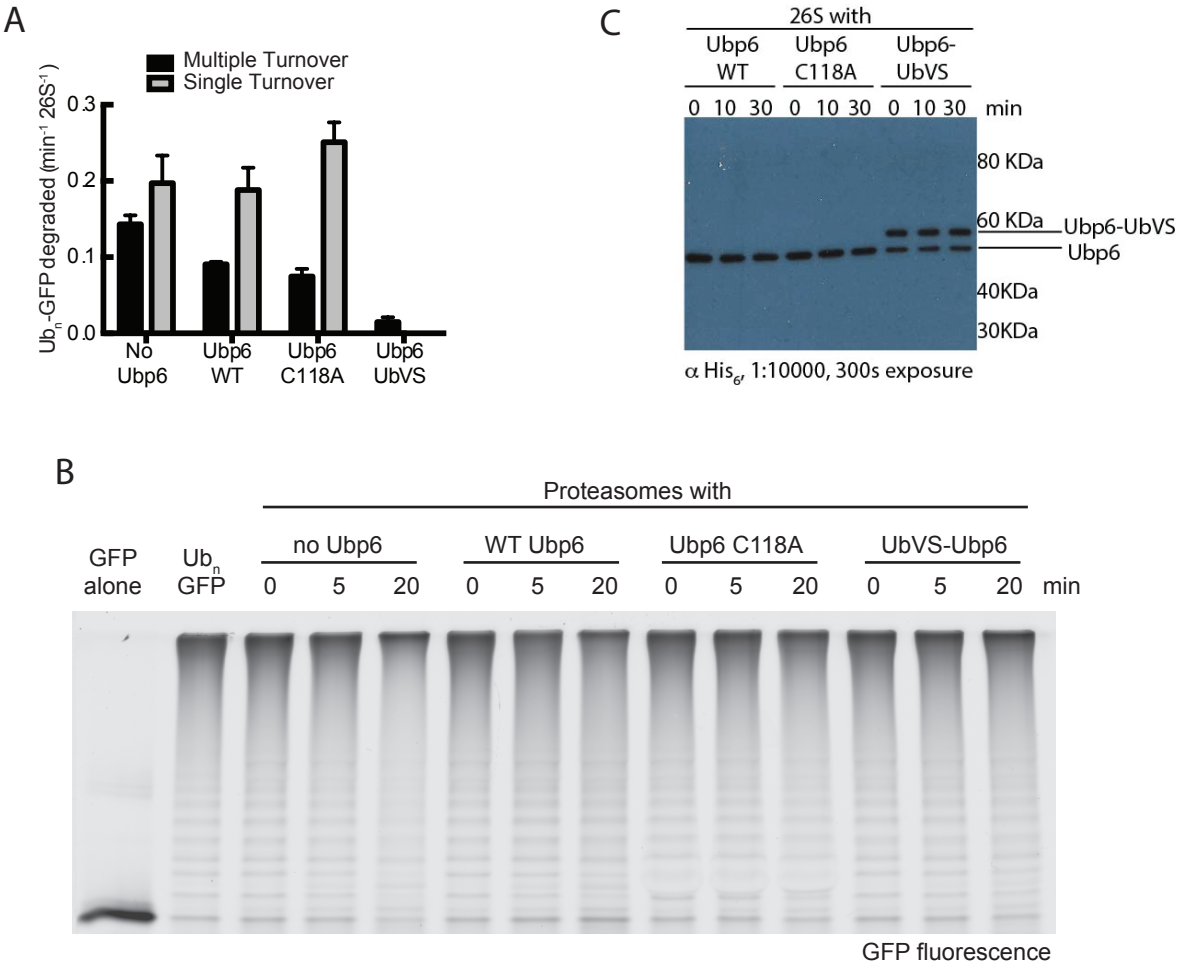

Figure 2.6: Ubp6 affects ubiquitin-dependent degradation. (a) Degradation of the polyubiquitinated GFP fusion substrate were measured with proteasome holoenzyme purified from an Ubp6-knockout yeast strain, with no Ubp6, His_6-Ubp6, His_6-Ubp6 C118A, or His_6-Ubp6-UbVS added back. Rate constants for single- and multiple-turnover degradation of the ubiquitinated GFP model substrate. Data shown are means and s.e.m. from three technical replicates. (b) SDS-PAGE of GFP fluorescence from representative multiple turnover reactions. (c) His_6-Ubp6 was visualized by western blot detecting His6 over the course of a multiple turnover reaction.

C118A does inhibit degradation when di-ubiquitin is added for both folded and unstructured substrates, which explains the non-catalytic inhibition of Ubp6-C118A reported previously for the degradation of ubiquitinated substrates (Hanna et al., 2006) (Figure 2.5b,c). The previously reported non-catalytic effects of Ubp6 on the proteasome have been contradictory, because Ubp6 is only inhibitory when ubiquitin-bound. By using a ubiquitin-independent substrate delivery system, we found that Ubp6-C118A inhibits degradation when ubiquitin-bound, but had no effect in other assays, such as ATPase activity where no ubiquitin chains were added.

Ubiquitin-bound Ubp6 stimulates the ATPase activity of the proteasome, but slows degradation. Ubiquitin-bound Ubp6, similar to ATPγS, acts by enforcing an engaged state on the proteasome and preventing conformational switching back to the pre-engaged state. To test this we reexamined degradation of the GFP substrate in a single turnover scenario, with an excess of enzyme over substrate. Under these conditions, using the $SspB_2$-mediated delivery to proteasomes, ubiquitin-bound Ubp6 did not inhibit degradation of the substrate, despite strongly inhibiting degradation in multiple turnover conditions (Figure 2.5c). However, using conventional recruitment through a ubiquitinated substrate, ubiquitin-bound Ubp6 abolishes degradation even in single turnover (Figure 2.6a,b). Ubiquitin-dependent degradation requires Rpn11 activity, which is inhibited by ubiquitin-bound Ubp6. Alternatively, Ubp6 might compete for substrate degradation by becoming a substrate itself, but Ubp6 levels remains constant over the course of degradations (Figure 2.6.c). These findings are consistent with a model where Ubp6 stabilizes the proteasome in an engaged state, and does not allow for the proteasome to switch back to the apo state until Ubp6 is no longer ubiquitin bound. This allows Ubp6 to act as both a sensor and a timer of the ubiquitin state of the proteasome depending on the context. Ubp6's DUB activity senses the conformational state of the proteasome and is activated by the engaged state. When a substrate is not actively being degraded, but ubiquitin chains remain on Ubp6, Ubp6 prevents the proteasome from returning to an apo state until these chains have been cleared. This allows Ubp6 to act as a ubiquitin-based timer on the proteasome and only allow degradation of the next substrate once the ubiquitin chains that may remain bound to ubiquitin receptors are cleared from the proteasome.

Defining Ubp6 substrates

To gain a better understanding of how Ubp6 may act as a timer for substrate degradation we sought to better define its substrates and to understand when in the cycle of degradation it acts on these substrates. All of our previous studies of Ubp6 relied on use of the non-physiological Ub-AMC. But, native substrates would likely involve chains of ubiquitin on a substrate where differences in the placement, length and linkage type linkage type of the ubiquitin could come into play.

We found that Ubp6, similar to Rpn11, preferentially cleaves not in between ubiquitin moieties in chains, but at the base of the chain removing the chain from the substrate *en bloc*. This has also been observed by the Finley lab, where they also observed that Ubp6 removes all but the last ubiquitin chain from proteasome substrates (Lee et al., 2016). In addition, these findings agree with the previous characterization of Ubp6 and Rpn11 of having similar activities on free chains. Both are more active on K63-linked chains than K48-linked chains, probably due to their more compact nature (Mansour et al., 2015). However, when presented with a substrate with long K63-linked chains, both Ubp6 and Rpn11 preferentially cleave at the base of the chain (Figure 2.7a). This can be observed by following deubiquitination at the proteasome. To measure deubiquitination, the core peptidases are catalytically inactivated by treatment with epoxomycin. Upon translocation and unfolding of a substrate, deubiquitination of the substrate still occurs, but the substrate is not

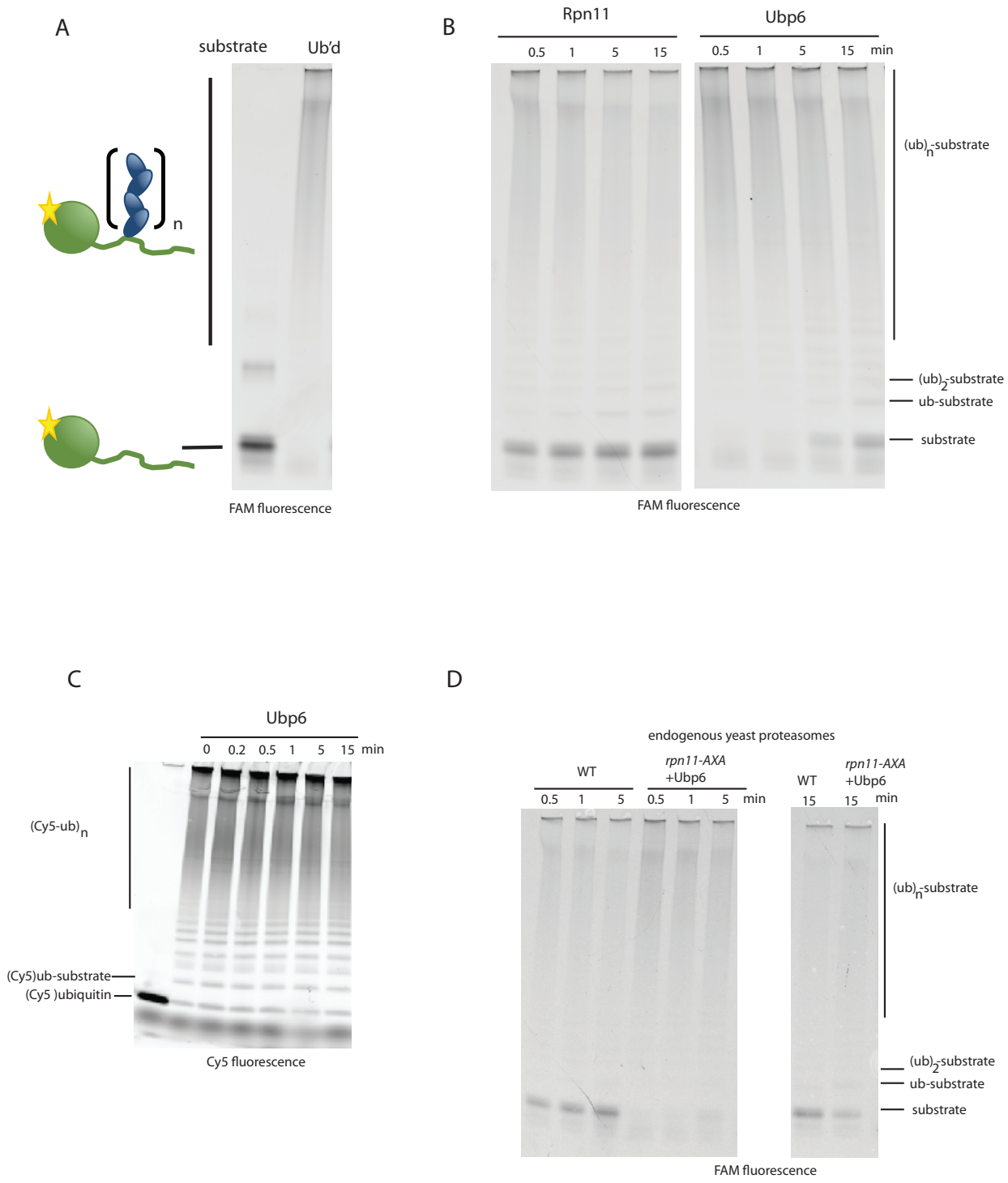

Figure 2.7: Ubp6 cleaves substrates at the base of the ubiquitin chain. (a) Schematic of gel-based deubiquitination assay: SDS-PAGE fluorescein labeled titin-cyclin substrate before and after ubiquitination. (b) Deubiquitination by reconstituted proteasomes containing either Rpn11 and no Ubp6 (Rpn11) or catalytically inactivated Rpn11 and Ubp6 (Ubp6) with an excess of proteasome over ubiquitinated substrate. Core was inactivated with epoxomicin before reconstitution to prevent cleavage of substrate into peptides. (c) Reaction performed under the same conditions as in (b) but using Cy5-labeled ubiquitin. Reaction performed as in (b) using endogenously purified yeast proteasomes. AXA proteasomes have additional Ubp6 added back. WT sample in (d) contains endogenous Ubp6.

clipped into peptides by the core particle. Using SDS-PAGE of a fluorescently-labeled substrate, the activity of Ubp6 and Rpn11 on a substrate can be directly assessed. Using this approach we observe the appearance of a fully deubiquitinated species without any preceding appearance of other substrates for either Rpn11 or Ubp6. However, Ubp6 is much slower than Rpn11 (Figure 2.7b). Using the same experimental setup we can instead label ubiquitin itself. If cleavage were occurring between ubiquitin moieties monoubiquitin would be produced over time. Instead we see little change in the ubiquitin ladder patterning over time, confirming that Rpn11 and Ubp6 cleave ubiquitin chains *en bloc* from substrates (Figure 2.7c). This DUB specificity for both Rpn11 and Ubp6 is seen not just with reconstituted holoenzyme, but also with yeast-purified holoenzymes (Figure 2.7d). Because the in-gel degradation assay relies on the inhibition of core for readout, it is unclear if the *en bloc* cleavage performed by Rpn11 and by Ubp6 are equivalent in terms of the location of the substrate on the proteasome. Ubp6 may act on non-engaged substrates, while Rpn11 acts on engaged ones in a co-translocational manner. The finding that Ubp6 cleaves at the base of the chain is perhaps less surprising now that the location of Ubp6 is known: when bound to the N-ring, Rpt1 and Rpt2 sterically block Ubp6 from efficiently cleaving in between ubiquitin chains. Because the activity of Ubp6 on these substrates is very slow, it is also possible that the current substrates are not ideally suited for Ubp6, for instance the in the number and placement of ubiquitin chains.

Using Ubp6 as a tool to test the conformational state of proteasome mutants

Ubp6's effect on ATPase activity and Ubp6's own Ub-AMC activity can be used as tools to readout the conformational state of proteasome mutants. Mutations in the AAA domain of Rpt subunits have differential defects in ATPase rate, core binding, and degradation rate (Beckwith et al., 2013). While degradation defects were correlated with location of subunits in the staircase of the apo proteasome, without structural data, the mechanism for why these mutations caused defects related to the apo staircase specifically was not clear.

Placing an E-to-Q mutation in the conserved Walker-B motif of the AAA+ ATPase site prevents ATP hydrolysis and traps that subunit into a nucleotide-bound state (Hersch et al, 2005). When previously characterized, the Walker-B mutations in the base were striking for their strong, but asymmetric effects on degradation. Mutations placed in Rpt3 or Rpt4 completely abolished degradation of proteasome substrates, while mutation in Rpt2 had little effect (Beckwith et al., 2013). These phenotypes correlate with the spiral staircase of the ATPase pore loops observed in the proteasome in the apo state. However, the ability of ATPγS to induce the substrate-engaged conformation suggests coupled with the asymmetric outcomes of mutation. The strongest defect in degradation is seen in those subunits in the highest position in the apo spiral staircase. Walker-B mutation of Rpt1 exhibited less than one third of the degradation activity of wild-type holoenzymes, and this mutation seems to sensitize the proteasome to ubiquitin-bound Ubp6 (Table 2.1). More strikingly, Ubp6's Ub-AMC cleavage is also hyperstimulated by this Rpt1 mutated proteasome. In ATPγS, Ubp6's Ub-AMC activity increases 3.5-fold rather than 1.5-fold seen in wild type holoenzymes (Figure 2.8b). Because Ubp6 makes direct contacts with Rpt1, this suggests that the ATP state of Rpt1 is insufficient to activate Ubp6, but that Ubp6 responds to a Walker-B Rpt1 in ATPγS more strongly than a wild type holoenzyme. This suggests that Walker-B substitution changes the response to ATPγS of neighboring other subunits, but because it is not know to which subunits ATPγS binding is required for inducing the conformational change, a model cannot yet be built to precisely explain these results (Figure 2.8a,b).

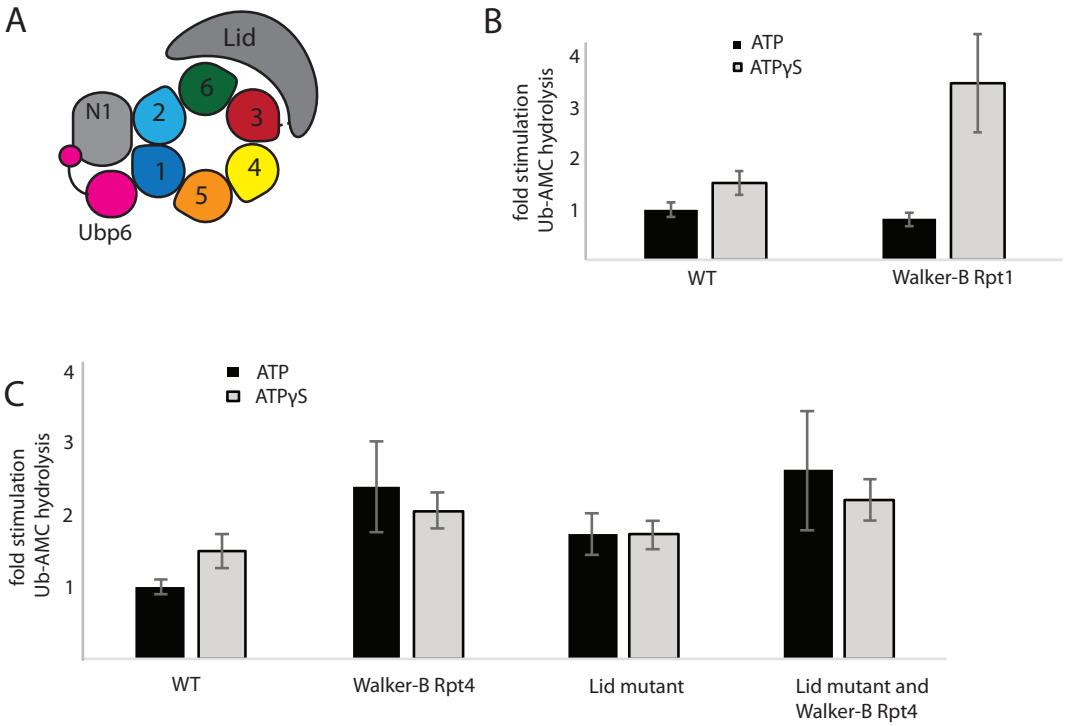

Figure 2.8: Ubp6 activity is a sensor for perturbations of the conformational state of the proteasome in ATPase-mutant proteasomes. (a) Schematic of the base ATPase from a top down view with each Rpt shown in a different color. Ubp6 (Pink) makes direct contact with Rpt1 (dark blue). A key contact between the lid and between the lid and Rpt3 is shown as a dotted line. Ubp6 activity as measured by Ub-AMC cleavage in wild type and Rpt1 Walker-B reconstituted holoenzymes (b) and in Rpt4 Walker-B, and Lid mutant reconstituted holoenzymes (c).

In contrast, a Walker-B mutation in Rpt4 completely abolishes the ATPase response to ubiquitin-bound Ubp6 (Table 2.1). Ubp6 makes no direct contacts with any part of Rpt4, but is more strikingly affected by ubiquitin-bound Ubp6. Ub-AMC activity of Ubp6 suggests that Walker-B Rpt4 proteasomes are insensitive to Ubp6 because they are in an engaged state even in the absence of ubiquitin-bound Ubp6 or ATP**γ**S (Figure 2.8c). Ubp6 activity behaves similarly when mutations disrupting a contact between base subunit Rpt3 and the lid are placed in the lid subunit Rpn5. But, when the Rpn5 lid mutation and Walker-B Rpt4 mutation are combined, there is no additive effect on ATPγS-dependent Ub-AMC activity. When this mutation is combined with a Walker-B Rpt4 mutation these mutations are not additive suggesting that they act on the proteasome similarly (Figure 2.8c).

Seeing a hyperstimulation of Ubp6 activity is also informative for translating the increasing number of conformational states of the proteasome into biochemical activity. Using only wild-type holoenzymes, we had previously thought that maximal Ub-AMC cleavage activity by Ubp6 was seen only with substrate present. Now, given the dynamic nature of the Ubp6 contact with the base, the increase in activity above wild type for mutants such as Walker-B Rpt1 or Walker-B Rpt4 could actually represent a more stable contact than is seen even in ATPγS, more similar to substrate. This parallels recent structures describing a more fully active conformation of the proteasome only seen when the holoenzyme is trapped with ADP-BeF_x rather than ATPγS (Wehmer et al., 2017). Notably,

Walker-B mutation	Holoenzyme ATPase activity (min^{-1} enz^{-1})	s.d.	ATPase activity with Ub-Ubp6 (min^{-1} enz^{-1})	s.d.	Fold change with addition of Ub-Ubp6
Wild type	51.10	5.6	111.66	10.6	2.2
Rpt1	42.06	5.6	107.55	23.2	2.6
Rpt2	119.32	12.0	197.43	24.8	1.7
Rpt3	51.26	4.7	86.57	19.3	1.7
Rpt4	84.97	8.2	92.78	20.9	1.1
Rpt5	69.02	10.1	110.54	0.9	1.6

Table 2.1: Summary of ATPase activity of holoenzymes reconstituted with Walker-B mutated bases

in the state trapped by ADP-BeF_X, Rpn1 is rotated closer to the N-ring than in the ATPγS or substrate bound state, which may allow for more stable association of Ubp6 with the N-ring.

Discussion

Our biochemical and structural data show that Ubp6 acts as a conformational sensor at the proteasome. Ubp6's activity is regulated by the proteasome, and in turn affects the conformational state of the proteasome. Balancing these two together, Ubp6 may act as a timer by specifically interfering with the conformational switching of the proteasome during degradation. Ubp6 sits opposite Rpn11 and makes contacts with the N-ring of the proteasome. This localization of Ubp6 was also observed by the Baumeister group by treating proteasomes with ubiquitin aldehyde, a similar suicide substrate as Ub-VS (Aufderheide et al., 2015). Ubp6 sits near the central the central pore through which proteasome substrates are threaded, but in contrast to Rpn11, its active site is not optimally positioned for acting on threaded substrates within the N-ring. The placement of Ubp6 also explains its preference for cleaving at the base of the ubiquitin chains because the N-ring and coiled coils sterically clash with cleavage between ubiquitin chains, similar to Rpn11 (Worden, Padovani, and Martin, 2014; Lee et al., 2016). However, the slow rates of cleavage of poly-ubiquitinated substrates relative to Rpn11 suggest we do not yet understand the ideal conditions for Ubp6 cleavage either in proteasome conformational state or in the precise geometry of ubiquitin chains on a substrate. In addition, these findings highlight context dependence of Ubp6's DUB activity. While Ubp6 shows much greater activity than Rpn11 on a non-translocation dependent substrate such as Ub-AMC, their relative activities on real proteasome substrates are the opposite. Examining substrates with ubiquitin chains of defined length or linkage-type may provide a clearer picture of Ubp6's preferred substrates in the future.

Ubp6's slower action and less ideal placement relative to the central pore explains its inability to substitute for Rpn11 *in vivo*, but Ubp6's true substrates in the cell remain to be identified (Guterman and Glickman 2004). In addition, while addition of Ubp6 decreases overall substrate degradation of model substrates, it is unclear if this is advantageous in degradation of some specific endogenous substrates or if the delaying of proteasome switching between substrates serves another role such as in quality control of the proteasome itself. Auto-ubiquitination of the proteasome occurs upon inhibition of the proteasome as a signal for autophagy of proteasomes (Marshall, McLoughlin, and Vierstra, 2016; Besche et al., 2014). It will be interesting to see how Ubp6's role as a conformational

sensor and as a DUB fit into this quality control pathway for proteasomes. Identifying the locations and biochemical interactions of other known proteasome interacting proteins such as the ligase Hul5, and the identification of other new and conditional proteasome interactors will hopefully address this in the future.

Methods:

Yeast strains

Yeast lid and holoenzyme were purified from strain YYS40 (genotype *MAT*a *ade2-1 his3-11,15 leu2-3,112 trp1-1 ura3-1 can1 Rpn11::Rpn11*-3× Flag(Saeki, Isono, and Toh-E., 2005). Core particle was prepared from either strain RJD1144 (genotype *MAT*a *his3Δ200 leu2-3,112 lys2-801 trpΔ63 ura3-52 PRE1*-Flag-His_6::*Ylpac211(URA3)*(Verma et al., 2000) or strain yAM14 (genotype *MAT*a *ade2-1 his3-11,15 leu2-3,112 trp1-1 ura3-1 can1-100 bar1 PRE1::PRE1*-3× Flag*(KanMX*),(Beckwith et al., 2013). To generate *UBP6* deletion strains, the KANMX6 sequence was integrated at the respective genomic locus, replacing the gene in YYS40 (Lander et al., 2012). To generate the *ubp6-c118a* strain, a C118A copy of UBP6 was cloned into pRS305 and was integrated into the *ubp6* deletion strain at the *leu2* locus.

Purification of yeast holoenzyme and subcomplexes

Wild-type and mutant proteasome was purified from *S. cerevisiae* essentially as described (Lander et al., 2012; Matyskiela et al., 2013). In summary, holoenzyme, lid, and core particle were purified from yeast strains listed above. Lysed cells were resuspended in lysis buffer containing 60 mM HEPES, pH 7.6, 50 mM NaCl, 50 mM KCl, 5 mM $MgCl_2$, 0.5 mM EDTA, 10% glycerol, and 0.2% NP-40. Holoenzyme lysis also included an ATP-regeneration mix (5 mM ATP, 0.03 mg/ml creatine kinase and 16 mM creatine phosphate). Complexes were bound to anti-Flag M2 affinity resin (Sigma) and washed with wash buffer (60 mM HEPES, pH 7.6, 50 mM NaCl, 50 mM KCl, 5 mM $MgCl_2$, 0.5 mM EDTA, 10% glycerol, 0.1% NP-40 and 500 mM ATP). Core particle was washed with wash buffer containing 500mM NaCl, and Lid was washed with wash buffer containing 1M NaCl. Complexes were eluted with Flag peptide and separation by size-exclusion chromatography over Superose-6 in gel-filtration (GF) buffer (60 mM HEPES, pH 7.6, 50 mM NaCl, 50 mM KCl, 5 mM $MgCl_2$, 0.5 mM EDTA and 0.5 mM ATP) containing 5% glycerol.

Recombinant expression and purification of proteins and complexes

Base subcomplexes were expressed and purified from *E. coli* as previously described (Beckwith et al., 2013). Nine integral subunits (Rpn1, Rpn2, Rpn13, Rpts-1-6,) and four RACs (Rpn14, Hsm3, Nas2 and Nas6) were expressed with rare tRNAs overnight at 18˚C after induction with 0.5mM IPTG for 5 hours at 30˚C. Cells were harvested by centrifugation and resuspended in buffer (60mM HEPES, pH 7.6, 100mM NaCl, 100mM KCl, 10% glycerol, 10mM $MgCl_2$, 0.5mM EDTA, and 20mM imidazole) supplemented with 2 mg ml^{-1} lysozyme, protease inhibitors, (aprotinin, pepstatin, leupeptin and PMSF) and benzonase (Novagen). Cells were lysed by sonication, and clarified by centrifugation. A two-step affinity purification of the base subcomplex was performed using nickel–nitrilotriacetic acid (Ni-NTA) agarose (Thermo) to select for His_6-Rpt3 and **α**-Flag M2 resin (Sigma-Aldrich) selecting for Flag-Rpt1. 0.5 mM ATP was present in all purification buffers. The Ni-NTA and anti-Flag M2 columns were eluted with nickel buffer containing 250mM imidazole and 0.15 mg ml^{-1} 3× Flag peptide, respectively. The Flag column eluate was concentrated and run on a Superose 6 10/300 size exclusion column (GE Healthcare) equilibrated with gel filtration buffer (60mM HEPES, pH 7.6, 50mM NaCl, 50mM KCl, 5% glycerol, 5mM $MgCl_2$,1mM DTT and 0.5mM ATP).

The GFP fusion substrate construct was cloned into a pET Duet (Novagen) vector, and consisted of a lysinesless superfolder GFP (Chu et al., 2013), lysineless, titin I27 V15P domain, and a random coil containing the ssrA sequence and the PPXY motif. The fluorescently labeled substrate for gel-based deubiquitination is the same as the previous substrate with the GFP replaced with an N-terminal cysteine. *E. coli* Bl21-star (DE3) cells were transformed with the construct and grown in Terrific Broth (EMD Millipore) at 30 °C. Cells were induced with 0.5mM IPTG at an OD_{600} of 1-1.5 and expression went for 5 hours at 30 °C.

The unfolded substrate was cloned into a pET 28A (Novagen) vector and consisted of a lysineless, disulfide-less N1 domain from gene-3-protein (Kather, Bippes, and Schmid, 2005) fused to a random coil containing an ssrA tag, ppxy motif, and a lysineless strepII tag. WT Ubp6 was amplified from genomic (W303) DNA, and cloned into pET Duet with an N-terminal His_6 tag. C118A and UBL**Δ** mutations were made by around-the-horn PCR. *E. coli* Bl21-star (DE3) cells were transformed with either the N1 construct or the Ubp6 constructs and grown in Terrific Broth at 37 °C. Cells were induced with 0.5mM IPTG at an OD_{600} of 0.6 and expression continued overnight at 18 °C.

GFP, titin substrate, unfolded substrate, or Ubp6 expressing cells were harvested by centrifugation and resuspended in nickel buffer (above) supplemented with 2mg ml^{-1} lysozyme, benzonase (Novagen), and protease inhibitors (aprotinin, pepstatin, leupeptin and PMSF). Cells were lysed by freeze thaw and sonication. Lyates were clarified by centrifugation at 15,000 rpm for 20 minutes at 4 C. Proteins were purified using Ni-NTA affinity chromatography followed by size exclusion chromatography on a Superdex 200 (GE Healthcare) using nickel and gel filtration buffers mentioned above.

Construction of the $SspB_2$ permutant base

To allow ubiquitin-independent substrate delivery to the proteasome, we created a base variant that is fused to a linked permutant dimer of the E.coli substrate adaptor SspB. A wild-type SspB monomer consists of a globular domain and a C-terminal tail of 38 residues. In simple dimer fusions, where we connected the C-terminus of the globular domain of one SspB monomer with the N-terminus of the second SspB monomer, the linker interfered with ssrA substrate binding to $SspB_2$. We therefore constructed a circular permutant SspB monomer, in which we created a new N-terminus at residue L26 and connected the preceding N-terminal helix to the C-terminus of the globular domain, and fused this monomer to the N-terminus of a second, wild-type SspB monomer. The connectivity of this covalently fused dimer is: (L26-D111) - GGASG - (S4-Q25) - GGGTGG - (wild-type monomer). This $SspB_2$ dimer was then fused to the N-terminus of Rpt2 of the base.

Ubiquitin purification and dimer synthesis

Ubiquitin was expressed and purified as previously described (Worden, et al., 2013; Pickart and Raasi, 2005). Briefly, Rosetta II (DE3) pLysS *E. coli* cells were transformed with a pET28a vector containing the ubiquitin gene from *S. cerevisiae* under control of a T7 promoter. Cells were grown in Terrific Broth supplemented with 1% glycerol at 37°C until OD_{600} = 1.5–2.0 and were induced with 0.5 mM IPTG overnight at 18 °C. The lysis buffer contained 50 mM Tris-HCl, pH 7.6, 0.02% NP-40, 2 mg mL^{-1} lysozyme, benzonase (Novagen), and protease inhibitors (aprotinin, pepstatin, leupeptin and PMSF). Cells were lysed by sonication and 20 min incubation at room temperature. Lysate was clarified by centrifugation at 15000 rpm. Clarified lysate was precipitated by adding 60%perchloric acid to a final concentration of 0.5%, and the solution was stirred on ice for a total of

20 min. A 5-mL HiTrap SP FF column (GE Life Sciences) was used for cation-exchange chromatography, and ubiquitin fractions were pooled and exchanged into Ub storage buffer (20 mM Tris-HCl, pH 7.6, and 150 mM NaCl) by repeated dilution and concentration. Lys-48 ubiquitin dimers were synthesized and purified as previously described (Dong et al, 2011).

Preparation of Ubiquitin fused Ubp6

50μM WT Ubp6 protein was reacted with 75uM ubiquitin vinyl sulfone or Ubiquitin Aldehyde (R&D Systems) in GF at 37°C. For the experiments in Figure 5D, which required complete inhibition of the active site cysteine, buffer, Ubp6 was reacted with ubiquitin aldehyde (R&D systems) for 16 hours at 37°C in the dark. This was further reacted with 500μM NEM for 30 min at 30°C, followed by quenching with 5mM DTT for another 30 min at 30 C. Ubiquitin-aldehyde, NEM, and DTT were removed by dilution and concentration in an Amicon 30K MWCO concentrator (EMD Milipore).

Ubiquitin AMC hydrolysis assays

Ubiquitin-AMC (R&D systems) hydrolysis was measured in a QuantaMaster spectrofluorimeter (PTI) by monitoring an increase of fluorescence emission at 435 nm with an excitation at 380nm. Reactions using reconstituted proteasome used 100nM Ubp6, 150nM Rpn1, 150nM recombinant base, 300nM CP, 300nM Lid, 300nM Rpn10, 20μM unfolded substrate, and 3-10uM Ub-AMC. Reactions using proteasomes purified from yeast used 100nM proteasome. Reactions were carried out either in the presence GF buffer (see above) with 1mM DTT and 1x ATP regeneration system or 1mM ATPγS. Samples were incubated at 30°C for 5-10 minutes prior to the addition of substrate to ensure Ubp6 association and nucleotide exchange.

Reactions with mutant bases were performed in a Synergy Neo2 plate reader with otherwise similar conditions. For Km curves 2.5nM Ubp6 was incubated with 400nM base or holoenzyme. 2uM Ubp6 was used for Ubp6 alone.

ATPase assays

ATPase activity was quantified by an NADH-coupled ATPase assay. Reconstituted proteasomes, (200nM base, 600nM core, 600nM lid, 600nM Rpn10) Ubp6, (200nM) Ub_2^{K48} (20uM), and unfolded gene-3-protein substrate (20uM) were incubated with 1× ATPase mix (3 U ml^{-1} pyruvate kinase, 3 U ml^{-1} lactate dehydrogenase, 1 mM NADH and 7.5 mM phosphoenol pyruvate) at 30°C. Reactions were done in GF buffer (see above) with 1mM DTT. Absorbance at 340nm was monitored at 30°C for 600 s at 1-s intervals by a UV-vis spectrophotometer (Agilent) or in Synergy Neo5 plate reader with 3-s intervals.

Multiple and Single turnover ubiquitin independent degradation assays

26S proteasomes were reconstituted using recombinant, heterologously-expressed $SspB_2$-Rpt2 base, recombinant Rpn10, and lid and core subcomplexes purified from yeast. Multiple turnover degradations were done with 200nM CP, 600nM Lid, 600 nM base, 600nM Rpn10, 900nM Ubp6 and 20uM Ub_2^{K48}. Reactions were done in the presence of 1x ATP regeneration system (5 mM ATP, 0.03 mg ml^{-1} creatine kinase, 16 mM creatine phosphate) in gel filtration buffer with 1mM DTT. Single turnover reactions were done with 3uM $SspB_2$-Rpt2 base, 4.5uM lid, 4.5uM base, 4.5uM Rpn10, 9uM Ubp6, 20uM Ub_2^{K48}, and 300nM substrate in the presence of 1x ATP regeneration system in gel filtration buffer with DTT and ATP regeneration system. GFP single- and multiple-turnover degradation activities were monitored by the loss of GFP fluorescence

(excitation, 467 nm; emission, 511 nm) using a QuantaMaster spectrofluorometer (PTI) Single turnover curves were fit to a single exponential in GraphPad Prism 6.

To track degradation of an unfolded substrate, purified N1 fusion substrates were labeled on a single cysteine with Alexa 647 maleimide at pH 7.2 for 3 hours at room temperature in the dark, before quenching unreacted dye with DTT. Free dye was removed on a Superdex 200. Substrate degradation was measured by taking time-points of a reaction at 30°C and assessed by SDS-PAGE followed by imaging on a Typhoon Trio (GE) with a 633 laser and 670BP emission filter. Band intensity was quantified using Image Quant software. Degradation reactions consisted of 8uM substrate against proteasomes reconstituted as above with either $SspB_2$-Rpt2 base or WT base to correct for any non-specific, $SspB_2$ independent substrate cleavage.

Deubiquitination in gel
For in gel DUB assays on Rpn11 and Ubp6 holoenzymes were reconstituted with 1.5uM base, lid (either wild type or *rpn11-axa)* rpn10, and 750uM core. Ubp6 was added only to Ubp6 activity samples. These proteasome were treated with epoxomycin for 30min at 30°C for 45min with ATP regeneration before the addition of 200nM ubiquitinated substrate. As above substrate was labeled and readout by typhoon scan but with fluoroscein-5-maleimide.

Preparation of Ubiquitinated substrates
GFP substrates (20uM) were modified with polyubiquitin chains by 5uM yeast Uba1, 5uM yeast Ubc1, 5uM Rsp5, 1x ATP Regeneration system, and 300uM ubiquitin. Reaction was carried out in a thermocycler for 2 hours at 25°C, then overnight at 4°C. titin -only substrates were modified with polyubiquitin chains as above but with 10uM substrate and with Cy3-labeled ubiquitin when ubiquitin was observed in gel-based assays.

Multiple and Single turnover ubiquitin dependent degradation assays
GFP constructs were ubiquitinated overnight and then used the next day without freezing. Single- and multiple-turnover degradation activities were monitored by the loss of GFP fluorescence (excitation, 467 nm; emission, 511 nm) using a QuantaMaster spectrofluorimeter (PTI) as above. Multiple turnover reactions consisted of 300nM purified proteasomes from a ubp6Δ strain, 600nM Ubp6, and 2μM substrate. Single-turnover reactions consisted of 3μM proteasome, 6μM Ubp6, and 300nM substrate.

Electron microscopy
Samples of 26S-bound Ubp6-UbVS were diluted to ~25 nM in 60 mM HEPES pH 7.6, 50 mM NaCl, 50 mM KCl, 5 mM $MgCl_2$, 0.5 mM EDTA, 1 mM TCEP and either 1 mM ATP or 1 mM ATP**γ**S (Sigma). A thin layer of carbon was applied to 400-mesh Cu-Rh maxtaform grids (Electron Microscopy Sciences) by chemical vapor deposition, and grids were subsequently exposed to a 95% Ar/5% O2 plasma for 20 seconds to glow-discharge/activate the carbon surface. Grids were pre-treated with 4 μl of 0.1% poly-L-lysine hydrobromide (Polysciences) to prevent preferred orientation of 26S particles on carbon. Poly-L-lysine solution was then wicked away, grids were washed with 4 μl of H_2O, and 4 μl of sample was applied. 252 and 357 images of negatively stained (2% uranyl formate) 26S-Ubp6-UbVS complexes in the presence of ATP or ATPγS, respectively, were collected at a nominal magnification of 52,000 X on an F416 CMOS 4K X 4K camera (TVIPS) with a pixel size of 2.05 Å/pixel at the sample level. Images were acquired on a Tecnai Spirit LaB_6 electron microscope operating at 120keV, with a random defocus range of -0.5 μm to -1.5 μm and an

electron dose of 20e-/Å^2. Data were acquired using the Leginon automated image acquisition software(Carragher et al., 2000).

Processing

All image preprocessing and 2D analysis was performed using the Appion image-processing pipeline(Lander et al., 2009). CTF was estimated using CTFFIND3, and only micrographs having a CTF confidence greater than 80% were used for processing. Particle picking was performed using the template-based FindEM software (Roseman, 2004). Micrographs were phase-flipped using EMAN's "applyctf" function, and particles were extracted with a box size of 384 pixels. Pixel values 4.5 sigma above or below the mean were replaced with the mean intensity of the extracted particle using XMIPP. Multiple rounds of iterative MSA/MRA was used for 2D classification and alignment of the particles, and class averages containing singly-capped proteasomes, as well as damaged, aggregated, or false particles, were removed, resulting in a dataset containing 24,411 and 18,565 double-capped proteasome particles in presence of 1mM ATP and 1mM ATPγS, respectively. 3D classification and 3D refinement were performed with C2 symmetry imposed using RELION v1.31(Scheres 2012). The 3D reconstructions for proteasomes in the presence of ATP and ATPγS resolved to 24.2 Å and 22.3 Å, respectively, according to a gold standard Fourier Shell Correlation at 0.143. Low resolution intensities were dampened using a SPIDER script in order to more clearly visualize domain features.

3D modeling

An atomic model of yeast Ub-bound Ubp6 was constructed by superimposing the yeast Ubp6 crystal structure (PDB 1VJV) onto the structure of the human Usp14 structure bound to Ubiquitin (PDB 2AYO), using UCSF Chimera's "MatchMaker" tool. These structures have high structural homology, and the resulting hybrid structure did not exhibit any clashes between the Ubiquitin and Ubp6. This Ubp6-Ub model was docked into the density putatively corresponding to Ubp6. PDB 4CR4 was used for docking other 26S core, base and lid subunits into the ATP**γ**S electron density map obtained here, with the exception of the Rpn8-Rpn11 dimer, for which PDB 4O8Y was used. All docking of PDB structures was performed using the "Fit in Map" tool of UCSF Chimera, and this software was also used to generate all figures displaying the EM density (Goddard, Huang, and Ferrin 2007).

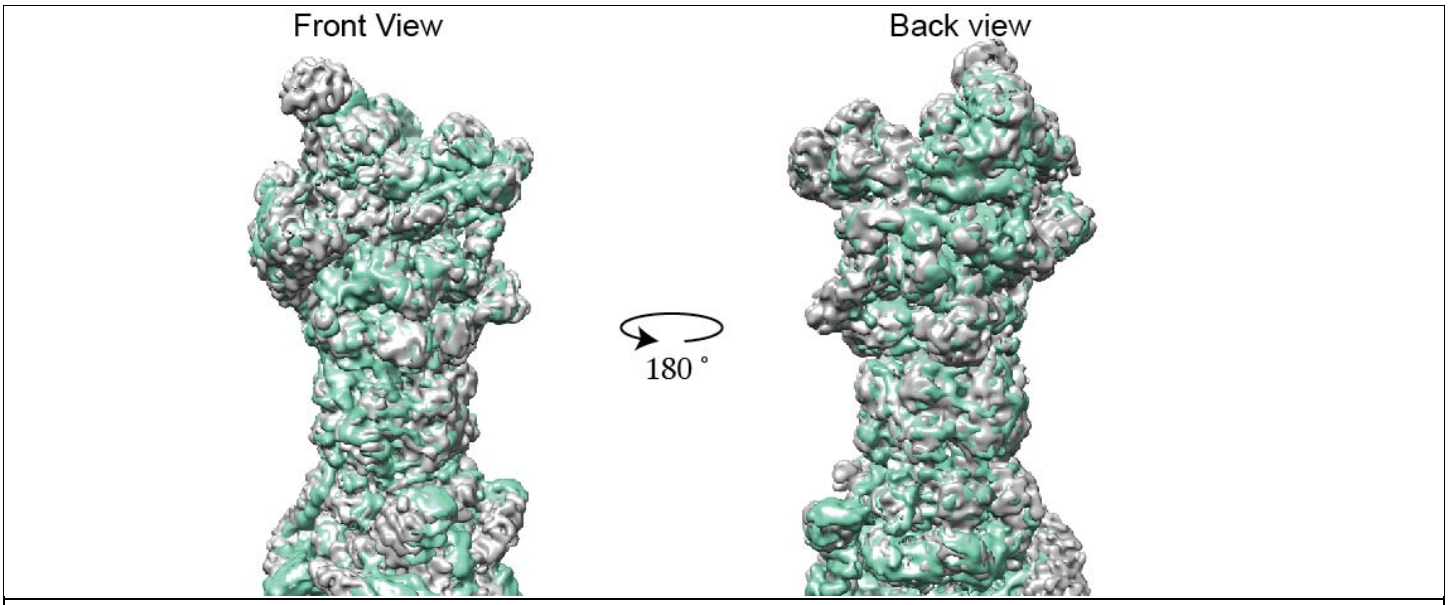

Supplementary Figure 2. 1

ATPγS-bound holoenzymes resemble a substrate-translocating proteasome conformation.

EM reconstruction of the ATPγS-bound proteasome agrees with EM reconstruction of substrate-bound, translocating proteasome. Font and back views of reconstructions of ATPγS-bound proteasome (EMDB 2596, gray) and substrate-bound proteasome (EMDB 5669, cyan) that were aligned in UCSF Chimera using the “fit in map tool”.

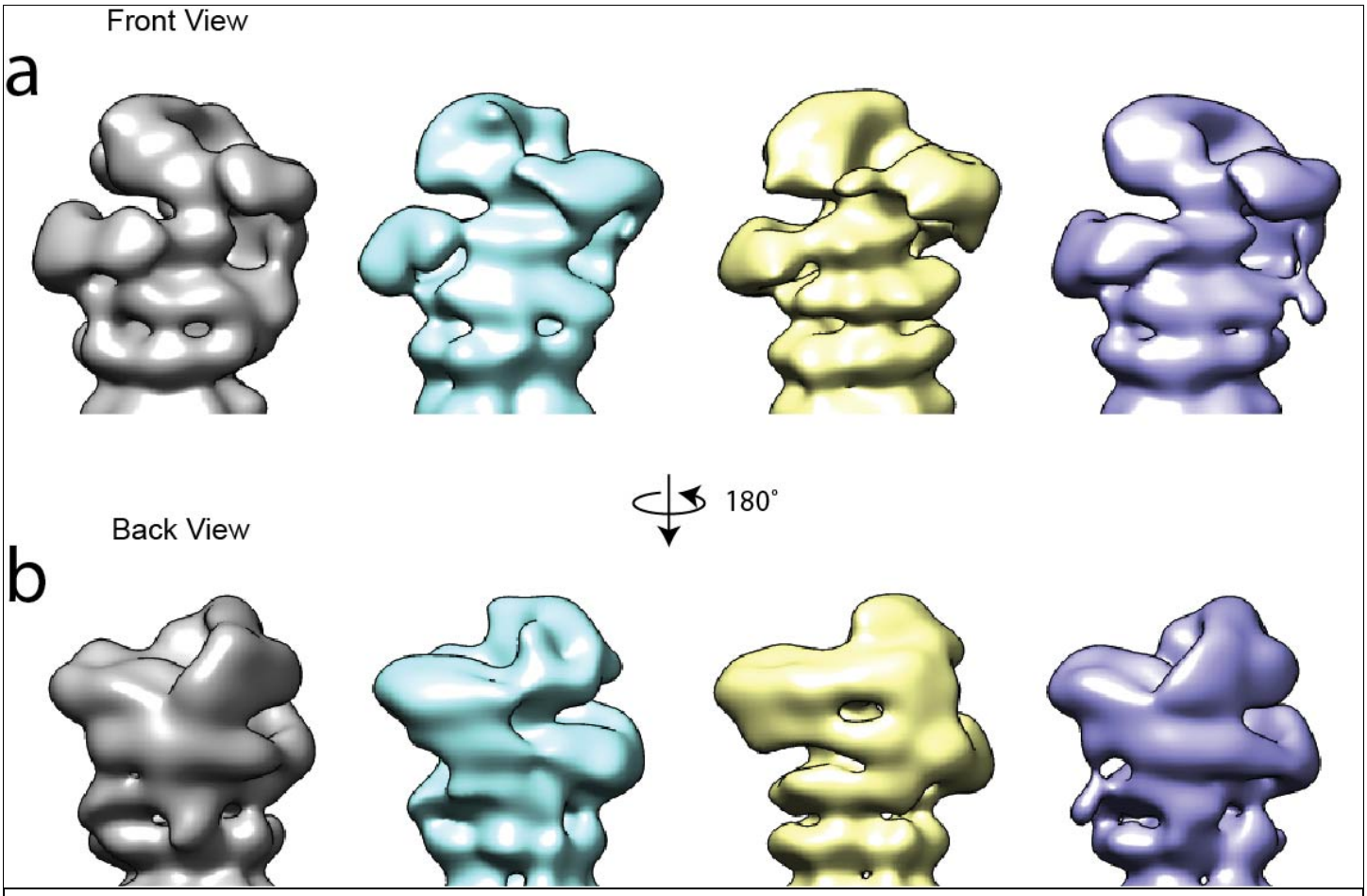

Supplementary Figure 2. 2

3D classes in ATP bound, Ub-Ubp6 proteasomes.

(a) Front and (b) back views of different proteasome conformations seen by negative stain EM.

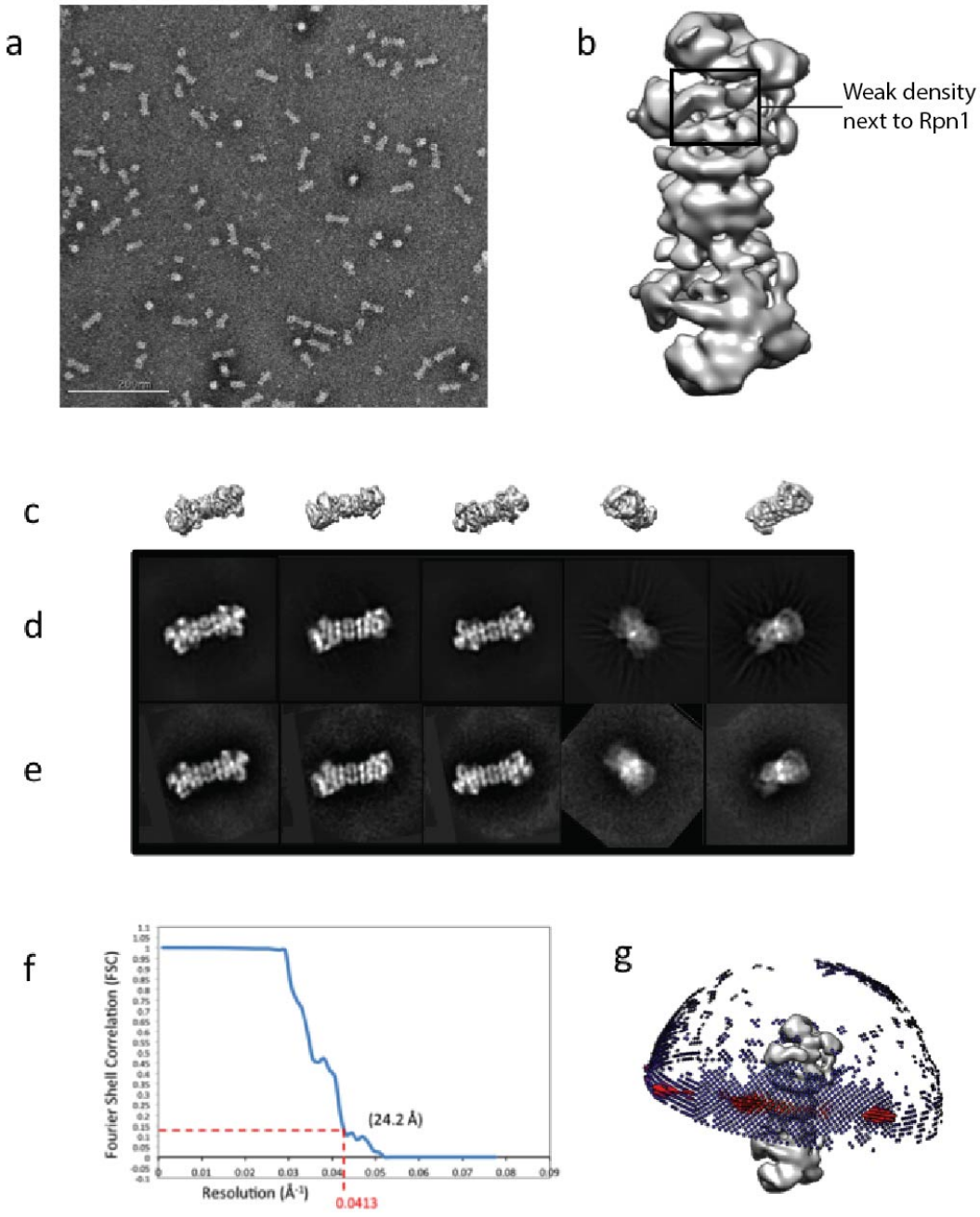

Supplementary Figure 2. 3

Ubp6-UbVS proteasome structure in ATP.

(a) Raw micrograph of the grids. (b) Sharpened reconstruction shows holoenzymes in an apo state. (c) Differential projections of the 3D model to match the 2D projections shown. (d) 2D projections calculated from the 3D model. (e) Reference-free 2D classes from actual data set. (f) FSC curve. (g) Angular distribution plot (Euler plot).

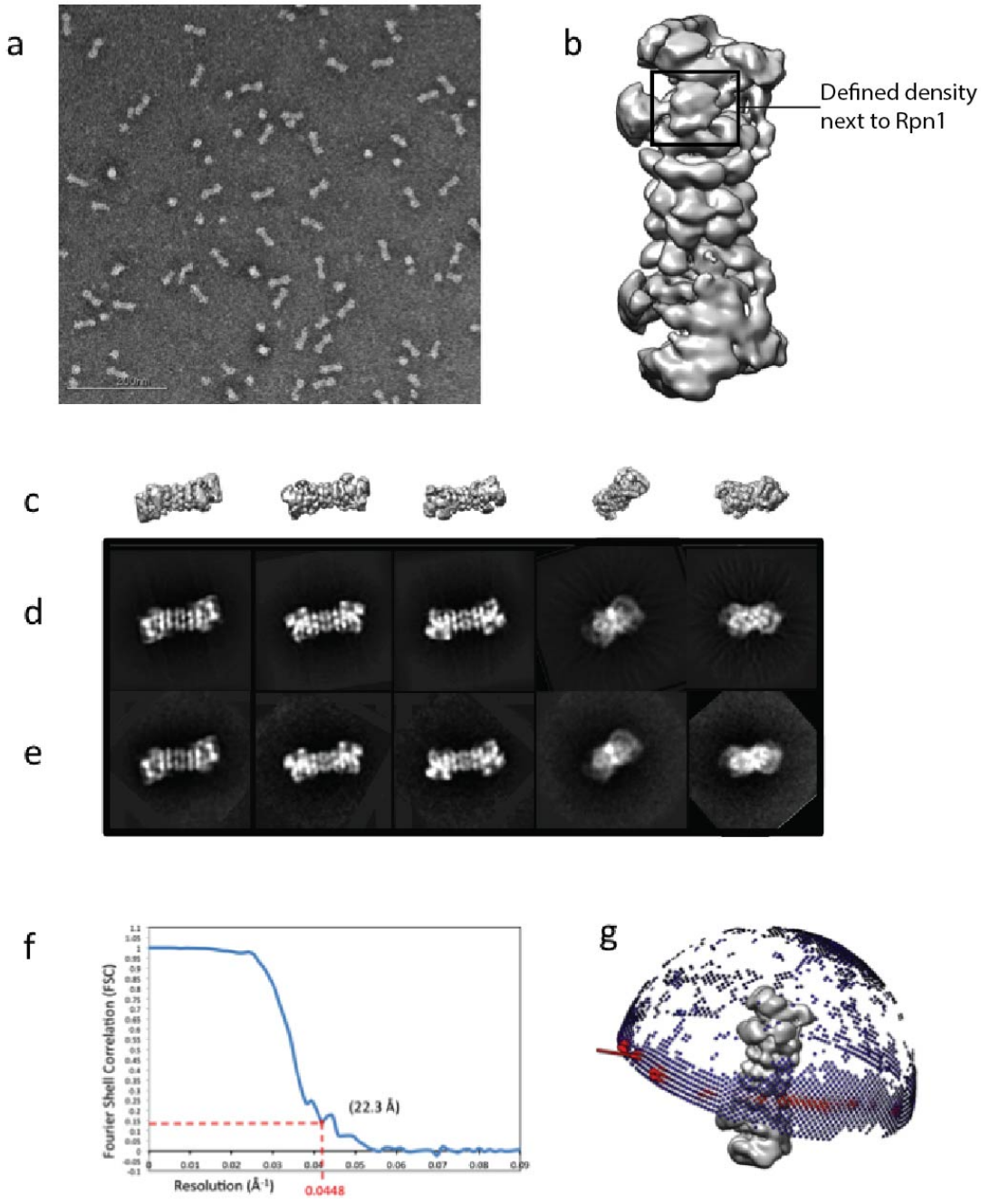

Supplementary Figure 2. 4

Ubp6-UbVS proteasome structure in ATPγS.

(a) Raw micrograph of the grids. (b) Sharpened reconstruction shows holoenzymes in an engaged state. (c) Differential projections of the 3D model to match the 2D projections shown. (d) 2D projections calculated from the 3D model. (e) Reference-free 2D classes from actual data set. (f) FSC curve. (g) Angular distribution plot (Euler plot).

Chapter 3: Shuttle factor-mediated degradation

Introduction

As the major ATP dependent protease in the eukaryotic cell, the proteasome must recognize a wide variety of substrates. The proteasome recognizes ubiquitin chains as one part of the degradation signal, but also requires an unstructured segment to be engaged by the ATPase motor (Prakash et al., 2004). One way that the proteasome accommodates differences in substrate geometry, relative placements of ubiquitin chains, and unstructured regions on substrates is the presence of multiple different ubiquitin receptors on the proteasome. The proteasome contains three intrinsic ubiquitin receptors: Rpn10, Rpn13, and the T1 site of Rpn1, which are placed in distinct locations (Shi et al., 2016; Husnjak et al., 2008; Elsasser et al., 2004). In addition to the stably bound ubiquitin receptors, yeast contain three 'shuttle factors,' Rad23, Dsk2, and Ddi1, that recognize and deliver ubiquitinated substrates to the proteasome, but do not remain stably bound (Chen and Madura, 2002; Wilkinson et al., 2001; Funakoshi et al., 2002).

These shuttle receptors are united in their domain architecture. Each contains an N-terminal UBL domain and at least one C-terminal UBA linked through flexible linkers. Through the UBL domain, shuttle receptors interact with E3 ligases or the proteasome, while the UBA domain binds polyubiquitin (Elsasser et al., 2004; Chen and Madura, 2002; Kim, Mi, and Rao, 2004). Together these interactions give rise to the shuttling model where interactions of the UBA and UBL intramolecularly compete with binding to the proteasome or E3 ligases. The competition of the UBA for UBL binding is relieved by binding to ubiquitin chains and couples production and removal of ubiquitin from a substrate to the shuttle receptor's interactions (Goh et al., 2008).

Substrates can be artificially recruited to the proteasome by N-terminally fusing either the UBL of Rad23 or linear tetra-ubiquitin to the substrate (Inobe et al., 2011). The requirements of unstructured tail length with these two recruitment methods are not identical despite the recruitment signal being located on the same site on the substrate (Inobe et al., 2011). In the cell this can be further complicated by attachment of ubiquitin chains at different lysines on the substrate. In the degradation of native substrates as well, it appears that some substrates are preferentially recruited to the proteasome through some receptors, but the mechanisms driving these preferences are unclear. Shuttle receptors and Rpn10 bind ubiquitin and the proteasome via different domains, but these proteasome-binding and ubiquitin-binding domains are both connected by unstructured linkers (Walters et al., 2003; Riedinger et al., 2010). This domain architecture likely allows more flexibility in the continued recognition of substrates during transition from initial binding to pulling the substrate into the unfoldase of the base. The precise locations of the ubiquitin binding domains are unknown because of this flexibility, but the locations of the proteasome binding domains of Rpn10 and Rad23 are in different places. Therefore substrates bound through the ubiquitin binding domains sample similar but not identical spaces on the proteasome. As a result, this diversity in ubiquitin receptors at the proteasome may allow the proteasome to accept a wider variety of ubiquitin chain lengths and geometries on substrates than a single ubiquitin receptor can offer.

While previous studies have used fusions of the UBL domain of Rad23 or linear tetra-ubiquitin to the substrate itself to test tail length dependence, this limits the ability to test preferences of proteasome receptors for the same substrate, and prevents variation in the placement of ubiquitin chains relative to an unfolded segment. Using *in vitro* reconstitution of the proteasome allows for selective inclusion of each ubiquitin receptor and examination of degradation of the same substrate with different receptors present. Because substrates bound to different receptors likely sample

different spaces on the proteasome, these substrates may have different accessibility to non-essential proteasome processes such as deubiquitination by Ubp6. In addition, while the location of Rpn10 on the proteasome well defined by structural studies, the binding site for Rad23 was somewhat ambiguous (Lander et al., 2012; Sakata et al., 2012). Rad23 binds Rpn1, but the region important for binding had not been narrowed down beyond a 320 amino acid portion of the 110kDa Rpn1 (Elsasser et al., 2002). To better be able to compare the spaces that proteasome substrates can sample on the proteasome when recruited through different receptors, I aimed to determine more precisely binding site on Rpn1 for Rad23.

Using model substrates ubiquitinated with Rsp5, recruitment through Rad23 is slower than recruitment through Rpn10, but the accessibility of these substrates to Ubp6 is similar. In addition, we confirmed that Rad23 binds directly to Rpn1, but were unable to more precisely identify the binding site on Rpn1 for Rad23. However, recent improvements in more uniform substrate delivery may soon offer clearer methods for comparing differently modified substrates.

Results

Determining Rad23 binding site on Rpn1

Before characterizing the binding site in more detail, we confirmed that Rad23 and Rpn1 bind directly when expressed and purified from *E. coli* by size exclusion chromatography (SEC) (Figure 3.1a). However, using the related shuttle factors Dsk2 and Ddi1 no co-elution was observed with Rpn1 (Figure 3.1b). In addition, some literature has proposed direct binding between some shuttle receptors and Rpn10 (Matiuhin et al., 2009; Walters et al., 2003), but using purified Rad23 and Rpn10, no interaction was observed by SEC (Figure 3.1c). The interaction between Rad23 and Rpn1 was confirmed and measured more quantitatively using isothermal titration calorimetry (ITC). This yielded a K_d of 1μM, in good agreement with the previously published affinity of 3.65 μM measured by surface plasmon resonance (Rosenzweig et al., 2012) (Figure 3.1d).

In our initial approach, we sought to localize Rad23 on Rpn1 using negative stain electron microscopy. Due to the relatively low-affinity interaction between Rpn1 and Rad23, samples were crosslinked with glutaraldehyde before SEC to select for non-aggregated, crosslinked species. However, despite the presence of higher molecular weight species with both Rad23 and Rpn1 present cross-linked samples still contained significant non-Rad23-bound Rpn1 (Figure 3.2b,d). Due to low occupancy of Rad23 and the small size of Rad23's UBL domain that interacts with Rpn1, negative stain samples for Rpn1 in the presence or absence of Rad23 were indistinguishable (Figure 3.2c). As a result I was unable to localize Rad23's binding site on Rpn1.

Using optimized crosslinking conditions, we aimed to narrow the location of Rad23 binding on Rpn1 by taking a crosslinking-MS approach. Here a deuterated, amine-reactive crosslinker was reacted with Rpn1 and Rad23, followed by trypsinization (Leitner, Walzthoeni, and Aebersold, 2014). Although crosslinks are rare within a sample, the use of a deuterated crosslinker allows for detection of crosslinker over non-crosslinked peptides due to its distinct doublet to be specifically selected for fragmentation. Very few crosslinks were observed and the two separate-peptide crosslinks detected were Rpn1 intralinks (Table 3.1). When the intralinks observed are mapped back to the structural model of Rpn1, they fit within the expected crosslinker distance of up to 26-30Å (Figure 3.3d, Table 3.1) (Merkley et al., 2014). Different chromatography post crosslinking or affinity purification of crosslinks using a biotinylated crosslinker might better select for crosslinked species if pursued further.

Figure 3.1: Rad23 and Rpn1 bind directly. (A) Purified Rpn1, Dsk2, Ddi1 and Rad23.
(B) Co-migration of Rpn1 and Rad23 by size exclusion chromatography (SEC) compared with Dsk2 or Ddi1 on Superdex 200 16 60 column. (C) SEC of Rpn10 and Rad23. (D) Isothermal titration calorimetry of Rad23 and Rpn1.

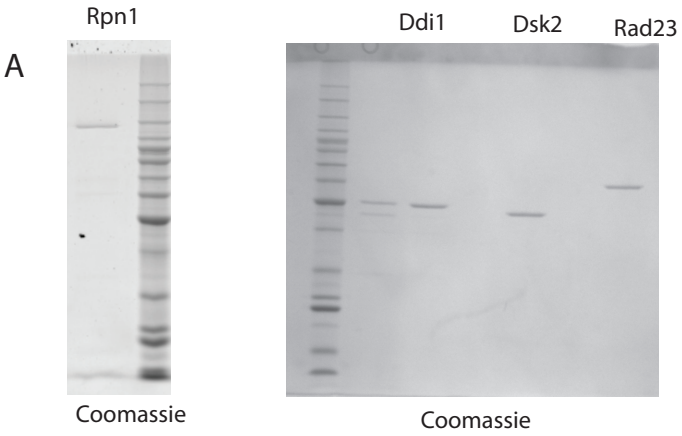

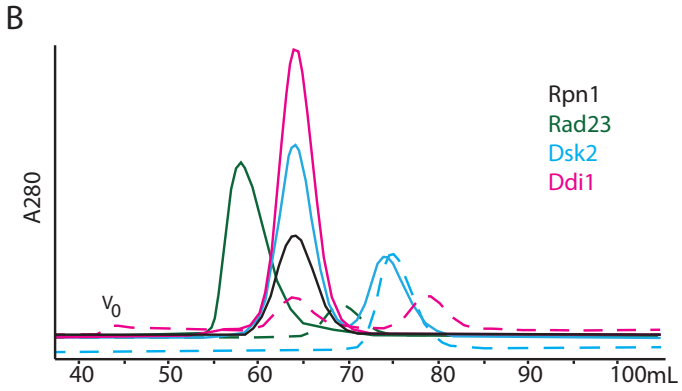

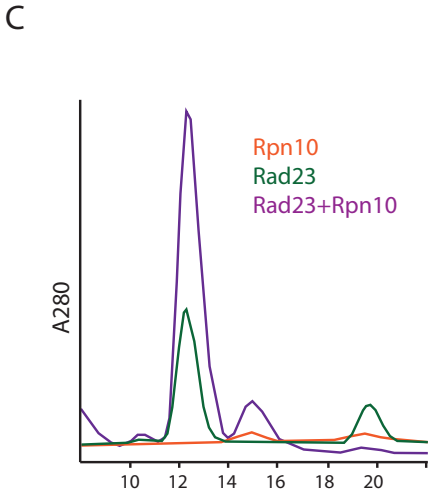

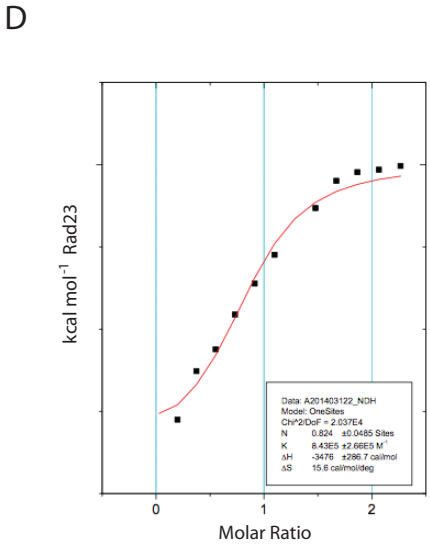

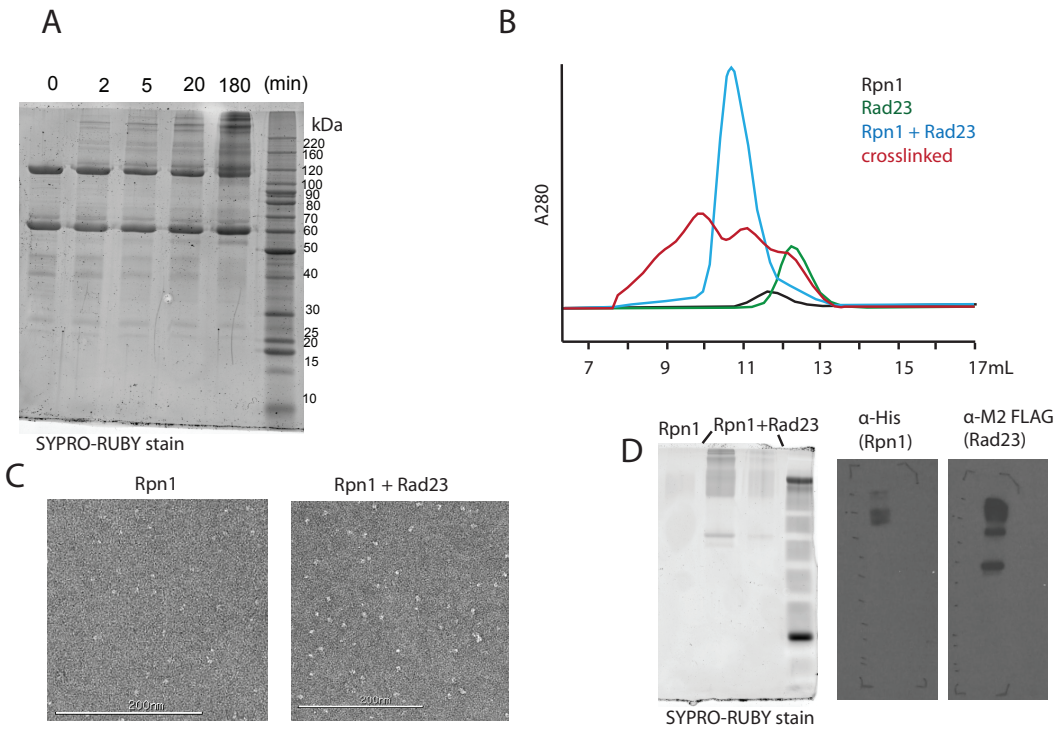

Figure 3.2: Rad23 and Rpn1 can be crosslinked to form a complex. (A) Appearance of higher molecular weight species during increasing time of incubation with glutaraldehyde. (B) crosslinked species contain a mixture of molecular weight species, with some at a similar SEC retention as native complex. (C) Crosslinked Rpn1 and Rad23 species contain particles, but look similar to Rpn1 alone as seen in representative micrographs. (D) By SDS page, higher molecular weight species seen in-gel contain both Rpn1 and Rad23 as visualized by western blotting against epitope tagged Rpn1 and Rad23.

Additionally, we hoped to narrow down the region of Rpn1 responsible for binding to Rad23 using hydrogen-deuterium exchange (HX). Protection of backbone hydrogens from exchange with solvent D_2O by binding of a ligand is usually monitored by comparing peptides of the protein of interest in the presence or absence of ligand at multiple timepoints (Engen 2009). However, when the binding site of a ligand is already protected from exchange in even the absence of ligand, it can be difficult to see interaction with the ligand simply because that well-ordered region of the protein cannot be any more protected by binding of a ligand. Mapping of amide-exchanged hydrogens for Rad23 and Rpn1 was consistent with structural models of these proteins: regions predicted to be unstructured or missing from structural models were readily exchanged with solvent (Figure 3.3a, b, e). For Rpn1, these regions include the acidic insertion into the LRR repeats making up the α-solenoid (Elsasser et al., 2004; Beck et al., 2012) (Figure 3.3a). Additional regions in Rpn1 predicted to be structured are highly exchanging, but some of these regions may make contacts with other base subunits and be more protected in a proteasome context (Figure 3.3b). For Rad23, the linkers connecting the UBL and UBA domains are unstructured, while the domains themselves are protected (Figure 3.3e). Peptide coverage for Rad23's UBL was poor, suggesting that the domain is not unfolded for digestion by pepsin (Figure 3.3e). As the UBL domain is structurally related to ubiquitin, it is unsurprising that the conditions required for pepsin digestion (pH 2.2, 1M Guanidine)

A

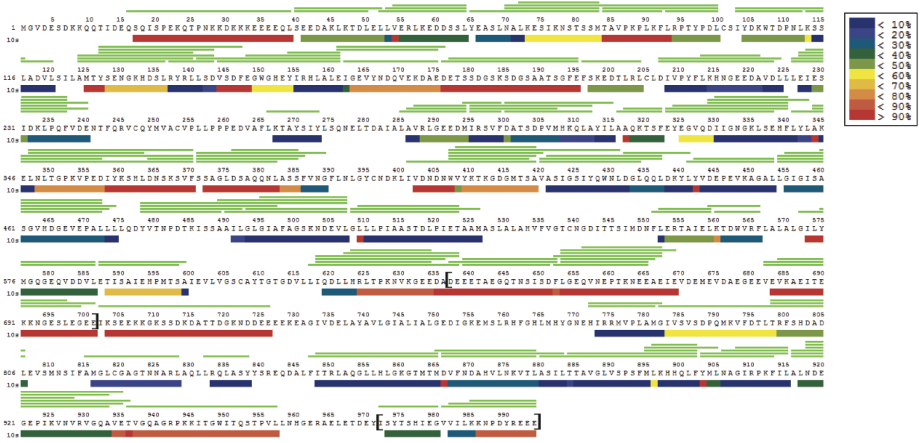

B

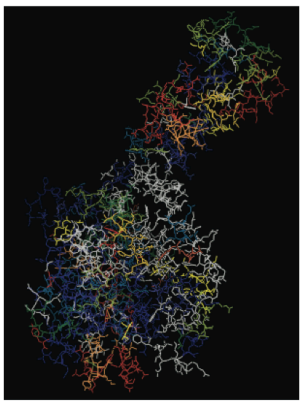

C

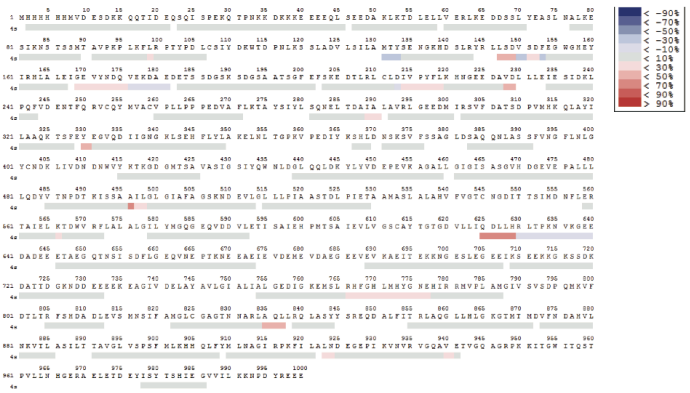

D

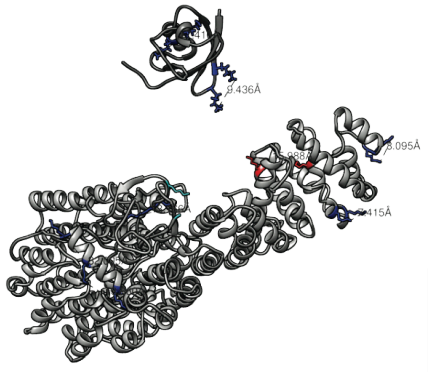

E

(Previous page) Figure 3.3 Hydrogen-Deuterium exchange (HX) and Crosslinking-MS of Rpn1 and Rad23 agree with structural models for each protein. (A) Exchange of Rpn1 mapped to the protein sequence of Rpn1 after 10s of exchange. Bracketed regions of the sequence are predicted to be unstructured in the context of the proteasome holoenzyme. Green bars denote the presence of high confidence peptides for the region. (B) information from (A) mapped to the structured model of Rpn1 (PDB: 4CR2.Z). (C) Comparison of Rpn1 exchange with 10s of exchange in the presence or absence of Rad23. (D) Intra-peptide (blue) and inter-peptide (red and cyan) crosslinks as shown in Table 3.1 mapped to a structural model of Rpn1 (PDB 4CR2.Z) and NMR structure of Rad23 UBL (PDB 2NBW.B). Cyan crosslink was between one ordered lysine and one thirteen residues outside the structural model. The structured lysine and end of the model are highlighted in cyan. (E) HX of Rad23 mapped to the sequence. Below the sequence α-helices and β-sheet portions of known structures are highlighted in yellow, structural elements in outside the yellow regions are PSIPred predictions.

Table 3.1: Rpn1 and Rad23 crosslinked by BS3

Dist. (Å)	peptide	(1)	(2)	Crosslink type:	aa (1)	aa (2)	Score
16	FLRPTYPDLCSIYDKWTDPNLK-LKEDDSSLYEASLNALK-a15-b2	Rpn1	Rpn1	intra-protein	112	72	28.07
n/a	FILALNDEGEPIKVNVR-KNPDYREEE-a13-b1	Rpn1	Rpn1	intra-protein	931	992	31.36
8.1	MHHHHHHMVDESDKK-K14-K15	Rpn1	-	intralink	14	n/a	42.55
7.4	NSTSSMTAVPKPLKFLRPTYPDLCSIY DK-K11-K14	Rpn1	-	intralink	94	n/a	32.6
7.4	NSTSSMTAVPKPLKFLRPTYPDLCSIY DKWTDPNLK-K11-K14	Rpn1	-	intralink	94	n/a	22.9
13.8	ELNLTGPKVPEDIYKSHLDNSK-K8-K15	Rpn1	-	intralink	359	n/a	33.91
32	ELNLTGPKVPEDIYKSHLDNSK-K8-K22	Rpn1	-	intralink	359	n/a	29.91
13.2	VGQAVETVGQAGRPKKITGWITQST PVLLNHGER-K15-K16	Rpn1	-	intralink	950	n/a	49.09
9.43	KEKVPLDLEPSNTILETK-K1-K3	Rad23	-	intralink	24	n/a	41.48
17.4	STKTKVTEPPIAPESATTPGR-K3-K5	Rad23	-	intralink	92	n/a	38.5

were unable to completely unfold the UBL of Rad23 even though these conditions are denaturing for many other proteins.

The α-solenoid portion of Rpn1 is the region expected to bind Rad23. However, these α-solenoid regions of Rpn1 are well folded and do not exchange much on the time scale of the exchanges measured. Due to the fast off rates previously reported for the Rad23-Rpn1 interaction and expected ~9s lifetime of the complex, we did not monitor long exchange times. Therefore it is perhaps unsurprising that very little difference was observed in Rpn1's exchange upon Rad23 binding (Figure 3.3c).

With isothermal titration calorimetry and size exclusion chromatography as functioning assays by which we could observe binding between these two subunits, looking at a few point mutations across the previously identified 320 amino acid region of Rpn1 was the most reasonable method to search for the Rad23 binding site. Using an improved structural model in combination with two previously described mutations in Rpn1 that affect Ddi1 binding, mutations were introduced in nearby loops (Gomez et al., 2011; Beck et al., 2012). However, none of these mutants showed defects in binding to Rad23 by SEC (Figure 3.4a). Differences in the behavior of these Rpn1 mutants in ITC despite identical reaction conditions prevented a more quantitative determination of

mutant effects (Figure 3.4B). Indeed, the mutations tested do not overlap with the binding site later identified by the Walters group (Chen et al., 2016)(Figure 3.4c).

Differences in degradation rate

Concurrent with efforts to identify the binding site for Rad23 on Rpn1, using an *in vitro* reconstitution system, we examined the differences in rate of degradation for model substrates ubiquitinated with Rsp5. In contrast to the 1μM affinity observed for Rpn1 and Rad23 interaction in isolation, the affinity for Rad23 in the context of active protein degradation is lower as estimated by the K_m for Rad23-mediated degradation of a single-lysine containing GFP substrate at 280nM (Figure 3.5b). This is in agreement with findings that the UBA competes for UBL-binding to the proteasome in an intramolecular interaction (Lowe et al., 2006). Therefore, when ubiquitin chains are present, the UBA's competition for binding with the UBL is relieved and the K_m is lower than the K_d of the isolated full-length protein. Unfortunately, ubiquitinated substrates are neither homogenous nor well behaved enough to be added to SEC or ITC to test this model directly. However, the Walters and Finley groups recently identified the binding site of Rad23 on Rpn1 by truncation of both components to portions of the protein that are suitable for NMR (Shi et al., 2016; Chen et al., 2016). Their affinity of 64nM for UBL alone confirms this model and their identification of the binding site on Rpn1 informed our further work.

Degradation mediated by Rad23 in the absence of Rpn10 *in vitro* is slower than Rpn10-mediated degradation (Figure 3.5a). This was not seen previously when using fusions of Rad23's UBL for degradation (Inobe et al., 2011) and seems to be dependent on properties of the substrate (Figure 3.5a). In addition, this slower overall rate cannot be overcome with the addition of more Rad23

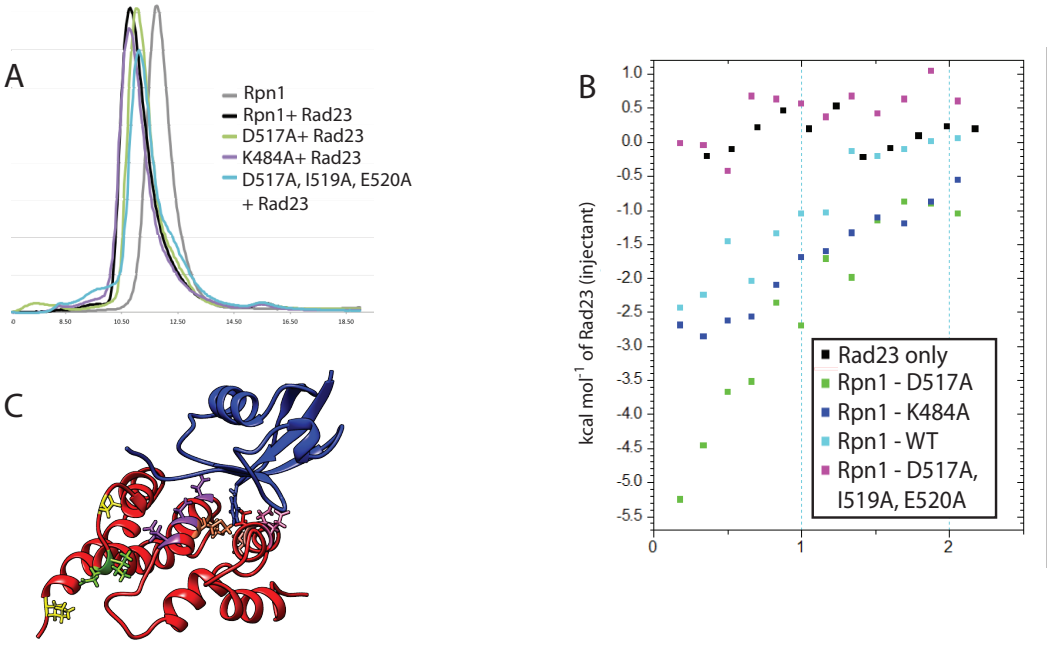

Figure 3.4 Binding of mutated Rpn1 to Rad23. (A) SEC of several point mutations Rpn1 iwith Rad23 as compared to wild-type Rpn1 with and without Rad23 present. (B) The same point mutant Rpn1 constructs in ITC with Rad23. Inconsistent baseline sloping prevents curve fitting. (C) Structure of a portion of Rpn1 (red) bound to Rad23 UBL (navy). Previously identified Ddi1-binding residues (K484, D517 in yellow) and the additional residues I mutated (I519, E520, green) do not overlap with residues involved in binding (orange and pink) (PDB: 2NBW).

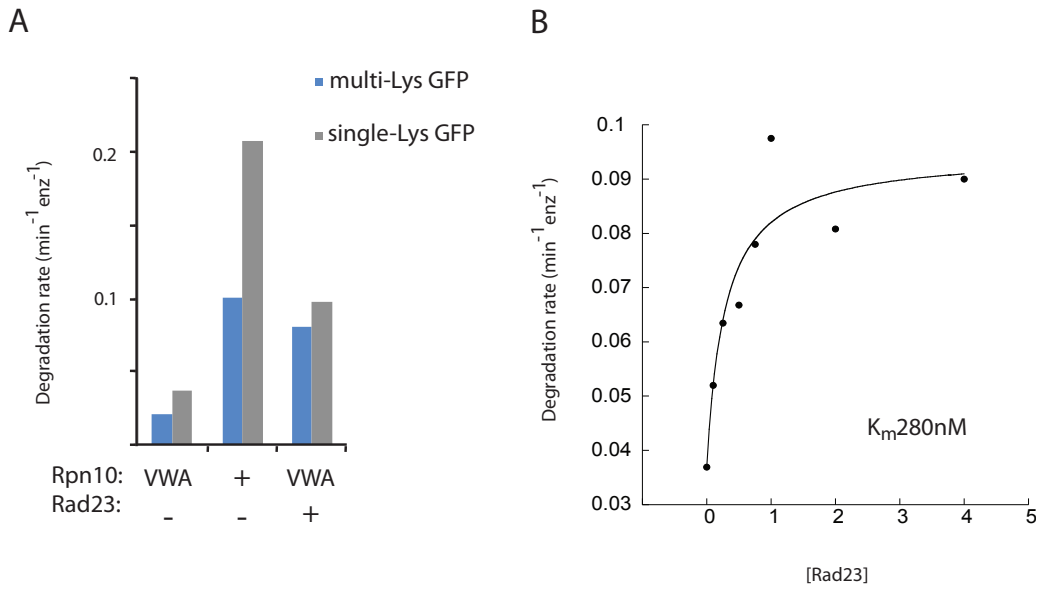

Figure 3.5 Proteasome degradation of model substrates with different ubiquitin receptors. (A) Degradation of 2uM substrate with 2uM of each of the designated ubiquitin receptors. All proteasomes contain Rpn13 and are at 2oonM. Rpn10-VWA maintains binding to the proteasome but is deficient in ubiquitin binding. (B) Titration of the multi-lysine GFP substrate with varying concentrations of Rad23.

(Figure 3.5b). As well, the relative rates of Rpn10 and Rad23 dependent substrate degradation are highly variable, perhaps because Rad23 is sensitive to the heterogeneity of the Rsp5 ubiquitinated substrate, auto-ubiquitination of Rsp5, or some other factor in ubiquitinations that varies from one to another. Overall, improvement in production of homogenous ubiquitinated substrate is required to better characterize the extent to which Rad23 and Rpn10-mediated degradation differ. However, the characterization of Rpn10-dependent and independent degradation (mediated through direct ubiquitin-binding to Rpn1) could provide similar answers as to how degradation through different means leads to differences in degradation rate.

To determine the kinetics of Rad23 recruitment to the proteasome, I aimed to develop a FRET-based binding assay. The proteasome can be site-specifically labeled on Rpn1 using the Schultz lab amber-suppression method to incorporate unnatural amino acids in place of the TAG stop codon (Chin et al., 2002). An amber stop codon introduced at position A555 in Rpn1 allowed for incorporation of 2-azidophenylalanine at that site for later labeling with a copper-free clickable fluorescent dyes (Figure 3.6b). Similarly, Rad23 can be labeled at positions V2, S3, T78 and T80 (Figure 3.6a). Proteasomes labeled at position A555 in Rpn1 are active in ATPase activity and degradation (Figure 3.6d). Labeled Rad23 is also functional in degradation and in ubiquitinated substrate binding (Figure 3.6c,e). However, using either labeled Rpn1 alone or in the context of the proteasome, FRET is not observed upon addition of labeled Rad23 (Figure 3.6f). In addition, anisotropy measurements using fluorescently labeled Rad23 suggests that Rad23 does not efficiently bind the proteasome (Table 3.2). This is in agreement with immunoprecipitations for substrate binding: Rad23 binds to ubiquitinated substrates and is released when ubiquitin chains are disassembled (Table 3.2). However, looking at interaction with Rpn1, proteasome base, or an E3 ligase binding partner, Ufd2, with either labeled full length Rad23 or the UBL alone does not show robust binding (Table 3.2). Perhaps fluorescent labeling of Rad23 disrupts UBL binding, and labeling at different positions either within Rad23 or Rpn1 will allow for a functional binding assay in the future.

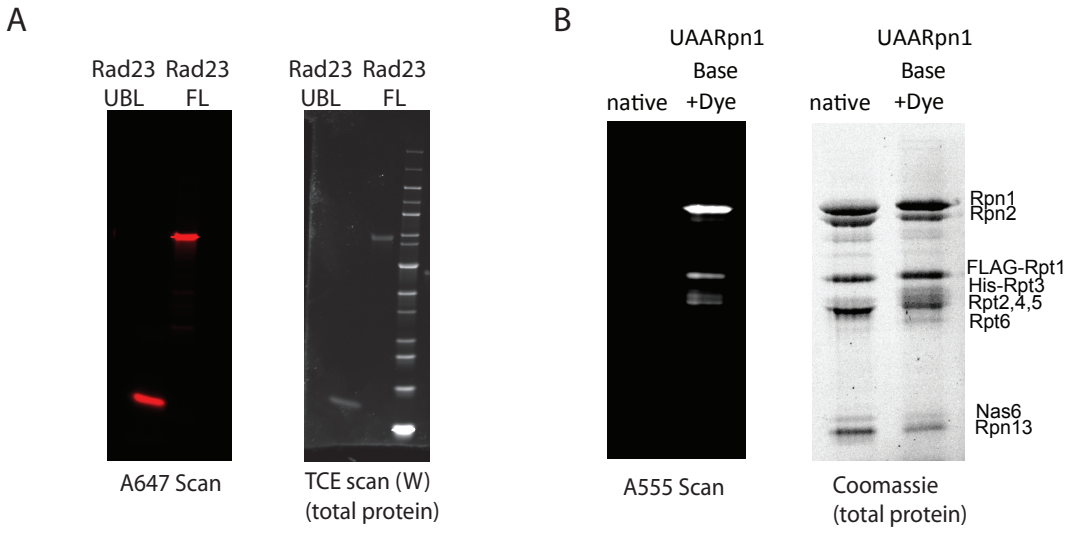
A
Rad23 UBL
Rad23 FL
Rad23 UBL
Rad23 FL
A647 Scan
TCE scan (W)
(total protein)
B
UAARpn1
Base
native
+Dye
UAARpn1
Base
native
+Dye
Rpn1
Rpn2
FLAG-Rpt1
His-Rpt3
Rpt2,4,5
Rpt6
Nas6
Rpn13
A555 Scan
Coomassie
(total protein)

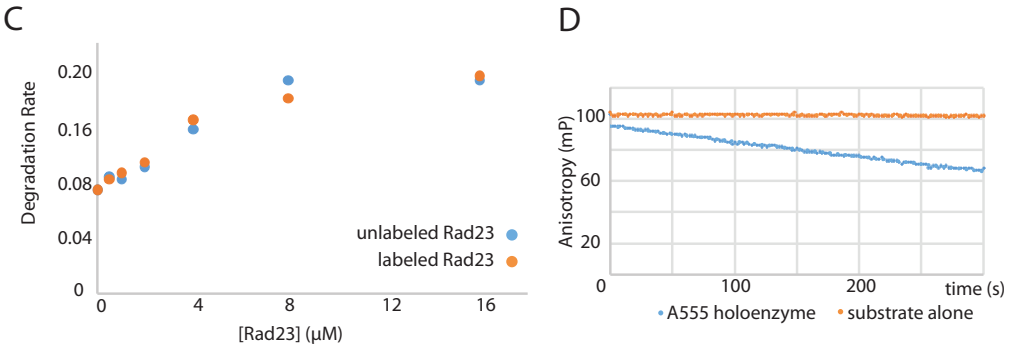
C
Degradation Rate
0.20
0.16
0.08
0.04
0
0
4
8
12
16
[Rad23] (μM)
unlabeled Rad23
labeled Rad23
D
Anisotropy (mP)
100
60
20
0
100
200
time (s)
A555 holoenzyme
substrate alone

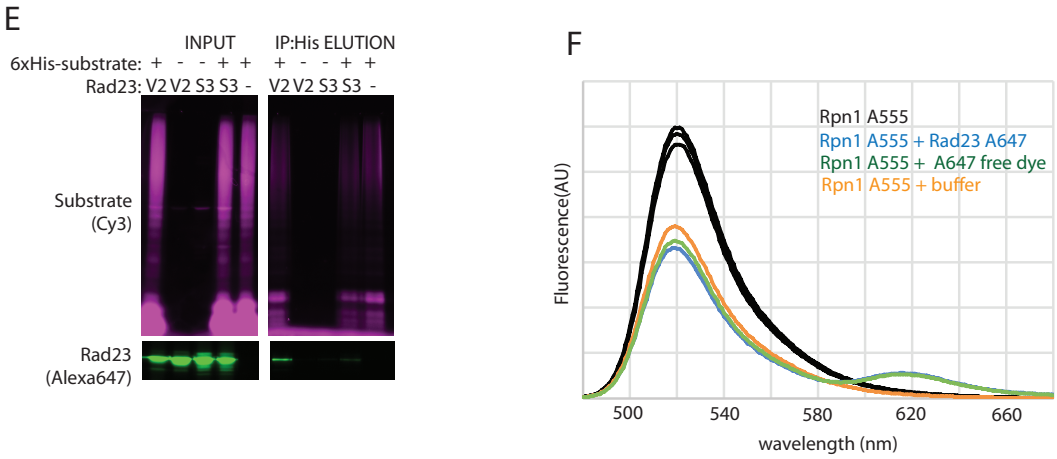
E
INPUT
IP:His ELUTION
6xHis-substrate: + - - + + + - - + +
Rad23: V2 V2 S3 S3 - V2 V2 S3 S3 -
Substrate
(Cy3)
Rad23
(Alexa647)
F
Fluorescence(AU)
Rpn1 A555
Rpn1 A555 + Rad23 A647
Rpn1 A555 + A647 free dye
Rpn1 A555 + buffer
500
540
580
620
660
wavelength (nm)

(Previous page) Figure 3.6 Labeling of Rpn1 and Rad23 for FRET and Anisotropy-based assays. (A) Rad23, either full length or the UBL alone, can be labeled with DIBO-Alexa647. (B) Rpn1 can be site specifically labeled with DIBO-Alexa555 and purifies as base. (C) Labeled Rad23 performs as native Rad23 in proteasome degradation. (D) Alexa555- labeled base is also capable of degrading a proteasome model substrate. (E) Labeled Rad23 can be affinity pulled down with His-tagged ubiquitinated substrate. (F) Quenching of Alexa555 fluorescence on Rpn1 with the addition of Buffer, free Alexa647 dye or labeled Rad23.

Table 3.2: Anisotropy response of Rad23 to binding partners

Change in anisotropy (mP)	Rad23 UBL	Rad23, Full length
BSA	2	2
Rpn1	19	-4
Base	8	3
Ufd2	16	12
Ub'd Substrate	-	44
Ub'd Substrate+ AMSH (DUB)	-	17

Differences in deubiquitination

Proteasome delivery through different ubiquitin receptors may allow substrates to sample different spaces surrounding the proteasome. As a result, a substrate's accessibility to the proteasome DUB Ubp6 might be altered by delivery mechanism. To address this, reconstituted proteasomes with inactivated core particle were reconstituted with either functional Rpn10 or functional Rad23. This allows for measurement of deubiquitination of proteasome substrates either by Rpn11 or Ubp6 depending on the reconstitution with either active or inactive Rpn11. Deubiquitination by Rpn11 occurs when the substrate is threaded and processed by the proteasome, but the action of Ubp6 in relation to the steps in proteasome processing is unclear. In agreement with fluorescence-based readouts of degradation, recruitment by Rpn10 results in more robust deubiquitination (Figure 3.7). Both DUBs cleave at the base of the ubiquitin chain, but Ubp6 acts more slowly, and this is discussed in more detail in Chapter 2. Through either Rpn10 or Rad23-mediated delivery, deubiquitination by Ubp6 occurs at a similar rate and is much slower than deubiquitination by Rpn11 (Figure 3.7). Monitoring deubiquitination of the substrate is complicated by recruitment through Rpn10-independent mechanisms, and in this assay Rpn10-independent mechanisms of substrate recruitment resulted in equivalent activity to those with Rad23 present (Figure 3.7a). Mutations that abrogate ubiquitin binding to Rpn1's T1 site cannot be used in this assay to prevent Rpn10-independent degradation because these mutations also disrupt binding of Rad23 (Shi et al., 2016). However, regardless of the exact mechanism of recruitment, different recruitment mechanisms result in differential deubiquitination by Rpn11, but not by Ubp6.

Discussion

Using model substrates delivered to the proteasome through different ubiquitin receptors, we observed the mechanism of substrate delivery affects the degradation rate. However, due to the recent discovery of an intrinsic ubiquitin receptor that overlaps with the Rad23 binding site, the difference in degradations for shuttle receptor-mediated delivery compared with direct Rpn1-ubiquitin binding is unclear. Improved sensitivity in degradation assays now allows differences in degradation through the Rpn10-mediated delivery or Rpn1-mediated delivery to be examined. Preliminarily, deubiquitination by Rpn11 and degradation are slower when recruitment through Rpn1 occurs. Without detailed knowledge of the kinetics and requirements of other steps in the process of degradation, such as tail-engagement, it is unclear if deubiquitination is rate-limiting for degradation, or if some other, preceding step is rate-limiting and deubiquitination is then slowed as a

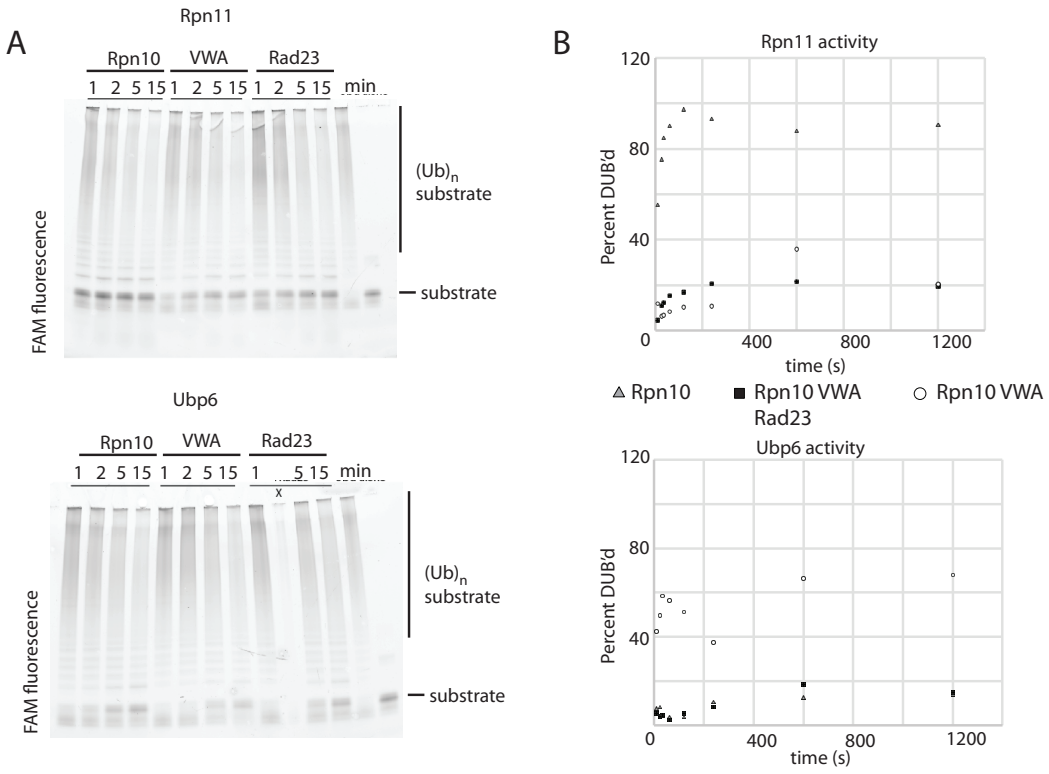

Figure 3.7: Accessibility of substrates to proteasome deubiquitinases with different substrate recruitment mechanisms. (A) Gel of deubiquitination mediated either by Rpn11 or by Ubp6 with reconstituted proteasome. Ubp6 samples contain a catalytically inactivated Rpn11 and both samples contain fully epoxomycin inhibited core particle so that deubiquitination is readout as a change in mobility and the substrate is not degraded into peptides. Both gels show non-ubiquitinated substrate and fully ubiquitinated substrate at the right side of the gel for reference. (B) Quantitation of reactions as in (A).

consequence. Given that Ubp6-mediated deubiquitination occurs equally slowly through either mechanism, it is clear that not all steps are slower through Rpn10-independent recruitment. Using fluorescence-based assays, these questions are currently under investigation by graduate students in the Martin lab.

In addition, while the methods employed here for determining the binding site on Rpn1 for Rad23 were unsuccessful, exploring the potential pitfalls of a variety of techniques for the same binding interaction provides a better picture of which techniques might be ultimately successful in describing other interactions at the proteasome. The majority of the methods described for searching for the binding site on Rpn1 for Rad23 would have been more easily accomplished for an interaction that is more stable than the one between full-length Rad23 and Rpn1, and usage of just the UBL of Rad23, which has a much higher affinity for the proteasome would likely have been more successful. In addition, techniques such as HX will likely still encounter issues, due to the large size of the proteasome and involvement of ubiquitin the inhibiting efficient production of peptides and chromatographic separation of peptides for the protein of interest. Meanwhile, techniques such as negative stain EM are limited by the small size of the UBL domain as well as the low affinity interaction. The ability to site-specifically label the proteasome provides the opportunity to build FRET-based assays to monitor activities such as tail insertion of a substrate directly, but also to build FRET-based binding assays for PIPs when their binding sites on the proteasome are well

known enough to engineer a dye nearby. Therefore, while this chapter does not provide satisfying mechanistic answers to the questions of how differential recognition and degradation of substrates occurs, it does provide a platform of techniques with which to address the interaction of other PIPs.

Methods

Purification

Base subcomplexes were expressed and purified from *E. coli* as previously described in Chapter 2. A555 base was expressed and purified with modification for incorporation and labeling of p-azidophenylalanine. A fourth pCDF plasmid containing the tRNA synthetase and tRNA under a T7-inducible promoter was coexpressed with the three base expression plasmids (Chin et al., 2002). Upon induction, cells were pelleted and transferred to fresh media containing 2mM amino acid and 0.5mM IPTG before expression. During purification, base was labeled with 400μM DIBO Alexa 647 (Thermo Fisher Scientific) at 4˚C with 200μM DTNB overnight before purification over Superose 6 10 300 (GE Healthcare). Lid, core, and ubiquitinated substrates were purified as described in Chapter 2.

Rad23, Dsk2, and Ddi1 were expressed as N-terminal His_6-fusion proteins in the pACYC plasmid and purified by Ni-NTA as previously described in Chapter 2. Rpn1 was similarly expressed as an N-terminal His_6 fusion co expressed with rare tRNAs (pRIL) Following Ni-purification, Shuttle proteins and Rpn1 were buffer exchanged into ion exchange binding buffer (50mM Tris pH 7.5 5% glycerol, 1mM DTT), loaded onto HiTrap Q HP (GE Healthcare) and eluted with gradient elution into 1M NaCl. Following anion exchange proteins were loaded onto HiLoad Superdex 200 16 60 (GE Healthcare) for Size exclusion chromatography. Labeled Rad23 or Rpn1 was treated as base and labeled overnight before anion exchange. Flag-tagged Rad23 was purified similarly, using M2-FLAG resin in place of the Ni-NTA step.

Analytical SEC

50μM of each protein in GF shuttle buffer (25mM HEPES 140mM NaCl, 5% glycerol, 10mM BME) was loaded onto Superdex 200 10 300 or Superdex 75 10 300 (GE healthcare) and run at 0.35mL/min at 4˚C and collected in 200uL fractions for visualization on SDS-PAGE. Comparison of Dsk2, Ddi1, and Rad23 was performed on a HiLoad Superdex 16 600 using the same buffers, but run at 0.8mL/min.

Isothermal Titration Calorimetry

Rad23 and Rpn1 were co-dialyzed with GF shuttle buffer overnight before loading into a MicroCal ITC for 11, 10μL injections of 110μM Rad23 into 10μM Rpn1 at 30˚C. Measurements were performed using samples all codialyzed together. Data analysis was performed using the MicroCal Analysis Software.

Glutaraldehyde crosslinking:

Rpn1 was mixed with a 3-fold excess of Rad23 and treated with a final concentration of glutaraldehyde of 0.02% for 2min before analysis by gel, SEC or for use in negative stain EM. Following crosslinking, SDS-PAGE of His-tagged Rpn1 and FLAG-tagged Rad23 was transferred to 0.22μ PVDF before blotting with α-His or α -M2-FLAG using conditions described in Chapter 2. Preparation and analysis of EM grids was performed by the Lander Lab as in Chapter 2.

Crosslinking with BS3 for XL-MS

Crosslinking for Rad23 and Rpn1 was performed as described in Leitner, Walzthoeni, and Aebersold, 2014. with modifications as described. Briefly, 4.5μM Rpn1 and 20μM Rad23 were crosslinked with BS3-H12/D12 (Creative Molecules) for 30min at 25˚C in GF buffer at pH 8.3. Samples were quenched with 50mM ammonium bicarbonate for 30min then dried under vacuum. Pellets were resuspended in 8M freshly prepared urea, 2.5mM TCEP and treated with 5mM iodoacetamide. Samples were diluted to 1M urea in 50mM ammonium bicarbonate, 5mM TCEP, and 1mM $CaCl_2$ for digestion with trypsin overnight at 37˚C. Following digestion samples were acidified with 0.05% TFA and desalted using C18 spin columns (Pierce). Samples were dried and resuspended in 0.2% formic acid and diluted 1:10 for injection onto nano-LC (Agilent 1260). Peptides were analysed on an Orbitrap Discovery mass spectrometer (ThermoFisher Scientific). Data analysis was performed using xQuest/xProphet using decoy databases generated to Rpn1 and Rad23 (Leitner, Walzthoeni and Aebersold 2014). Crosslinking, sample preparation and mass-spectrometry was done collaboratively with Goran Stjepanovic.

Hydrogen-deuterium exchange mass spectrometry experiments

As with the crosslinking, MS was collaboratively performed with Goran Stjepanovic. 5μL samples of 20μM Rpn1 and 40μM Rad23, or 20μM Rpn1 or Rad23 alone were mixed with 95μL D_2O buffer (25mM HEPES, 140mM NaCl, pD 7.6) at 25˚C. After 4 seconds, the reaction was quenched by cooling the reaction to 0˚C and adjusting the pH to 2.2 with the addition of 100μL of ice cold quench buffer (400 mM KH2PO4/K2HPO4, pH 2.2, and 3 M guanidine HCl) Samples were next injected into a modified HPLC (Agilent 1100) with and inline pepsin column followed by a reverse phase column (Biobasic-8, 50mm x 0.5mm, Thermo Scientific) submerged in an ice-water bath. Eluted peptides were injected onto an Orbitrap Discovery mass spectrometer (ThermoFisher Scientific) for analysis. For fully deuterated controls, samples were prepared by diluting Rpn1 and Rad23 into D_2O buffer in 6M guanidine. The samples were dried to pellets and solubilized in this buffer three times sequentially. For non-deuterated controls, samples were diluted into H_2O (25mM HEPES, 140mM NaCl, pH 7.6) buffer for exchange rather than D_2O buffer. Initial peptide sequencing runs were performed using tandem MS/MS. Analysis of peptide centroids shifts for exchanging samples was performed using HD-Examiner (Sierra Analytics) and all peptides were manually verified for retention time, charge state, and the absence of multiple overlapping peptides.

Anisotropy of labeled Rad23

15μL samples of 100nM Rad23, either full length or UBL only, labeled with c-terminally sortase labeled with a FAM-labeled peptide of the sequence GGGK were incubated with 0.72mg/mL BSA, 79.2μM Rpn1, 2μM base, 10.4μM Ufd2, or 1μM ubiquitinated substrate. DUB treated samples were incubated with 5uM AMSH for 30min before measuring anisotropy. Measurements were performed using dual PMTs on a Synergy Neo2 platereader.

Pulldown of Rad23 and Ubiquitinated substrates

10μM Rsp5 ubiquitinated substrate, labeled with FAM-maleimide on an engineered cysteine in the titin substrate was incubated with 20μM Rad23 labeled with DIBO-Alexa 647 at the site of 2-azido phenylalanine incorporation in Rad23 (V2, S3, T78, T80) in Ni wash buffer (25mM HEPES, 150mM NaCl, 2mM $MgCl_2$, 5% glycerol, 15mM imidazole, pH 7.6). Samples were incubated 10min at room temperature before adding 5μL of buffer-washed Magnetic Ni beads (Promega). After incubation for 30min, samples were washed three times with Ni wash buffer, 750μL each using a magnetic stand. Samples were eluted with elution buffer (25mM HEPES, 150mM NaCl, 2mM

$MgCl_2$, 5% glycerol, 500 mM imidazole, pH 7.6) for 30 minutes before samples were collected for SDS-PAGE. Substrate and labeled Rad23 were visualized by Typhoon scan (GE Healthcare).

Gel-based Deubiquitination Assay

Deubiquitination of FAM-labeled ubiquitinated substrate was measured as described in Chapter 2 for reconstituted proteasome. For Rpn11-dependent deubiquitination, Ubp6 was not included in the reconstitution. For Ubp6-dependent deubiquitination, Rpn11-AXA containing lid was included.

Chapter 4: Investigating assembly of the proteasome base

Introduction

The proteasome consists of more than 33 different subunits in either one or two copies that assemble to form a 2.5MDa complex containing multiple, coordinated enzymatic activities. In order to ensure proper functioning, the proteasome and its subcomplexes must assemble properly and efficiently. The biochemically characterized lid, base, and core subcomplexes were identified by dissociating holoenzyme in high salt conditions, and these subcomplexes are also the building blocks for assembling the proteasome holoenzyme. Each of the subcomplexes can be further broken down into modules that specifically assemble to form a subcomplex.

When base assembly is disrupted, modules containing coiled-coil pairs of Rpts and RP-specific chaperones (RACs) (Rpt1-Rpt2-Hsm3-Rpn1, Rpt3-Rpt6-Nas6-Rpn14, Rpt4-Rpt5-Nas2) are observed in yeast cells and are assumed to be intermediates in base assembly (Park et al., 2009; Roelofs et al., 2009; Funakoshi et al., 2009; Saeki et al., 2009). Each module contains at least one stably associated RAC for which the module is named. First, the Nas6/Rpn14 module, containing Rpt3 and Rpt6, joins with the Nas2 module containing Rpt4, Rpt5, and Nas2. Rpn2 and Rpn13 are thought to join the base at this point (Funakoshi et al., 2009; Saeki et al., 2009). Next, joining of the Hsm3 module, containing Hsm3, Rpn1, Rpt1, and Rpt2, displaces Nas2 from the base (Park et al., 2009; Roelofs et al., 2009) (See Figure 1.4). It seems clear that the RACs do not contain all of the information for proper assembly of the base, not only because they are not essential *in vivo*, but because each RAC makes contacts only with a single module (Funakoshi et al, 2009; Saeki et al., 2009). Furthermore, during the assembly process Nas2 is released from the base, but Nas6, Rpn14, and Hsm3 remain bound to assembled base until it is incorporated into holoenzyme. RAC-independent mechanisms of assembly templated by the core particle have been proposed, but seem unlikely given the promiscuity of Rpt C-terminal tails in core binding (Park et al., 2009; Park et al., 2012). Neither lid nor core is required for base assembly, because base can be heterologously expressed in *E. coli*. But, the heterologous expression system requires the RACs for efficient assembly, whereas the RACs are not essential *in vivo* (Beckwith et al., 2013).

This heterologous expression system for the base provided a system for determining more specifically the role of RACs in assembly of the base because it is more sensitive to RAC function than base assembly *in vivo*. This system allowed separation of the effects of other subcomplexes from the effects of RACs. Using both a subtractive and additive approach, we determined that the heterologous expression system does not 'perfectly' assemble base subcomplex, but that it recapitulates other aspects of the proteasome assembly process such as that RACs are not released until the base is incorporated into holoenzyme. The RACs improve the assembly of the base from modules in part by improving the solubility of their direct binding partners, but the RACs cannot prevent the incorrect assembly of modules into higher order complexes. Finally, other components of the proteasome, core and Ubp6, discriminate between properly and improperly assembled complexes by making contacts with multiple subunits of the base.

Results

Heterologous expression of proteasome base requires RACs

Previous heterologous expression of the base required the RACs, however the contributions to assembly of each individual RAC was not known. To purify assembled base, two-step affinity purification is required to get a single population of assembled base (Figure 4.1a-c). Importantly, this two-step purification selects for subunits not within the same module. From immunoblots against

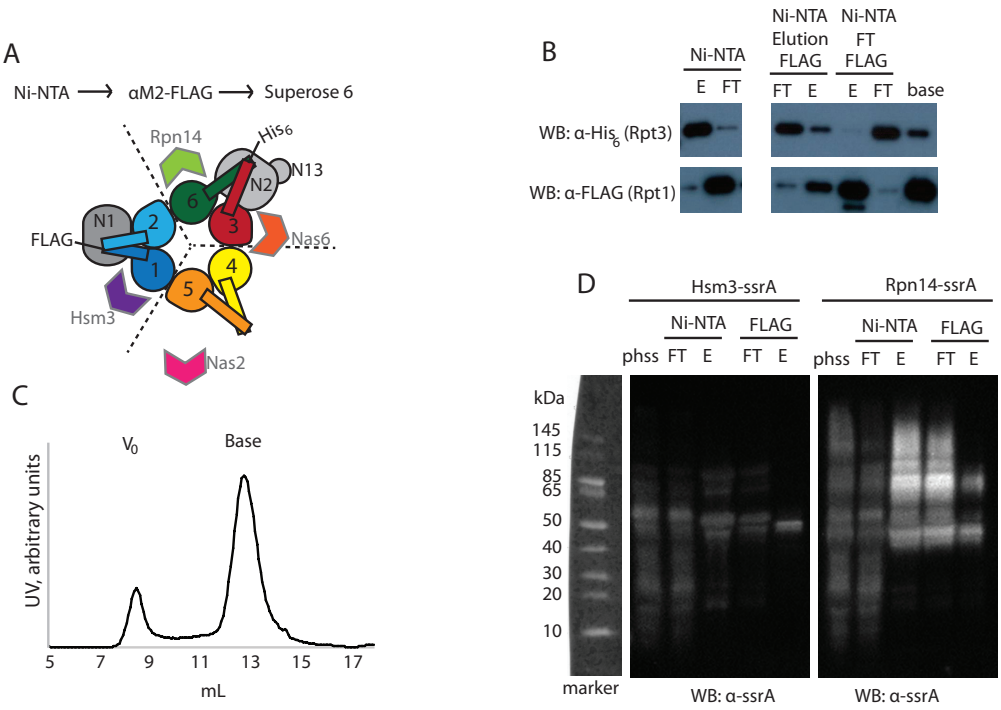

Figure 4.1: Heterologous expression and purification of base. His_6-Rpt3 and FLAG-Rpt1 are used for sequential affinity purification of base, selecting for subunits in two different modules of the base (A). Analysis of the flow through (FT) and elution of each step by immunoblot (B). Following FLAG elution, a representative trace of base over a Superose 6 10 300 Size exclusion chromatography column with the void volume (Vo) and base peaks noted (C). Visualization by immunoblot against ssrA tagged Hsm3 or Rpn14 over the course of base purification. As the ssrA tag is present in *E. coli*, non-specific reactivity is present in less purified samples such as cleared lysate (phss) and flow through (FT) (D).

His_6-tagged Rpt3 and FLAG-tagged Rpt1 it is clear that this is necessary to select for assembled base. It does not appear that expression of either of these subunits is limiting in the amount of base recovered because in both steps un-incorporated base subunits flow through the affinity column (Figure 4.1b). In addition, all three RACs assumed to remain bound to yeast base, Hsm3, Rpn14, and Nas6, do remain stably bound to heterologously-expressed base. Nas6 can be observed by Coomassie (Figure 4.5a), but Rpn14 and Hsm3 are of a similar molecular weight to most of the Rpts. By tagging these RACs with an epitope tag (ssrA), Hsm3 and Rpn14 can be followed throughout the purification by immunoblotting. Hsm3 and Rpn14 bind to both the properly assembled base and mis-assembled complexes (Figure 4.1d).

Although the RACs compete with core and lid binding, increasing the apparent K_d of base for lid or core, heterologously expressed base with bound RACs is competent to form holoenzyme and otherwise behaves similarly to yeast-purified base (Beckwith et al., 2013; Park et al., 2013; Park et al., 2017). To overcome the holoenzyme stability defects that come with co-purifying the base with RACs in the heterologous expression system, C-terminally tagging the RACs with the ssrA tag offers a mechanism for recognition and selective degradation by the ClpXP protease (Figure 4.2a). Preliminarily, Hsm3 and Rpn14 can be selectively degraded by added ClpXP, with untagged subunits remaining untouched (Figure 4.2b). Degradation of the RACs was much slower than degradation of a model ClpXP substrate (titin-V15P-ssrA), but could perhaps be improved by extending a flexible linker between the ssrA recognition tag and the end of the folded domain of the RAC.

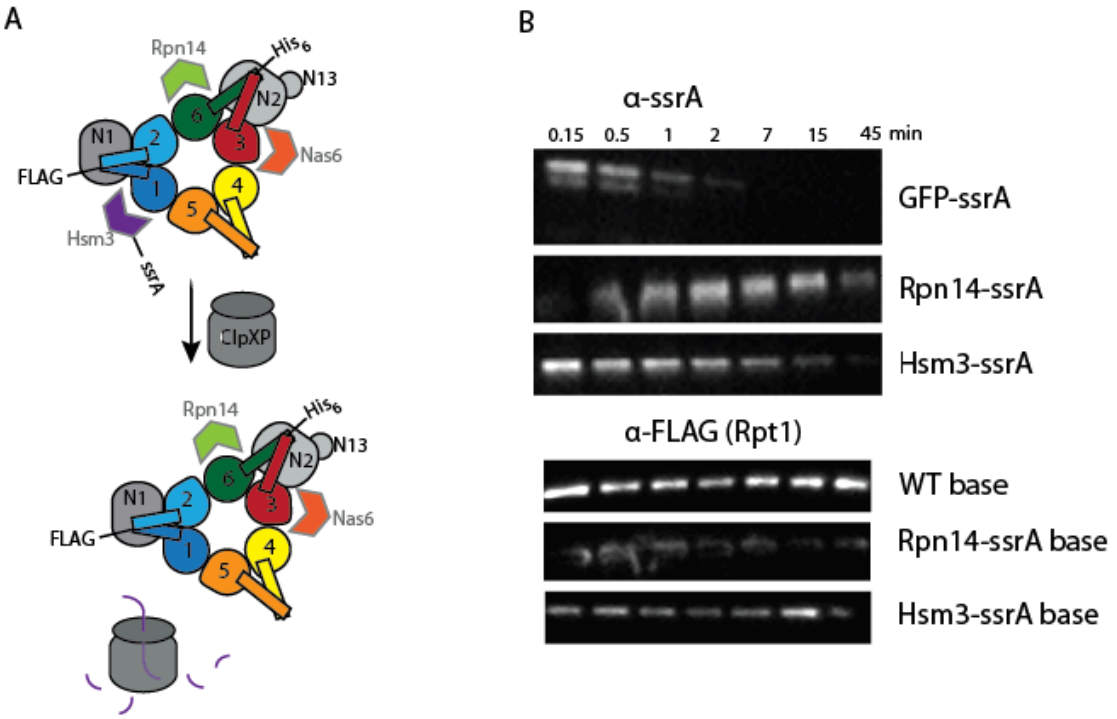

Figure 4.2: Specific degradation of associated RACs using ClpXP targeted degradation to the ssrA tag. Addition of the 11 amino acid sequence to the C-terminus of a RAC targets it, but not untagged subunits for degradation (A). Degradation of ssrA-tagged RACs upon incubation with ClpXP by Immunoblot. In the same reactions Rpt1 followed by α-M2-FLAG immunoblot remains constant (B). Note that a bubble in the transfer obscures signal in the 0.15min sample for Rpn14-ssrA base

When any of the three RACs that remain stably bound are deleted from the heterologous expression system, the amount of the soluble base subunits produced from their respective module decreases. For example, Rpt3 soluble levels are diminished when either Rpn14 or Nas6 is removed, however other base subunits that can be expressed individually such as Rpn1 are still present (Figure 4.3a). When only Nas2 is removed from the expression system, some Rpt1 remains associated with Rpt3 throughout the purification, however the majority of the sample ends up in the void volume or a peak larger than the base (Figure 4.3c,d). When only Nas2 is included, some soluble Rpt3, Rpt1, and other base subunits are still produced, but assembly is disrupted (Figure 4.3a,b). Because three of the RACs bind to the outside of the base, it is unclear how they might pair subunits together for proper assembly. However, the observation that removal of RACs decreases not just assembly but the solubility of many of the Rpts is consistent with previous observations that some of the Rpts express poorly in *E. coli* (Takeuchi and Tamura, 2004). For example, the AAA domain of Rpt3 is only soluble in the presence of Nas6 (Nakamura et al., 2007). Because pairing of subunits also stabilizes them, it is difficult to determine to how removal of single RACs from the base expression system affects assembly.

Heterologous Expression of RAC modules

To understand how base assembly occurs we sought to develop a heterologous expression of each module with the goal of developing an *in vitro* reconstitution of base assembly. Although we did not attain an *in vitro* reconstitution of modules, the properties of these heterologously expressed modules are informative in understanding how specificity for base assembly is encoded in Rpt subunits and

RACs. First, the previously described Hsm3 and Nas2-containing modules can be purified as complexes from *E. coli* (Figure 4.4). The Nas6/Rpn14 module does not remain stably associated and does not purify as a complex. The Hsm3 and Nas2 modules form higher order assemblies that are not easily dissociated with high salt and are larger in size than the base (Figure 4.4b,c). As both modules were poorly behaved, a further characterization of just the Hsm3 was performed to understand what this complex is and how it is assembled.

The base subunits are not totally selective in their incorporation into base. In the heterologous base expression system some Rpt3 and Rpt1 are soluble but are not incorporated into proper base (Figure 4.1b, Figure 4.3). The large complexes that Hsm3 module forms are likely one example of the inappropriate complexes formed in the complete base expression system in addition to base. Surprisingly, the Hsm3 module still contains significant ATPase activity when compared with base (Table 4.1). To confirm that this activity is truly from base subunits, Walker-B mutations would need to be placed in each of the ATPase subunits of the module to abolish activity. Because the modules purify as complexes that are already larger than the proteasome base and harbor ATPase activity, following assembly of base from these components would be difficult without adding lid and core. Addition of lid or core could directly affect the assembly process itself, but the response of proteasome subcomplexes to modules illustrates how the final steps in the assembly process can act as a checkpoint on proper assembly.

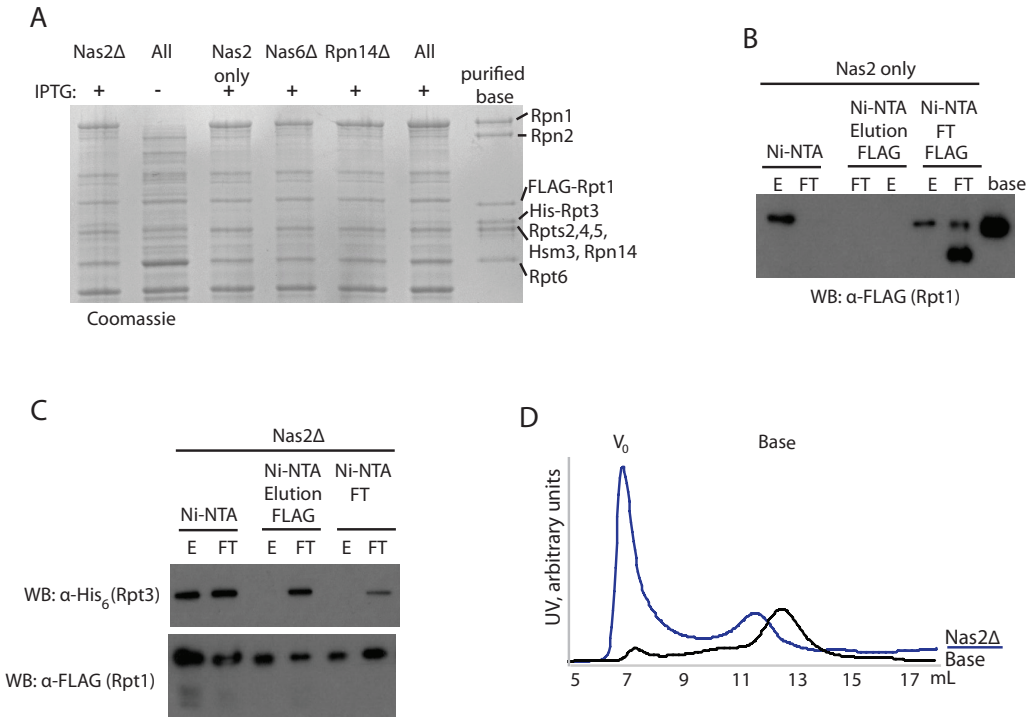

Figure 4.3: Removal of RACs disrupts base assembly. Coomassie-stained induction samples of base subunits in the presence of subsets of RACs (A). Presence of FLAG-Rpt1 or His-Rpt3 followed over the course of a base purification when only Nas2 is included (B) or when Hsm3, Rpn14, and Nas6 are included (C). E and FT refer to the eluate and flow through of the affinity step. Comparison of Superose 6 traces for base lacking Nas2 to a normal purification (D).

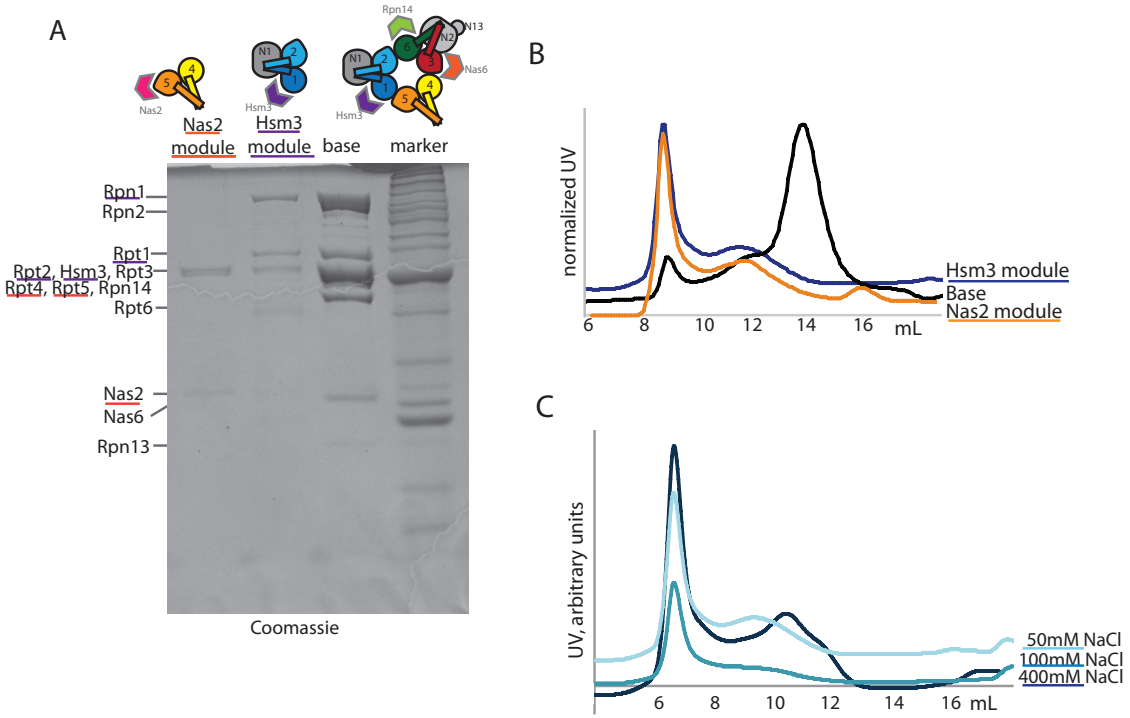

Figure 4.4: Expression and purification of base modules. SDS-PAGE (A) and SEC traces (B) for Hsm3 and Nas2 modules. Comparison of Superose 6 traces for Hsm3 module purified in varying salt conditions (C).

Proteasome subcomplexes selectively interact with properly assembled base

Binding of base C-terminal tails to the core peptidase opens the gates of the core, and this gate opening can be monitored by a stimulation of core-mediated cleavage of a fluorogenic substrate. While the Hsm3 module contains ATPase activity, it is not able to stimulate gate opening of the core (Table 4.1). The core peptidase stimulation by base is also abolished when the C-terminus of Rpn1, a non-ATPase subunit of the base, is extended. In both of these samples, subunits containing HbYX motifs normally capable of stimulating gate opening are present. While this base containing a short C-terminal epitope tag extension of Rpn1 is normally behaved in affinity purification and size exclusion chromatography, SDS-PAGE of this prep indicates some subunits are missing, likely Hsm3, Rpn14, or Rpt5 (Figure 4.5). This suggests that the non-ATPase subunits of the base may act directly in the proper pairing of subunits in base assembly. This misassembled base also largely lacks ATPase activity (Table 4.1). While potential loss of contacts between the C-terminus of Rpn1 and the core may explain the loss in core peptidase stimulation, the loss of base subunits and lack of ATPase activity cannot be explained solely by this core-base interaction.

Ubp6 is a proteasome associated DUB that binds two sites on the proteasome: it binds strongly to Rpn1 and more weakly to the OB- domain of Rpt1. Ubp6 is activated by binding to the proteasome, and has been described as a component of the Hsm3 module (Park et al., 2009; Sakata et al., 2011) (see chapter 2 for more details). Despite containing the subunits to which Ubp6 binds,

	ATPase activity (min^{-1} •enz^{-1})	s.d.	% base activity	Core peptidase stimulation	s.d.	% base activity	Ubp6 activity (min^{-1} •enz^{-1})	s.d.	% base activity
Base	79.7	7.48	100	13.3	0.21	100	51.2	2.1	100
C-terminal Rpn1 extended 'base'	6.16	2.81	0.77	1.05	0.01	7.9	29.1	0.7	61
Hsm3 module	48.0	9.03	60.2	1.06	0.03	7.5	0.20	1.2	3.2

Table 4.1: Summary of ATPase activity, core peptidase stimulation (LLVY-AMC cleavage), and Ubp6 activity stimulation (Ub-AMC cleavage) by base, Hsm3 module and Rpn1-C-terminally-extended base. Values for each assay are expressed as a rate and in terms of relative activity compared with base.

the Hsm3 module does not activate Ubp6, and the C-terminally extended Rpn1 base has an intermediate activation of Ubp6 (Table 4.1). While Ubp6 is implicated as a sensor of conformational changes in the proteasome, its activation at the proteasome is also selective for properly assembled base.

Discussion

Using the heterologous expression system to study base assembly offers the advantage that it is more sensitive to perturbations in the assembly pathway than in yeast. This has allowed for the discovery of new contributions to assembly such as the C-terminus of Rpn1. In yeast, C-terminal tagging of Rpn1 allows for robust purification of properly assembled proteasome holoenzyme, but in the heterologous expression system gives a clear assembly defect (Lander et al., 2012). The sensitivity of the heterologous expression system to RACs and base subunit changes supports models that the core particle facilitates assembly of the proteasome base (Park et al., 2009). By looking at base assembly in the absence of core, in the absence of RACs, or with changes to the base subunits themselves, assembly is disrupted. That the core can distinguish between properly assembled base and multiple misassembled base complexes offers one mechanism by which core

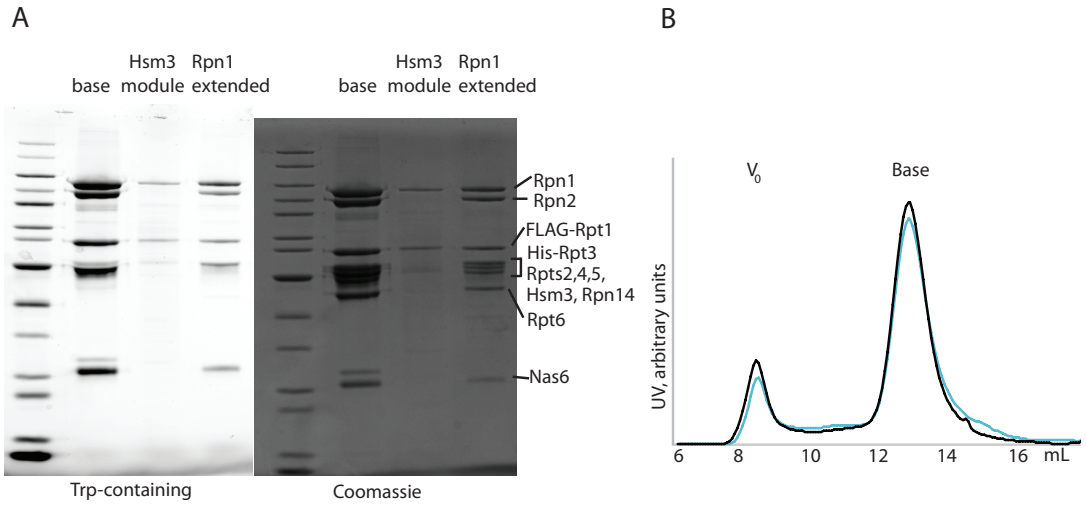

Figure 4.5: Comparison of Hsm3 module and C-terminally extended Rpn1 base. Imaging of the same samples by TCE, staining of only proteins containing tryptophan, and with Coomassie staining of total protein side-by-side (A). C-terminally extended Rpn1 base (light blue) runs similarly to base (black) by SEC (B).

may aid assembly. However, this sensitivity to loss of the RACs has also been a drawback of this approach, because it has been difficult to determine more specifically how an individual RAC acts when the entire process is disrupted by small changes. Additionally, the unexpected finding that these modules form complexes larger than the fully assembled base raises the question as to whether the modules purified and described here are ever formed *in vivo* and are on pathway to assembly. Using similar purifications of these modules from yeast could address these questions.

While complexes of Rpt1 and Rpt2 coexpressed in *E. coli* were known to form higher order complexes and have ATPase activity, it is surprising that the addition of both Hsm3 and Rpn1, two factors that affect assembly, does not prevent these ATPase-active, large complexes from forming (Takeuchi and Tamura, 2004). Interestingly, while the Rpt1-Rpt2 complex reported previously has gate opening activity, this is not observed for the Hsm3 module. While Hsm3 does not seem to be able to prevent this higher order assembly from occurring, perhaps it is able to prevent this module from binding to the core unless it is assembled into base. It is still unclear if this complex is even competent to assemble into base, and this could be addressed by mixing the purified modules together to see if any active base could be detected using core peptidase stimulation. While, this would not address the role of core-templated base assembly, it could be a tool for investigating effects of the base subunits themselves on assembly.

The role of the non-ATPase subunits of the base (Rpn1, Rpn2, and Rpn13) remains an incompletely explored aspect of proteasome assembly. Hsm3 has been previously reported to make direct contacts with Rpn1 during the formation of the Hsm3 module, but the portion of Rpn1 involved in this interaction is unknown (Barrault et al., 2011). The defects seen in assembly with C-terminal extension of Rpn1 suggest that Hsm3 might interact with the C-terminus of Rpn1. Recent proteasome structures have also uncovered connecting density between Rpn1 and Rpn2 that may be formed by contact between long disordered regions in the middle of the PC solenoids of each subunit (Schweitzer et al., 2016). A direct contact between Rpn1 and Rpn2 could explain the role of Rpn2 in module joining. Rpn2 is proposed to join the Nas2 and Nas6/Rpn14 modules, but was only previously known to make direct contacts with subunits in the Nas6/Rpn14 module of the base (Tomko and Hochstrasser, 2013). The Nas6/Rpn14 module was difficult to purify and seems to fall apart more easily than the other modules, however it was never coexpressed with Rpn2. It is therefore possible that Rpn2 also stabilizes this module besides participating in pairing of modules.

Characterizing the heterologous expression of base modules highlights the multiple mechanisms employed by subunits to properly assemble proteasome, specificity for assembly encoded in base subunits themselves, RACs, and other proteasome subcomplexes. Over the course of this work, conditionally-expressed RACs, Adc17 and Spg5, have been described and could be investigated in the expression of modules or the base expression system as whole (Hanssum et al., 2014; Hanna et al., 2012). Adc17 had no effect in the heterologous base expression system, but aids in formation of the Nas6/Rpn14 module *in vivo*, and therefore might allow that module to be purified if added. In addition, the tolerance of this system to substitution of subunits in the context of the RACs should also be considered. *In vivo*, each yeast Rpt can be substituted for by the mouse or human version (Inobe and Genmei, 2015; Kachroo et al., 2015). Investigating whether the yeast RACs still recognize mouse or human Rpt subunits in the heterologous expression system could address how RACs recognize a specific Rpt despite similarities of Rpts to each other. This could be quickly tested with the sensitivity of the heterologous expression system. While we now know more pieces of what is important for assembly, the exact order of assembly in yeast cells and how each protein's functions in assembly may overlap remains to be seen.

Methods

Recombinant expression and purification of proteins and complexes

Base subcomplex was purified as described in Chapter 2 modified by the removal of RACs from the expression plasmid where noted. When following assembly of base by immunoblot, both the flow-through and the eluate from Ni-NTA steps were separately passed over FLAG columns as otherwise described in Chapter 2. Joshua Cofsky provided purified Rpn1-extended base.

Expression and purification of modules was similar except the Ni-NTA step was omitted. Briefly, after clarification by centrifugation lysates were loaded directly onto α-M2-FLAG agarose resin and eluted with FLAG peptide. Hsm3 module contains a FLAG-tag on Rpt1 as in the base expression system. Nas2 module contains a FLAG-tag on the N-terminus of Rpt4.

SDS-PAGE 'Tryptophan staining'

For examining the subunit differences between C-terminally extended Rpn1 base and native base, gels containing 2,2,2-Trichloroethanol were imaged with UV light on a Chemidoc XRS+ (Bio Rad). Proteins containing tryptophans are visible in-gel after crosslinking with this compound.

Immunoblotting for base assembly

SDS PAGE samples were normalized by Bradford before running SDS-PAGE for transfer to 0.22μ PVDF. Blots were incubates with 6% milk (w/v) in TBST overnight before incubation with the appropriate antibody. α-His (Santa Cruz Biotech sc-8036HRP) was used at 1:5000 and α-M2 FLAG (Sigma- A8592) 1:20000. Rb-α-ssrA (gift from R. Sauer and T. Baker) was used at 1:10000, followed by α-Rb-HRP at 1:20000.

ClpXP degradation

1.5μM ClpX and 4.5μM ClpP were incubated with 250nM ssrA-containing complexes: Rpn14-ssrA base, Hsm3-ssrA base, or titin-ssrA with ATP Regeneration mix. Reactions were started with the addition of ClpXP and followed by α-ssrA Immunoblot blot. FLAG-Rpt1 levels were also over the same timecourse by stripping and reblotting. Immunoblots were performed as above.

ATPase assays

Data were collected on Synergy Neo2 as described in Chapter 2. All measurements were collected in at least triplicate.

Core peptidase stimulation

Cleavage of the LLVY-AMC fluorogenic peptide was measured on a plate reader (Synergy Neo2) using excitation at 345nm and emission at 445nm. Reactions monitored the stimulation in activity of 50nM core on 1μM LLVY-AMC substrate incubated with 400nM base-like complex for 5 minutes at 25°C. All reactions were measured in at least triplicate.

Chapter 5: Conclusions

Summary

Together this work illustrates the how interactions between the subunits of the proteasome template its assembly and coordinate the conformational changes required for substrate degradation. As more structures of the proteasome in different states are revealed, the functions of substoichiometric proteasome subunits and the mechanisms of proteasome assembly are becoming more easily determined. I have shown here that assembly of the proteasome base is governed by dedicated RACs in the absence of other proteasome subcomplexes, and these RACs participate in the proper pairing of subunits despite each making stable contacts with only a single proteasome subunit. The *E. coli* expression of proteasome base reveals the importance of the proteasome subunits themselves, specifically Rpn1, in encoding assembly. In addition, proteasome components such as the core and PIPs including Ubp6 can discriminate between complete base and other base subunit-containing complexes. These interactions may act as checkpoints in proteasome assembly to prevent assembly of sick proteasomes.

PIPs like Ubp6 and Rad23 can be used as tools to understand the function of the proteasome better, not only in allowing for characterization of the proteasome's interaction with cellular partners, but because these partners offer insights into mechanisms for modulating proteasome activity. Delivery through different ubiquitin receptors at the proteasome leads to differences in degradation rates. By gaining a better understanding of what properties of a proteasome substrate's ubiquitin chain placement and linkage type shift the efficiency of degradation by any receptor on the proteasome, we can better address how the proteasome accomplishes protein degradation of the proteome.

Understanding the role PIPs like Ubp6 can also give insight into the fundamental mechanisms of proteasome degradation through Ubp6's allosteric actions regulating proteasome activity. From contacts that Ubp6 makes directly with the ATPase subunits of the base, Ubp6 acts as a conformational sensor but also stabilizes an engaged state of the proteasome in response to ubiquitin. By separating substrate recruitment from ubiquitin, we have been able to use Ubp6's conformational sensing to probe the effect other mutations have on the proteasome. Using Ubp6 as a tool, we have begun to uncover the allosteric network driving the conformational changes seen in response to substrate. While contacts between Rpn5 and the rigid body formed by Rpt3's small AAA with Rpt4's AAA are clearly an important part of this switch, Ubp6 will continue to be useful in further probing other contacts in the proteasome mediating the conformational change.

The assays I have developed for following the binding of Rad23 to the proteasome and probing the conformational state of the proteasome with Ubp6 can act as platforms to answer other questions about proteasome mechanism. In addition, a better characterization of the *E. coli* base expression system provides a platform to tease apart the relative contributions to assembly and subunit communication during of mutations in proteasome base components. These new tools coupled with the enormous strides in the structural understanding of the proteasome leave a wide variety of questions about the proteasome at an ideal state to be addressed. A few open questions are outlined below.

What triggers the proteasome conformational change and how is this change communicated through the complex?

Substrate processing is associated with a variety of biochemical responses from the proteasome such as core gate opening and an increase in ATPase activity. Recent structures of the proteasome (Wehmer et al., 2017; Matyskiela et al., 2013) show that the conformational changes associated with substrate or non-hydrolyzable nucleotides move the ATPases into an flatter translocation-competent

ring from a cracked washer and open the gates of the core, but substrate is not yet visible. Visualizing substrate by structural means or by using FRET-based assays to assess the binding and translocation of substrate will aid in understanding what series of events at the proteasome trigger this conformational change and allows the switch back to the apo state of the proteasome. Proteasome structures also provide us with contact points between proteasome subunits that may be important for this conformational change and can now be addressed by incorporating mutations at these contact sites.

This approach is already underway for Rpn5-base contacts, but other contacts are also worth pursuing. Especially interesting is the connection between Rpn1 and Rpn2 possibly mediated by unstructured insertions into the PC repeats of each protein (Schweitzer et al., 2016). This contact could serve roles in both base assembly and in propagation of the conformational change. As with substrate, it is unclear how Ubp6 triggers the engaged state of the proteasome despite now having a picture of the Ubp6-bound state (Bashore et al., 2015, Aufderheide et al., 2015). A connection between Rpn1 and Rpn2 is an attractive explanation here given that Rpn2 makes direct contacts with Rpn11. This Rpn2-Rpn11 contact may also be important for this conformational change, because we know that deletion of the loop in Rpn11 that makes contacts with Rpn2 prevents activation of the lid, by the holoenzymes, but the communication of this contact to the rest of the proteasome remains to be clarified (Dambacher et al., 2016).

Understanding what contacts contribute to the conformational change of the proteasome may also give insight into posttranslational modifications mediating the balance between these states of the proteasome. Recently, phosphorylation of the loops of Usp14/Ubp6 has been described and partially activates DUB activity without the contact of the proteasome (Xu et al., 2015). A wealth of posttranslational-modifications of the proteasome exist, but the effect of these modifications on function of the proteasome remains to be tested (Guo, Huang, and Chen, 2017). Similar to PIPs, some of these modifications likely tie into the allosteric network controlling conformational switching of the proteasome while others may regulate assembly.

Is the proteasome's degradation of model substrates in vitro *a good mimic of proteasomal processing* in vivo*?*
Proteasomal degradation *in vitro* occurs at a rate of between 0.1-1 min^{-1} $enzyme^{-1}$ and is slower than related AAA+ motors. This is especially surprising given the degradation of APC/C substrates driving the metaphase-anaphase transition must occur within minutes in the cell. One possibility is that model substrates, despite often being derived from these cell cycle substrates, behave differently in cells due to differences in the ubiquitination of substrates *in vitro*. Recent work adding preformed chains to APC/C substrates demonstrates that multiple short chains can be a more efficient signal for degradation than the long chains that are often produced *in vitro* (Lu et al., 2015). Another possibility is that the proteasome may have other activating factors or modifications that are lost during purification of proteasomes and have not yet been identified. Regulation of proteasome function during the cell cycle or by other conditions may modulate proteasome activity by posttranslational modifications that are lost in the bulk purification of proteasome from unsynchronized cells. Or, the proteasome really may be as slow as is observed *in vitro* because it is subject to more regulation than similar bacterial motors, but is able to accomplish efficient degradation due to its high abundance in the cell. The proteasome is perhaps is at a high enough concentration that the observed *in vitro* rates are consistent with the timing of the cell cycle. However, in a survey of proteasomes in rat neurons by EM tomography, only 20% of proteasomes were in a substrate-engaged conformation (Asano et al., 2015).

How are malfunctioning proteasomes recognized and degraded?

The specific autophagy of proteasomes, termed 'proteaphagy,' was described in arabidopsis (Marshall et al., 2015). Here, Vierstra and colleagues see specific autophagy of proteasomes, but not general autophagy, upon treatment of cells with the proteasome inhibitor MG132 or with the introduction of proteasome mutations. In addition, autophagy mutants displayed elevated proteasome levels without elevated proteasome activity. Together these data suggest that autophagy of proteasomes is a response to a loss of proteasome function, but the mechanisms by which proteasomes are recognized as sick remain unclear. Ubiquitination of proteasome ubiquitin receptors changes in response to stress is one possible part of this signal. Rpn13 is ubiquitinated by the proteasome-associated Hul5/UBE3C ubiquitin ligase, which could be part of the signal for proteaphagy (Besche et al., 2014). However, under some of the same stress conditions, heat shock or heavy metal treatment, inhibitory monoubiquitination of the proteasome receptor Rpn10 is lessened (Isasa et al., 2010). This mono-ubiquitinated Rpn10 has decreased affinity for the proteasome and for ubiquitin conjugates (Isasa et al., 2010; Keren-Kaplan et al., 2016).

In addition, PIPs such as Ecm29 seems to paradoxically stabilize proteasome association, while inhibiting proteasome activity (Leggett et al., 2002; De La Mota-Peynado et al., 2013). However, Ecm29's importance under stress conditions and its ability to recognize specific proteasome mutations points to a role in proteasome quality control (Park et al., 2011; Haratake et al., 2016). Ecm29-bound proteasomes are also enriched at endosomal membranes, perhaps pointing to connection between recognition of dysfunctional proteasomes and lysosomal degradation (Gorbea et al., 2010).

In addition to direct degradation of proteasomes by autophagy, recent work on proteasome assembly factors has uncovered signaling links between the proteasome and the lysosome/vacuole where sensing of proteasome function is mediated by the supply of amino acids to the cell, and TORC1 signaling can respond to this by inducing the production of more proteasomes (Rousseau and Bertolotti, 2016; Suraweera et al., 2012). It will be interesting to see how the regulatory mechanisms concerning proteasome assembly and proteasome turnover fit together with a deeper understanding of the mechanics of proteasome degradation.

References

Aufderheide, A., Beck, F., Stengel, F., Hartwig, M., Schweitzer, A., Pfeifer, G., Goldberg, A.L., Sakata, E., Baumeister, W., and Förster, F. (2015). Structural characterization of the interaction of Ubp6 with the 26S proteasome. Proc Natl Acad Sci U S A *112*, 8626–8631.

Arendt, C.S., and Hochstrasser, M. (1999). Eukaryotic 20S proteasome catalytic subunit propeptides prevent active site inactivation by N-terminal acetylation and promote particle assembly. EMBO J. *18*, 3575–3585.

Asano, S., Fukuda, Y., Beck, F., Aufderheide, A., Förster, F., Danev, R., and Baumeister, W. (2015). Proteasomes. A molecular census of 26S proteasomes in intact neurons. Science *347*, 439–442.

Barrault, M.-B., Richet, N., Godard, C., Murciano, B., Le Tallec, B., Rousseau, E., Legrand, P., Charbonnier, J.-B., Le Du, M.-H., Guérois, R., Ochsenbein F., Peyroche, A. (2012). Dual functions of the Hsm3 protein in chaperoning and scaffolding regulatory particle subunits during the proteasome assembly. Proc. Natl. Acad. Sci. U.S.A. *109*, E1001-1010.

Beck, F., Unverdorben, P., Bohn, S., Schweitzer, A., Pfeifer, G., Sakata, E., Nickell, S., Plitzko, J.M., Villa, E., Baumeister, W. Forster, F. (2012). Near-atomic resolution structural model of the yeast 26S proteasome. Proc Natl Acad Sci U S A *109*, 14870–14875.

Beckwith, R., Estrin, E., Worden, E.J., and Martin, A. (2013). Reconstitution of the 26S proteasome reveals functional asymmetries in its AAA+ unfoldase. Nat. Struct. Mol. Biol. *20*, 1164–1172.

Bengtson, M.H., and Joazeiro, C.A.P. (2010). Role of a ribosome-associated E3 ubiquitin ligase in protein quality control. Nature *467*, 470–473.

Besche, H.C., Sha, Z., Kukushkin, N.V., Peth, A., Hock, E.-M., Kim, W., Gygi, S., Gutierrez, J.A., Liao, H., Dick, L., Goldberg, A.L. (2014). Autoubiquitination of the 26S proteasome on Rpn13 regulates breakdown of ubiquitin conjugates. EMBO J. *33*, 1159–1176.

Biggins, S., Ivanovska, I., and Rose, M.D. (1996). Yeast ubiquitin-like genes are involved in duplication of the microtubule organizing center. J. Cell Biol. *133*, 1331–1346.

Brandman, O., Stewart-Ornstein, J., Wong, D., Larson, A., Williams, C.C., Li, G.-W., Zhou, S., King, D., Shen, P.S., Weibezahn, J., Dunn, J.G., Rouskin, S., Inada, T., Frost, A., Weissman, J. (2012). A ribosome-bound quality control complex triggers degradation of nascent peptides and signals translation stress. Cell *151*, 1042–1054.

Carragher, B., Kisseberth, N., Kriegman, D., Milligan, R.A., Potter, C.S., Pulokas, J., and Reilein, A. (2000). Leginon: an automated system for acquisition of images from vitreous ice specimens. J. Struct. Biol. *132*, 33–45.

Chen, L., and Madura, K. (2002). Rad23 promotes the targeting of proteolytic substrates to the proteasome. Mol. Cell. Biol. *22*, 4902–4913.

Chen, X., Randles, L., Shi, K., Tarasov, S.G., Aihara, H., and Walters, K.J. (2016). Structures of Rpn1 T1:Rad23 and hRpn13:hPLIC2 Reveal Distinct Binding Mechanisms between Substrate Receptors and Shuttle Factors of the Proteasome. Structure *24*, 1257–1270.

Chin, J.W., Santoro, S.W., Martin, A.B., King, D.S., Wang, L., and Schultz, P.G. (2002). Addition of p-azido-L-phenylalanine to the genetic code of Escherichia coli. J. Am. Chem. Soc. *124*, 9026–9027.

Chu, B.W., Kovary, K.M., Guillaume, J., Chen, L., Teruel, M.N., and Wandless, T.J. (2013). The E3 ubiquitin ligase UBE3C enhances proteasome processivity by ubiquitinating partially proteolyzed substrates. J. Biol. Chem. *288*, 34575–34587.

Dambacher, C.M., Worden, E.J., Herzik, M.A., Martin, A., and Lander, G.C. (2016) Atomic structure of the 26S proteasome lid reveals the mechanism of deubiquitinase inhibition. eLife *5 :e13027*.

Dantuma, N.P., Heinen, C., and Hoogstraten, D. (2009). The ubiquitin receptor Rad23: at the crossroads of nucleotide excision repair and proteasomal degradation. DNA Repair (Amst.) *8*, 449–460.

D'Arcy, P., Brnjic, S., Olofsson, M.H., Fryknäs, M., Lindsten, K., De Cesare, M., Perego, P., Sadeghi, B., Hassan, M., Larsson, R., Linder, S. (2011). Inhibition of proteasome deubiquitinating activity as a new cancer therapy. Nat. Med. *17*, 1636–1640.

De La Mota-Peynado, A., Lee, S.Y.-C., Pierce, B.M., Wani, P., Singh, C.R., and Roelofs, J. (2013). The proteasome-associated protein Ecm29 inhibits proteasomal ATPase activity and in vivo protein degradation by the proteasome. J. Biol. Chem. *288*, 29467–29481.

Deng, H.-X., Chen, W., Hong, S.-T., Boycott, K.M., Gorrie, G.H., Siddique, N., Yang, Y., Fecto, F., Shi, Y., Zhai H., Jiang, H., Hirano, M., Rampersaud, E., Jansen, G.H., Donkervoort, S., Bigio, E.H., Brooks, B.R., Ajroud, K., Sufit, R.L., Haines, J.L., Mugnaini, E., Pericak-Vance, M.A., Siddique, T. (2011). Mutations in UBQLN2 cause dominant X-linked juvenile and adult-onset ALS and ALS/dementia. Nature *477*, 211–215.

Dick, T.P., Nussbaum, A.K., Deeg, M., Heinemeyer, W., Groll, M., Schirle, M., Keilholz, W., Stevanović, S., Wolf, D.H., Huber, R., Rammensee, H.G., Schild, H. (1998). Contribution of proteasomal beta-subunits to the cleavage of peptide substrates analyzed with yeast mutants. J. Biol. Chem. *273*, 25637–25646.

Ding, Z., Fu, Z., Xu, C., Wang, Y., Wang, Y., Li, J., Kong, L., Chen, J., Li, N., Zhang, R., Cong, L. (2017). High-resolution cryo-EM structure of the proteasome in complex with ADP-AlFx. Cell Res. *27*, 373–385.

Dong, K.C., Helgason, E., Yu, C., Phu, L., Arnott, D.P., Bosanac, I., Compaan, D.M., Huang, O.W., Fedorova, A.V., Kirkpatrick, D.S., Hymowitz, S.G., Dueber, E.C. (2011). Preparation of distinct ubiquitin chain reagents of high purity and yield. Structure *19*, 1053–1063.

Eddins, M.J., Varadan, R., Fushman, D., Pickart, C.M., and Wolberger, C. (2007). Crystal structure and solution NMR studies of Lys48-linked tetraubiquitin at neutral pH. J. Mol. Biol. *367*, 204–211.

Elsasser, S., Gali, R.R., Schwickart, M., Larsen, C.N., Leggett, D.S., Müller, B., Feng, M.T., Tübing, F., Dittmar, G.A.G., and Finley, D. (2002). Proteasome subunit Rpn1 binds ubiquitin-like protein domains. Nat. Cell Biol. *4*, 725–730.

Elsasser, S., Chandler-Militello, D., Müller, B., Hanna, J., and Finley, D. (2004). Rad23 and Rpn10 serve as alternative ubiquitin receptors for the proteasome. J. Biol. Chem. *279*, 26817–26822.

Engen, J.R. (2009). Analysis of Protein Conformation and Dynamics by Hydrogen/Deuterium Exchange MS. Anal Chem *81*, 7870–7875.

Estrin, E., Lopez-Blanco, J.R., Chacón, P., and Martin, A. (2013). Formation of an intricate helical bundle dictates the assembly of the 26S proteasome lid. Structure *21*, 1624–1635.

Finley, D. (2009). Recognition and processing of ubiquitin-protein conjugates by the proteasome. Annu. Rev. Biochem. *78*, 477–513.

Fishbain, S., Prakash, S., Herrig, A., Elsasser, S., and Matouschek, A. (2011). Rad23 escapes degradation because it lacks a proteasome initiation region. Nat Commun *2*, 192.

Funakoshi, M., Sasaki, T., Nishimoto, T., and Kobayashi, H. (2002). Budding yeast Dsk2p is a polyubiquitin-binding protein that can interact with the proteasome. Proc. Natl. Acad. Sci. U.S.A. *99*, 745–750.

Funakoshi, M., Tomko Jr., R.J., Kobayashi, H., and Hochstrasser, M. (2009). Multiple Assembly Chaperones Govern Biogenesis of the Proteasome Regulatory Particle Base. Cell *137*, 887–899.

Goddard, T.D., Huang, C.C., and Ferrin, T.E. (2007). Visualizing density maps with UCSF Chimera. J. Struct. Biol. *157*, 281–287.

Goh, A.M., Walters, K.J., Elsasser, S., Verma, R., Deshaies, R.J., Finley, D., and Howley, P.M. (2008). Components of the ubiquitin-proteasome pathway compete for surfaces on Rad23 family proteins. BMC Biochem. *9*, 4.

Gomez, T.A., Kolawa, N., Gee, M., Sweredoski, M.J., and Deshaies, R.J. (2011). Identification of a functional docking site in the Rpn1 LRR domain for the UBA-UBL domain protein Ddi1. BMC Biol. *9*, 33.

Gorbea, C., Pratt, G., Ustrell, V., Bell, R., Sahasrabudhe, S., Hughes, R.E., and Rechsteiner, M. (2010). A Protein Interaction Network for Ecm29 Links the 26 S Proteasome to Molecular Motors and Endosomal Components. J Biol Chem *285*, 31616–31633.

Groll, M., Ditzel, L., Löwe, J., Stock, D., Bochtler, M., Bartunik, H.D., and Huber, R. (1997). Structure of 20S proteasome from yeast at 2.4 A resolution. Nature *386*, 463–471.

Guo, X., Huang, X., and Chen, M.J. (2017). Reversible phosphorylation of the 26S proteasome. Protein Cell *8*, 255–272.

Guterman, A., and Glickman, M.H. (2004). Complementary roles for Rpn11 and Ubp6 in deubiquitination and proteolysis by the proteasome. J. Biol. Chem. *279*, 1729–1738.

Hanna, J., Leggett, D.S., and Finley, D. (2003). Ubiquitin depletion as a key mediator of toxicity by translational inhibitors. Mol. Cell. Biol. *23*, 9251–9261.

Hanna, J., Hathaway, N.A., Tone, Y., Crosas, B., Elsasser, S., Kirkpatrick, D.S., Leggett, D.S., Gygi, S.P., King, R.W., and Finley, D. (2006). Deubiquitinating enzyme Ubp6 functions noncatalytically to delay proteasomal degradation. Cell *127*, 99–111.

Hanna, J., Waterman, D., Boselli, M., and Finley, D. (2012). Spg5 protein regulates the proteasome in quiescence. J. Biol. Chem. *287*, 34400–34409.

Hanssum, A., Zhong, Z., Rousseau, A., Krzyzosiak, A., Sigurdardottir, A., and Bertolotti, A. (2014). An inducible chaperone adapts proteasome assembly to stress. Mol. Cell *55*, 566–577.

Haratake, K., Sato, A., Tsuruta, F., and Chiba, T. (2016). KIAA0368-deficiency affects disassembly of 26S proteasome under oxidative stress condition. J. Biochem. *159*, 609–618.

Husnjak, K., and Dikic, I. (2012). Ubiquitin-binding proteins: decoders of ubiquitin-mediated cellular functions. Annu. Rev. Biochem. *81*, 291–322.

Husnjak, K., Elsasser, S., Zhang, N., Chen, X., Randles, L., Shi, Y., Hofmann, K., Walters, K.J., Finley, D., and Dikic, I. (2008). Proteasome subunit Rpn13 is a novel ubiquitin receptor. Nature *453*, 481–488.

Inobe, T., and Genmei, R. (2015). N-Terminal Coiled-Coil Structure of ATPase Subunits of 26S Proteasome Is Crucial for Proteasome Function. PLoS ONE *10*, e0134056.

Inobe, T., Fishbain, S., Prakash, S., and Matouschek, A. (2011). Defining the geometry of the two-component proteasome degron. Nat Chem Biol *7*, 161–167.

Isasa, M., Katz, E.J., Kim, W., Yugo, V., González, S., Kirkpatrick, D.S., Thomson, T.M., Finley, D., Gygi, S.P., and Crosas, B. (2010). Monoubiquitination of Rpn10 Regulates Substrate Recruitment to the proteasome. Mol Cell *38*, 733–745.

Kachroo, A.H., Laurent, J.M., Yellman, C.M., Meyer, A.G., Wilke, C.O., and Marcotte, E.M. (2015). Systematic humanization of yeast genes reveals conserved functions and genetic modularity. Science *348*, 921–925.

Kang, Y., Vossler, R.A., Diaz-Martinez, L.A., Winter, N.S., Clarke, D.J., and Walters, K.J. (2006). UBL/UBA ubiquitin receptor proteins bind a common tetraubiquitin chain. J. Mol. Biol. *356*, 1027–1035.

Kather, I., Bippes, C.A., and Schmid, F.X. (2005). A stable disulfide-free gene-3-protein of phage fd generated by in vitro evolution. J. Mol. Biol. *354*, 666–678.

Keren-Kaplan, T., Zeev Peters, L., Levin-Kravets, O., Attali, I., Kleifeld, O., Shohat, N., Artzi, S., Zucker, O., Pilzer, I., Reis, N., et al. (2016). Structure of ubiquitylated-Rpn10 provides insight into its autoregulation mechanism. Nat Commun *7*, 12960.

Kim, H.C., and Huibregtse, J.M. (2009). Polyubiquitination by HECT E3s and the determinants of chain type specificity. Mol. Cell. Biol. *29*, 3307–3318.

Kim, I., Mi, K., and Rao, H. (2004). Multiple interactions of rad23 suggest a mechanism for ubiquitylated substrate delivery important in proteolysis. Mol. Biol. Cell *15*, 3357–3365.

Kim, W., Bennett, E.J., Huttlin, E.L., Guo, A., Li, J., Possemato, A., Sowa, M.E., Rad, R., Rush, J., Comb, M.J.,Harper J.W., Gygi, S.P. (2011). Systematic and quantitative assessment of the ubiquitin-modified proteome. Mol. Cell *44*, 325–340.

Komander, D., and Rape, M. (2012). The ubiquitin code. Annu. Rev. Biochem. *81*, 203–229.

Kriegenburg, F., Ellgaard, L., and Hartmann-Petersen, R. (2012). Molecular chaperones in targeting misfolded proteins for ubiquitin-dependent degradation. FEBS Journal *279*, 532–542.

Kunjappu, M.J., and Hochstrasser, M. (2014). Assembly of the 20S proteasome. Biochim. Biophys. Acta *1843*, 2–12.

Lander, G.C., Stagg, S.M., Voss, N.R., Cheng, A., Fellmann, D., Pulokas, J., Yoshioka, C., Irving, C., Mulder, A., Lau, P.-W., et al. (2009). Appion: an integrated, database-driven pipeline to facilitate EM image processing. J. Struct. Biol. *166*, 95–102.

Lasker, K., Förster, F., Bohn, S., Walzthoeni, T., Villa, E., Unverdorben, P., Beck, F., Aebersold, R., Sali, A., and Baumeister, W. (2012). Molecular architecture of the 26S proteasome holocomplex determined by an integrative approach. Proc. Natl. Acad. Sci. U.S.A. *109*, 1380–1387.

Le Tallec, B., Barrault, M.-B., Guérois, R., Carré, T., and Peyroche, A. (2009). Hsm3/S5b participates in the assembly pathway of the 19S regulatory particle of the proteasome. Mol. Cell *33*, 389–399.

Lee, B.-H., Lu, Y., Prado, M.A., Shi, Y., Tian, G., Sun, S., Elsasser, S., Gygi, S.P., King, R.W., and Finley, D. (2016). USP14 deubiquitinates proteasome-bound substrates that are ubiquitinated at multiple sites. Nature *532*, 398–401.

Leggett, D.S., Hanna, J., Borodovsky, A., Crosas, B., Schmidt, M., Baker, R.T., Walz, T., Ploegh, H., and Finley, D. (2002). Multiple Associated Proteins Regulate Proteasome Structure and Function. Molecular Cell *10*, 495–507.

Leitner, A., Walzthoeni, T., and Aebersold, R. (2014). Lysine-specific chemical cross-linking of protein complexes and identification of cross-linking sites using LC-MS/MS and the xQuest/xProphet software pipeline. Nat Protoc *9*, 120–137.

Levchenko, I., Seidel, M., Sauer, R.T., and Baker, T.A. (2000). A specificity-enhancing factor for the ClpXP degradation machine. Science *289*, 2354–2356.

Li, F., Tian, G., Langager, D., Sokolova, V., Finley, D., and Park, S. (2017). Nucleotide-dependent switch in proteasome assembly mediated by the Nas6 chaperone. Proc. Natl. Acad. Sci. U.S.A. *114*, 1548–1553.

Lowe, E.D., Hasan, N. 'il, Trempe, J.F., Fonso, L., Noble, M.E.M., Endicott, J.A., Johnson, L.N., and Brown, N.R. (2006). Structures of the Dsk2 UBL and UBA domains and their complex. Acta Crystallogr. D Biol. Crystallogr. *62*, 177–188.

Lu, Y., Wu, J., Chen, S., Sun, S., Ma, Y.-B., Ouyang, Q., Finley, D., Kirschner, M.W., and Mao, Y. (2016). Conformational landscape of the p28-bound human proteasome regulatory particle. bioRxiv 088492. *Not yet peer reviewed.

Lu, Y., Lee, B., King, R.W., Finley, D., and Kirschner, M.W. (2015). Substrate degradation by the proteasome: a single-molecule kinetic analysis. Science *348*, 1250834.

Mansour, W., Nakasone, M.A., von Delbrück, M., Yu, Z., Krutauz, D., Reis, N., Kleifeld, O., Sommer, T., Fushman, D., and Glickman, M.H. (2015). Disassembly of Lys11 and mixed linkage polyubiquitin conjugates provides insights into function of proteasomal deubiquitinases Rpn11 and Ubp6. J. Biol. Chem. *290*, 4688–4704.

Marshall, R.S., McLoughlin, F., and Vierstra, R.D. (2016). Autophagic Turnover of Inactive 26S Proteasomes in Yeast Is Directed by the Ubiquitin Receptor Cue5 and the Hsp42 Chaperone. Cell Rep *16*, 1717–1732.

Martin, A., Baker, T.A., and Sauer, R.T. (2008). Pore loops of the AAA+ ClpX machine grip substrates to drive translocation and unfolding. Nat. Struct. Mol. Biol. *15*, 1147–1151.

Matyskiela, M.E., and Martin, A. (2013). Design Principles of a Universal Protein Degradation Machine. J Mol Biol *425*, 199–213.

McDowell, G.S., and Philpott, A. (2013). Non-canonical ubiquitylation: mechanisms and consequences. Int. J. Biochem. Cell Biol. *45*, 1833–1842.

Merkley, E.D., Rysavy, S., Kahraman, A., Hafen, R.P., Daggett, V., and Adkins, J.N. (2014). Distance restraints from crosslinking mass spectrometry: Mining a molecular dynamics simulation database to evaluate lysine–lysine distances. Protein Sci *23*, 747–759.

Nakamura, Y., Umehara, T., Tanaka, A., Horikoshi, M., Padmanabhan, B., and Yokoyama, S. (2007). Structural basis for the recognition between the regulatory particles Nas6 and Rpt3 of the yeast 26S proteasome. Biochem. Biophys. Res. Commun. *359*, 503–509.

Nakayama, K.I., and Nakayama, K. (2005). Regulation of the cell cycle by SCF-type ubiquitin ligases. Semin. Cell Dev. Biol. *16*, 323–333.

Nathan, J.A., Kim, H.T., Ting, L., Gygi, S.P., and Goldberg, A.L. (2013). Why do cellular proteins linked to K63-polyubiquitin chains not associate with proteasomes? EMBO J. *32*, 552–565.

Park, S., Roelofs, J., Kim, W., Robert, J., Schmidt, M., Gygi, S.P., and Finley, D. (2009). Hexameric assembly of the proteasomal ATPases is templated through their C-termini. Nature *459*, 866–870.

Park, S., Kim, W., Tian, G., Gygi, S.P., and Finley, D. (2011). Structural defects in the regulatory particle-core particle interface of the proteasome induce a novel proteasome stress response. J. Biol. Chem. *286*, 36652–36666.

Park, S., Li, X., Kim, H.M., Singh, C.R., Tian, G., Hoyt, M.A., Lovell, S., Battaile, K.P., Zolkiewski, M., Coffino, P., et al. (2013). Reconfiguration of the proteasome during chaperone-mediated assembly. Nature *497*, 512–516.

Peth, A., Besche, H.C., and Goldberg, A.L. (2009). Ubiquitinated proteins activate the proteasome by binding to Usp14/Ubp6, which causes 20S gate opening. Mol. Cell *36*, 794–804.

Pickart, C.M., and Raasi, S. (2005). Controlled synthesis of polyubiquitin chains. Meth. Enzymol. *399*, 21–36.

Prakash, S., Tian, L., Ratliff, K.S., Lehotzky, R.E., and Matouschek, A. (2004). An unstructured initiation site is required for efficient proteasome-mediated degradation. Nat. Struct. Mol. Biol. *11*, 830–837.

Pruneda, J.N., Littlefield, P.J., Soss, S.E., Nordquist, K.A., Chazin, W.J., Brzovic, P.S., and Klevit, R.E. (2012). Structure of an E3:E2~Ub complex reveals an allosteric mechanism shared among RING/U-box ligases. Mol. Cell *47*, 933–942.

Riedinger, C., Boehringer, J., Trempe, J.-F., Lowe, E.D., Brown, N.R., Gehring, K., Noble, M.E.M., Gordon, C., and Endicott, J.A. (2010). Structure of Rpn10 and Its Interactions with Polyubiquitin Chains and the Proteasome Subunit Rpn12. J. Biol. Chem. *285*, 33992–34003.

Roelofs, J., Park, S., Haas, W., Tian, G., McAllister, F.E., Huo, Y., Lee, B.-H., Zhang, F., Shi, Y., Gygi, S.P., et al. (2009). Chaperone-mediated pathway of proteasome regulatory particle assembly. Nature *459*, 861–865.

Roseman, A.M. (2004). FindEM--a fast, efficient program for automatic selection of particles from electron micrographs. J. Struct. Biol. *145*, 91–99.

Rosenzweig, R., Bronner, V., Zhang, D., Fushman, D., and Glickman, M.H. (2012). Rpn1 and Rpn2 coordinate ubiquitin processing factors at proteasome. J. Biol. Chem. *287*, 14659–14671.

Rousseau, A., and Bertolotti, A. (2016). An evolutionarily conserved pathway controls proteasome homeostasis. Nature *536*, 184–189.

Saeki, Y., Saitoh, A., Toh-e, A., and Yokosawa, H. (2002). Ubiquitin-like proteins and Rpn10 play cooperative roles in ubiquitin-dependent proteolysis. Biochem. Biophys. Res. Commun. *293*, 986–992.

Saeki, Y., Isono, E., and Toh-E, A. (2005). Preparation of ubiquitinated substrates by the PY motif-insertion method for monitoring 26S proteasome activity. Meth. Enzymol. *399*, 215–227.

Saeki, Y., Toh-e, A., Kudo, T., Kawamura, H., and Tanaka, K. (2009). Multiple Proteasome-Interacting Proteins Assist the Assembly of the Yeast 19S Regulatory Particle. Cell *137*, 900–913.

Sakata, E., Bohn, S., Mihalache, O., Kiss, P., Beck, F., Nagy, I., Nickell, S., Tanaka, K., Saeki, Y., Förster, F., Baumeister, W. (2012). Localization of the proteasomal ubiquitin receptors Rpn10 and Rpn13 by electron cryomicroscopy. Proc. Natl. Acad. Sci. U.S.A. *109*, 1479–1484.

Scheres, S.H.W. (2012). RELION: implementation of a Bayesian approach to cryo-EM structure determination. J. Struct. Biol. *180*, 519–530.

Schreiner, P., Chen, X., Husnjak, K., Randles, L., Zhang, N., Elsasser, S., Finley, D., Dikic, I., Walters, K.J., and Groll, M. (2008). Ubiquitin docking at the proteasome through a novel pleckstrin-homology domain interaction. Nature *453*, 548–552.

Schweitzer, A., Aufderheide, A., Rudack, T., Beck, F., Pfeifer, G., Plitzko, J.M., Sakata, E., Schulten, K., Förster, F., and Baumeister, W. (2016). Structure of the human 26S proteasome at a resolution of 3.9 Å. PNAS *113*, 7816–7821.

Shi, Y., Chen, X., Elsasser, S., Stocks, B.B., Tian, G., Lee, B.-H., Shi, Y., Zhang, N., de Poot, S.A.H., Tuebing, F., Sun, S., Vannoy, J., Tarasov, S.G., Engen, J.R., Finley, D., Walters, K.J. (2016). Rpn1 provides adjacent receptor sites for substrate binding and deubiquitination by the proteasome. Science *351*.

Singh, C.R., Lovell, S., Mehzabeen, N., Chowdhury, W.Q., Geanes, E.S., Battaile, K.P., and Roelofs, J. (2014). 1.15 Å resolution structure of the proteasome-assembly chaperone Nas2 PDZ domain. Acta Crystallogr F Struct Biol Commun *70*, 418–423.

Smith, D.M., Chang, S.-C., Park, S., Finley, D., Cheng, Y., and Goldberg, A.L. (2007). Docking of the proteasomal ATPases' carboxyl termini in the 20S proteasome's alpha ring opens the gate for substrate entry. Mol. Cell *27*, 731–744.

Suraweera, A., Münch, C., Hanssum, A., and Bertolotti, A. (2012). Failure of amino acid homeostasis causes cell death following proteasome inhibition. Mol. Cell *48*, 242–253.

Takagi, K., Kim, S., Yukii, H., Ueno, M., Morishita, R., Endo, Y., Kato, K., Tanaka, K., Saeki, Y., and Mizushima, T. (2012). Structural basis for specific recognition of Rpt1p, an ATPase subunit of 26 S proteasome, by proteasome-dedicated chaperone Hsm3p. J. Biol. Chem. *287*, 12172–12182.

Takeuchi, J., and Tamura, T. (2004). Recombinant ATPases of the yeast 26S proteasome activate protein degradation by the 20S proteasome. FEBS Lett. *565*, 39–42.

Thrower, J.S., Hoffman, L., Rechsteiner, M., and Pickart, C.M. (2000). Recognition of the polyubiquitin proteolytic signal. EMBO J. *19*, 94–102.

Tomko, R.J., and Hochstrasser, M. (2011a). Incorporation of the Rpn12 subunit couples completion of proteasome regulatory particle lid assembly to lid-base joining. Mol. Cell *44*, 907–917.

Tomko, R.J., and Hochstrasser, M. (2011b). Order of the proteasomal ATPases and eukaryotic proteasome assembly. Cell Biochem. Biophys. *60*, 13–20.

Tomko, R.J., and Hochstrasser, M. (2013). Molecular architecture and assembly of the eukaryotic proteasome. Annu. Rev. Biochem. *82*, 415–445.

Tomko, R.J., and Hochstrasser, M. (2014). The intrinsically disordered Sem1 protein functions as a molecular tether during proteasome lid biogenesis. Mol. Cell *53*, 433–443.

Torres, E.M., Dephoure, N., Panneerselvam, A., Tucker, C.M., Whittaker, C.A., Gygi, S.P., Dunham, M.J., and Amon, A. (2010). Identification of aneuploidy-tolerating mutations. Cell *143*, 71–83.

Unverdorben, P., Beck, F., Śledź, P., Schweitzer, A., Pfeifer, G., Plitzko, J.M., Baumeister, W., and Förster, F. (2014). Deep classification of a large cryo-EM dataset defines the conformational landscape of the 26S proteasome. Proc Natl Acad Sci U S A *111*, 5544–5549.

Verma, R., Chen, S., Feldman, R., Schieltz, D., Yates, J., Dohmen, J., and Deshaies, R.J. (2000). Proteasomal proteomics: identification of nucleotide-sensitive proteasome-interacting proteins by mass spectrometric analysis of affinity-purified proteasomes. Mol. Biol. Cell *11*, 3425–3439.

Verma, R., Aravind, L., Oania, R., McDonald, W.H., Yates, J.R., Koonin, E.V., and Deshaies, R.J. (2002). Role of Rpn11 metalloprotease in deubiquitination and degradation by the 26S proteasome. Science *298*, 611–615.

Vijay-Kumar, S., Bugg, C.E., and Cook, W.J. (1987). Structure of ubiquitin refined at 1.8 A resolution. J. Mol. Biol. *194*, 531–544.

Vodermaier, H.C. (2004). APC/C and SCF: controlling each other and the cell cycle. Curr. Biol. *14*, R787-796.

Voloshin, O., Bakhrat, A., Herrmann, S., and Raveh, D. (2012). Transfer of Ho endonuclease and Ufo1 to the proteasome by the UbL-UbA shuttle protein, Ddi1, analysed by complex formation in vitro. PLoS ONE *7*, e39210.

Walters, K.J., Lech, P.J., Goh, A.M., Wang, Q., and Howley, P.M. (2003). DNA-repair protein hHR23a alters its protein structure upon binding proteasomal subunit S5a. Proc. Natl. Acad. Sci. U.S.A. *100*, 12694–12699.

Wehmer, M., Rudack, T., Beck, F., Aufderheide, A., Pfeifer, G., Plitzko, J.M., Förster, F., Schulten, K., Baumeister, W., and Sakata, E. (2017). Structural insights into the functional cycle of the ATPase module of the 26S proteasome. Proc. Natl. Acad. Sci. U.S.A. *114*, 1305–1310.

Wilkinson, C.R., Seeger, M., Hartmann-Petersen, R., Stone, M., Wallace, M., Semple, C., and Gordon, C. (2001). Proteins containing the UBA domain are able to bind to multi-ubiquitin chains. Nat. Cell Biol. *3*, 939–943.

Worden, E.J., Padovani, C., and Martin, A. (2014). Structure of the Rpn11-Rpn8 dimer reveals mechanisms of substrate deubiquitination during proteasomal degradation. Nat Struct Mol Biol *21*, 220–227.

Wu, N., Liu, C., Bai, C., Han, Y.-P., Cho, W.C.S., and Li, Q. (2013). Over-expression of deubiquitinating enzyme USP14 in lung adenocarcinoma promotes proliferation through the accumulation of β-catenin. Int J Mol Sci *14*, 10749–10760.

Xu, D., Shan, B., Lee, B.-H., Zhu, K., Zhang, T., Sun, H., Liu, M., Shi, L., Liang, W., Qian, L., et al. (2015) Phosphorylation and activation of ubiquitin-specific protease-14 by Akt regulates the ubiquitin-proteasome system. eLife *4 e10510*.

Xu, P., Duong, D.M., Seyfried, N.T., Cheng, D., Xie, Y., Robert, J., Rush, J., Hochstrasser, M., Finley, D., and Peng, J. (2009). Quantitative proteomics reveals the function of unconventional ubiquitin chains in proteasomal degradation. Cell *137*, 133–145.

Yao, T., and Cohen, R.E. (2002). A cryptic protease couples deubiquitination and degradation by the proteasome. Nature *419*, 403–407.

Ye, Y., Blaser, G., Horrocks, M.H., Ruedas-Rama, M.J., Ibrahim, S., Zhukov, A.A., Orte, A., Klenerman, D., Jackson, S.E., and Komander, D. (2012). Ubiquitin chain conformation regulates recognition and activity of interacting proteins. Nature *492*, 266–270.

Zhang, F., Hu, M., Tian, G., Zhang, P., Finley, D., Jeffrey, P.D., and Shi, Y. (2009). Structural insights into the regulatory particle of the proteasome from Methanocaldococcus jannaschii. Mol. Cell *34*, 473–484.

Ziv, I., Matiuhin, Y., Kirkpatrick, D.S., Erpapazoglou, Z., Leon, S., Pantazopoulou, M., Kim, W., Gygi, S.P., Haguenauer-Tsapis, R., Reis, N., Glickman, M.H., Kleifeld, O. (2011). A perturbed ubiquitin landscape distinguishes between ubiquitin in trafficking and in proteolysis. Mol. Cell Proteomics *10*, M111.009753.